This document includes a point-by-point response to the reviews, a list of all major changes made in the manuscript, and a marked-up manuscript version.

Response to Referee #1

We are very grateful for the Referee #1's critical comments and suggestions, which have helped us improve the paper quality substantially. We have addressed all of the comments carefully as detailed below in our point-by-point responses. Our responses start with "R:".

General comments:

This study presents the optical and physical properties of anthropogenic soil dust and natural mineral dust near the dust source regions in East Asia. This information is the key to evaluate the impacts of dust on the regional climate. Results and discussions are comprehensive, some valuable information have been generated. I would recommend the paper to be accepted for publication after a few comments as listed below have been addressed.

R: We have addressed all of the comments carefully as detailed below.

I strongly suggest the authors to reorganize the introduction section. The relevant studies on aerosol optical properties over East Asia should be reviewed. Accordingly, significance of this study could be further summarized and focus. For example, page 3 and page 4 all discussed the research importance of dust aerosol rather than their optical properties.

R: We have reconstructed the introduction section and added one section in reviewing the aerosol optical properties over East Asia based on previous dust field campaigns.

I suggest the authors to more pay attention to the logics between the sentences and paragraphs. For example, the logic in line 15-22 in page 3 is confusing. Organic matters and sulfate are the dominant chemical compositions of aerosol, why the authors only mentioned BC here?

R: We agree with the reviewer. For this research mainly discuss the properties of natural and anthropogenic dust near the dust sources regions, we deleted the description of the other air pollutions in the introduction section, such as BC, OC, and sulfate aerosols.

I also strongly suggest authors to break down the result section into several topics or sections for reading friendly.

R: We have separated the result section into individual topics based on the reviewer's suggestion.

I suggest the authors to reorganize the abstract and conclusions due to these two sections are too similar.

R: The abstract has been rewritten, and the conclusions has been reorganized based on reviewer's suggestions.

The QA/QC of all instruments should be addressed in section 2.2.

R: The QA/QC information for all instruments have been given as Table 1, and the corresponding description is also added in Section 2.2.

Generally, the MAC of BC could be determined by its size distribution and coating. Why authors choose 6.6 m^2 g^{-1}?

R: Thanks very much for your comments and suggestions. To convert data into BC mass loadings, a precise knowledge of the mass absorption coefficient (MAC) is of great importance. Actually, a narrow range of BC for MAC (6.4–6.6 m^2 g^{-1}) was found to provide a good fit to urban particles collected by previous studies (Petzold et al., 1997; Penner et al., 1998; Sharma et al., 2002; Arnott et al., 2003; Bond and Bergstrom, 2006; Schwarz et al., 2008).

In this study, there are three reasons for us to use this MAC value as follows.

(1) Petzold et al. (2002) obtained the MAC= 6.5 ± 0.5 m^2 g^{-1} at the wavelength of 670 nm for the black carbon particles using ambient aerosol samples.

(2) The MAAP (Model 5012) provides the absorption information as an equivalent black carbon concentration (EBC), which is obtained by dividing the measured absorption coefficient by a default MAC of 6.6 $m^2 \cdot g^{-1}$, recommended by the manufacturer.

(3) Müller et al. (2011) found that the optical wavelength of MAAP is 637 ± 1 nm instead of 670nm during the GAW2005 workshop. For an Ångström exponent of 1.02, the absorption coefficient at 637 nm should be 5% higher than that at 670 nm. Hence, the MAC at 637 nm is 5% lower and should be corrected by multiplication with a factor of 1.05, and the corrected equation was given by Müller: $\sigma_{ap,\ 637} = m_{BC} \cdot MAC \cdot 1.05$

But we also admit that the BC particles may tend to be mixed with other aerosols during aging process, and the MAC of BC can vary during its lifetime due to changes in its chemical composition. However, it must be noted that our research area is very close to the desert source regions. Therefore, as we used the same MAC value as the MAAP

recommended in our calculation, we consider that the variability in MAC as a source of uncertainty can be neglected.

Above all, we prefer to use the MAC of BC as 6.6 m^2 g^{-1} in this study.

Table 1. The main aerosol observations and ground-based instrumentations at three sites.

Observation	Instrumentation	Model & manufacturer	Accuracy
Meteorological elements	Weather transmitter	WXT 520, Vaisala, Helsinki, Finland	*T*: ± 0.3; RH: 0.1 %; *P*: 0.1 hPa; WS: 0.1 m s^{-1}; WD: 1°
$PM_{2.5}$ concentration	Ambient particulate monitor	RP1400a, R&P Corp., Albany, NY, USA	0.1 μg m^{-3}
Aerosol total scattering/backscattering coefficient	Integrating nephelometer	TSI 3563, TSI Inc., Shoreview, MN, USA	0.44, 0.17, and 0.26 Mm^{-1} at the wavelengths of 450, 550, and 700 nm, respectively
Aerosol absorption coefficient	Multi-angle absorption photometer	MAAP 5012, Thermo Scientific, Waltham, MA, USA	0.66 Mm^{-1}
Aerosol size distribution	Aerodynamic particle sizer	APS 3321, TSI Inc., Shoreview, MN, USA	0.001 cm^{-3}

References

Arnott, W. P., Moosmuller, H., Sheridan, P. J., Ogren, J. A., Raspet, R., Slaton, W. V., Hand, J. L., Kreidenweis, S. M., and Collett, J. L.: Photoacoustic and filter-based ambient aerosol light absorption measurements: Instrument comparisons and the role of relative humidity, J. Geophys. Res-Atmos, 108, 4034, doi:10.1029/2002jd002165, 2003.

Bond, T. C. and Bergstrom, R. W.: Light Absorption by Carbonaceous Particles: An Investigative Review, Aerosol Sci. Tech., 40, 27–67, doi:10.1080/02786820500421521, 2006.

Müller, T., Henzing, J. S., de Leeuw, G., Wiedensohler, A., Alastuey, A., Angelov, H., Bizjak, M., Collaud Coen, M., Engström, J. E., Gruening, C., Hillamo, R., Hoffer, A., Imre, K., Ivanow, P., Jennings, G., Sun, J. Y., Kalivitis, N., Karlsson, H., Komppula,

M., Laj, P., Li, S. M., Lunder, C., Marinoni, A., Martins dos Santos, S., Moerman, M., Nowak, A., Ogren, J. A., Petzold, A., Pichon, J. M., Rodriquez, S., Sharma, S., Sheridan, P. J., Teinilä, K., Tuch, T., Viana, M., Virkkula, A., Weingartner, E., Wilhelm, R., and Wang, Y. Q.: Characterization and intercomparison of aerosol absorption photometers: result of two intercomparison workshops, Atmos. Meas. Tech., 4, 245–268, doi:10.5194/amt-4-245-2011, 2011.

Penner, J. E., Chuang, C. C., and Grant, K.: Climate forcing by carbonaceous and sulfate aerosols, Clim. Dynam., 14, 839–851, doi:10.1007/s003820050259, 1998.

Petzold, A., Kopp, C. and Niessner, R.: The Dependence of the Specific Attenuation Cross-section on Black Carbon Mass Fraction and Particle Size, Atmos. Environ., 31, 661–672, doi:10.1016/s1352-2310(96)00245-2, 1997.

Petzold, A., Kramer, H., and Schonlinner, M.: Continuous measurement of atmospheric black carbon using a multi-angle absorption photometer, Environ. Sci. Pollut. R., 78–82, 2002.

Schwarz, J.P., Gao, R.S., Spackman, J.R., Watts, L.A. and Thomson, D.S.: Measurement of the Mixing State, Mass, and Optical Size of Individual Black Carbon Particles in Urban and Biomass Burning Emissions, Geophys. Res. Lett., 35, 13810–13814, doi:10.1029/2008gl033968, 2008.

Sharma, S., Brook, J.R. and Cachier, H.: Light Absorption and Thermal Measurements of Black Carbon in Different Regions of Canada, J. Geophys. Res.-Atmos, 107, 4771, doi:10.1029/2002jd002496, 2002.

Response to Referee #2

We greatly appreciate the Referee #2's insightful and constructive comments and suggestions, which are helpful and valuable for greatly improving our manuscript. We have addressed all of the comments carefully as detailed below in our point-by-point responses. Our responses start with "R:".

General comments:

The paper presents measurements, results and analyses of optical properties and size distributions of surface layer aerosols in Northwestern China. Mineral dust affects air quality and climate over very large areas and they can be observed very far from their sources. In observations far from the sources the aerosol is typically aged and mixed with other particles. Therefore, it is very valuable that measurements are conducted also near the sources. This manuscript presents measurements very close to or essentially at the source and is valuable as such. One of the weaknesses of the work is that particle size range of the optical measurements was limited to 2.5 μm. In dust storms there are often larger particles like the authors' own APS measurements show. But now the data are here and also they yield good information. The authors could use the full extent of the data to obtain also more information as I will suggest below.

I can recommend publishing the paper in ACP, but I did find something to be revised.

R: Thanks very much for your good suggestions and the acceptance of this work, we have addressed all of the comments carefully as detailed below.

Detailed comments:

There is no text on the calibration of any of the instruments. In dusty conditions such as the sites where the measurements were conducted, instruments get quickly dirty and calibrations change. How did you deal with this? Write about calibrations, flow checks etc.

R: We have added the details of the calibration and flow checks for all the aerosol-related instruments in Section 2.2, and the accuracy for each instrument is also listed in Table 1.

In addition to calibrations, also data processing needs some revision.

The nephelometer suffers from a problem called truncation which leads to underestimation of scattering. The error is the larger the particles are. Read and cite Anderson and Ogren: Aerosol Sci. Tech., 29, 57–69, 1998 and Müller et al.: Aerosol Sci. Tech., 43, 581–586, 2009. and use their algorithms to correct the scattering. The corrected scattering coefficients will be larger than the ones presented now. And so will the corrected single scattering albedos also be.

R: We are sorry for the misleading. In this study, the datasets of the aerosol optical properties have already been corrected based on the nonideal detection developed by Anderson and Ogren (1998), and one of the sentence has been added in Section 2.2 as "For reducing and quantifying the uncertainties in aerosol optical properties measured by the nephelometers, the data reduction and uncertainty analysis for the scattering datasets due to nonideal detection are followed by Anderson and Ogren (1998)."

The nephelometer used in the campaign also measures backscatter coefficient. Why is there nothing about that in the whole manuscript? It would be a valuable addition to the paper. If the instrument was working I strongly recommend presenting and discussing also

backscatter coefficients and backscatter fractions at 3 wavelengths, both in figures and tables.

R: Due to the backscatter coefficients shows the same trends with the total scattering coefficients but in a relatively small magnitude, we plotted a new figure suggested by the reviewer (Figure 4a). Then, we calculate the backscattering fractions at the wavelengths of 550 nm shown as Figure 4c in the revised manuscript. Additionally, the detailed information of backscatter coefficients and backscattering fractions of $PM_{1.0}$ and $PM_{2.5}$ at the wavelengths of 450, 550, 700 nm are listed in Table 2.

There was the APS. Why was that not utilized more? I have some suggestions, not requirements. First, calculating integrated volume concentrations for PM2.5 would yield some quality control when compared with the TEOM. And if they correlate well, they would together yield an estimate of the dust particle density, at least in such cases when particles were dominated by supermicron particles. That would be valuable.

R: Following the reviewer's suggestion, we found that the integrated volume concentrations of $PM_{2.5}$ measured by APS and the mass concentration measured by TEOM are correlated well as Figure S2 shown. Then, we calculated the dust particle density under different atmospheric conditions during the dust field campaign, and the relative discussion were added in the result section in Page 23, Line 2–9, and Table 3.

Second: estimation of scattering coefficient would not be difficult either. If you don't have a Mie code, you can find them in the internet, calculate scattering efficiencies for the size channels of the APS and then calculate scattering coefficient of each size and finally

integrate over the size range. An important question would be, for instance, how large a fraction of scattering did you not get measured because of the impactors in front of the nephelometers? Sure, the particles were not spherical and Mie theory not accurate but it would yield an estimate.

R: Thanks very much for your comments and suggestions. We use the Mie theory and the aerosol number size distribution measured by APS to estimate the scattering coefficient compared with that derived by the nephelometer. The real part of the refractive index was assumed to be 1.53, which was widely used for mineral dust in literatures (Müller et al., 2009; McConnell et al., 2010) the imaginary part of the refractive index was determined using Mie calculations. As shown in Figure 13, the Mie-calculated scattering coefficient and measured scattering coefficient are highly correlated. For instance, the imaginary part of the refractive index (0.0010) for natural dust during dust storm in Zhangye and the background weather condition in Dunhuang are similar to the result of SAMUM-1 in Saharan (Müller et al., 2009). Based on the Mie calculation in this study, the $PM_{2.5}$ scattering fraction, which defined as the contribution of the light scattering of $PM_{2.5}$ to the total scattering (the calculated scattering coefficient in the size range of 0.5–20 μm), is ~36.4 % during dust storm, while is in the range of ~37.9–85.1 % during floating dust episode. Detailed information of Mie-calculated and measured scattering coefficient is summarized in Table 3. Generally, most of the $\sigma^{2.5}_{sp,\,Mie}$ agree well with $\sigma^{2.5}_{sp,\,neph}$, which can reflect a good quality of the datasets of $\sigma^{2.5}_{sp}$ during this dust field campaign.

Third: the APS data could also be used for calculating some weighted mean diameter, e.g., volume-weighted mean diameter VMD of the size distribution and compare that with the

Åsp. That would be valuable since satellite-derived products use wavelength dependency for estimating size.

R: We use the APS data to calculate the volume-weighted mean diameter (VMD) under the diameter of 2.5 μm and 1.0 μm. We found that the $VMD_{2.5}$ and $Å_{sp}^{2.5}$ are correlated well during the whole dust field campaign (Figure S3 in Supplement). However, there is no significant linear correlation between $VMD_{1.0}$ and $Å_{sp}^{1.0}$. The highly possible explanation is that the $VMD_{1.0}$ is calculated based on the aerosol size diameter ranging from ~0.5 to 1 μm measured by APS, while the variation of $Å_{sp}^{1.0}$ is affected by the aerosol diameter under 1 μm.

There was also an SP2 in the campaign, at least according to Fig 3. Why was it and its data not discussed at all? It would potentially yield also interesting and important results. Comparison with MAAP in different cases for instance. The MAAP measures light absorption which may also be due to absorbing mineral aerosols, not just BC.

R: We feel sorry for the misleading. Yes, we also measure the BC concentration and its size distribution by using the SP2 instrument shown as Figure 3. But the major innovation of this manuscript is the difference of the optical and physical properties of natural and anthropogenic dust. Therefore, the datasets measured by SP2 are used to analyze the mixing status of BC with the other aerosols during this dust field campaign in another manuscript (In preparation). A comparison of the BC mass concentration between SP2 and MAAP instruments is given in Figure S1 in the Supplement. The result indicates that the tendency of BC mass concentrations are much similar, but the values measured by MAAP

was relatively larger than that measured by SP2. We note the relative large bias between MAAP and SP2 instruments may result from the size distribution of BC measured by using different sampler inlet impactors of 2.5 μm and 1 μm.

P6, L5 – What is Hexi corridor? Not well-known for non-Chinese.

R: The explanation of the geographical location of Hexi corridor is given in Section 2.1 based on the reviewer's suggestion as follow: "The Hexi Corridor is a ~1000km northwest-southeast-oriented chain of oases in northwestern China (mainly in the Gansu Province), surrounded by the Qilian Mountains (elevation: ~4000 m), the Beishan Mountains (elevation: ~2500 m), Heli Mountains (elevation: ~2000 m) and the Wushao Mountains (elevation: ~3000 m). The Hexi Corridor is considered to be a heavily polluted area because of the combination of local topography and the human activities occurring over northwestern China."

P7, L3- Define or explain floating dust.

R: The definition of floating dust has been added in Section 3.1 as "Floating dust is generally defined as a weather phenomenon in which fine mode dust particles suspended in the lower troposphere under calm or low-wind condition, with horizontal visibility less than 10 km."

P8, L3-4, The detection limits of the scattering coefficients were obviously taken from the Table 4 of Anderson et al., 1996 for 300 min averaging time. But in that table there is not the multiplication by 10. So, the detection limit of total scattering at 450 nm is 0.44 Mm^{-1},

not 0.44 × 10 Mm^{-1} like the authors claim on L3.

R: We have corrected this sentence as "the detection limits are 0.44 Mm^{-1}, 0.17 Mm^{-1}, and 0.26 Mm^{-1} (1 Mm^{-1} = 10^{-6} m^{-1}), respectively" in Page 8, Line 20–21.

P8, L7: MAAP wavelength: the MAAP manual claims it is 670 nm but Müller et al. Atmos. Meas. Tech., 4, 245–268, 2011 measured it to be 637 nm. You should reprocess the data. First correct scattering for truncation, then use MAAP data for calculating SSA. But, instead of assuming the wavelength dependence of absorption, use the wavelength dependency ($Å_{sp}$) of truncation-corrected scattering and interpolate the scattering to 637 nm and present SSA at 637 nm. This way you avoid assumptions. The point is that the wavelength dependency and Ångström exponent of absorption by absorbing mineral dust may significantly differ from 1.

R: We have adjusted the absorption estimated by MAAP to 637nm following the method of Müller et al. (2011). Then, we interpolate the scattering coefficients to 637 nm in order to calculate SSA at 637 nm. We also replotted all of the related Figures as well as Table 2 based on the corrected datasets in the revised manuscript.

In Figure 1, show

- Hexi corridor – not well-known for most readers of ACP

R: The same with the above explanation.

- show a kilometer scale also in the upper panel

R: We have added the kilometer scale in the upper panel of Figure 1.

- use and show sub-panel letters a – d. Also for the upper panel.

R: We have added the sub-panel letters a–d in Figure 1.

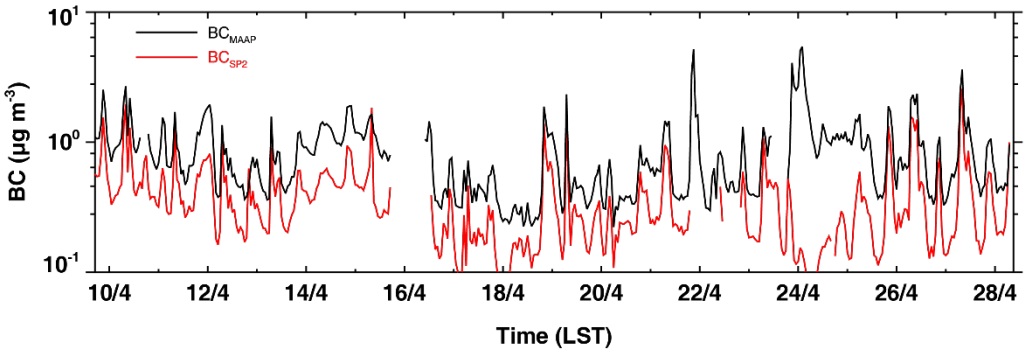

Figure S1. Temporal variations of BC mass concentration under the diameter of 1 μm and 2.5 μm measured by SP2 and MAAP in Zhangye from 9 to 28 April, respectively.

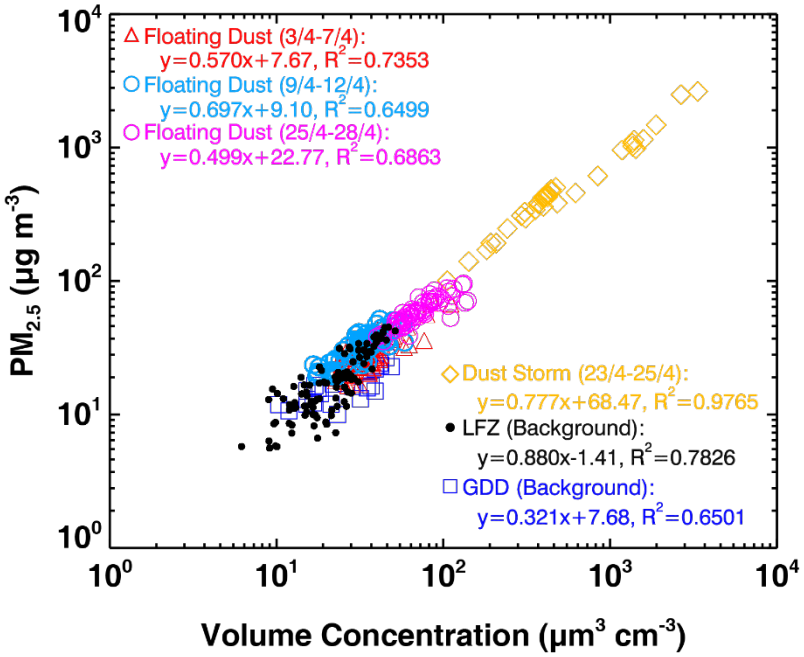

Figure S2. Scatter plot of mass concentration of $PM_{2.5}$ versus the integrated volume concentration under the diameter of 2.5 μm during the dust field campaign. The color symbols represent different atmospheric conditions during the dust field campaign.

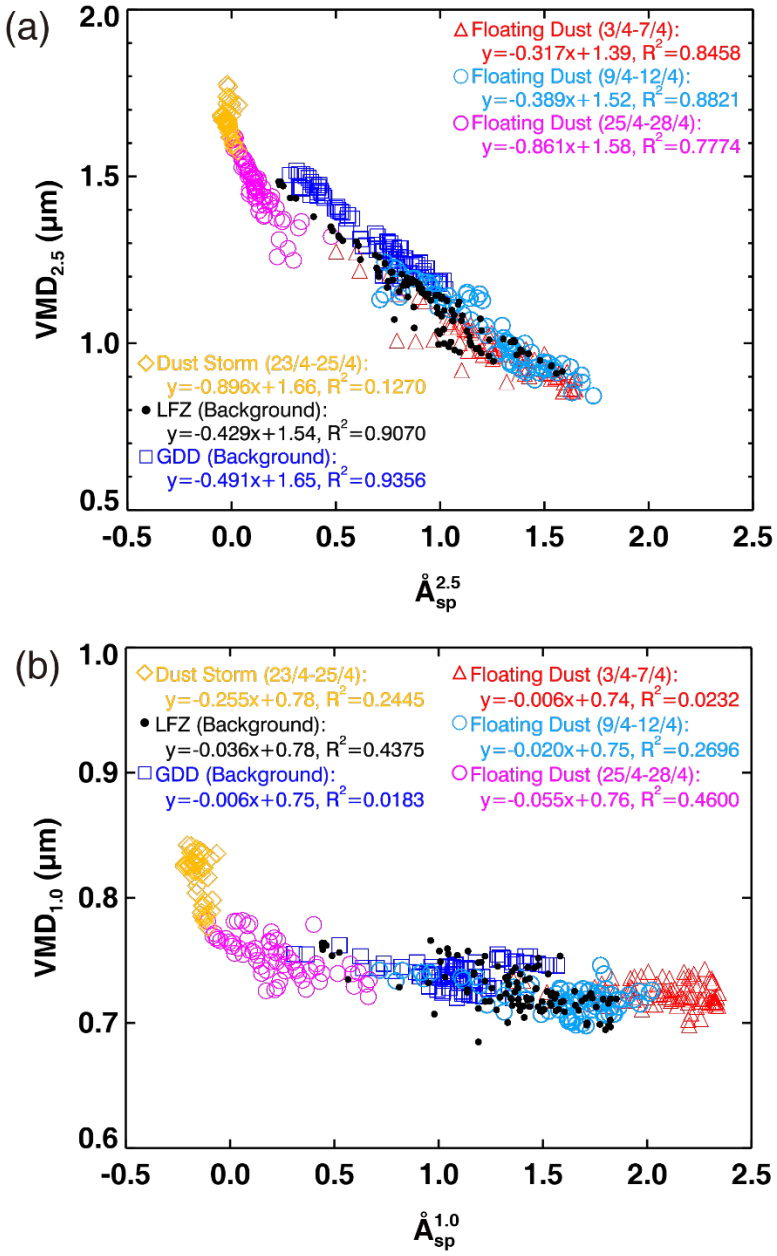

Figure S3. Scatter plot of the volume-weighted mean diameter (VMD) versus scattering Ångström exponent at 450–700 nm for **(a)** $PM_{2.5}$ and **(b)** $PM_{1.0}$. The color symbols represent different atmospheric conditions during the dust field campaign.

Table 3. Statistical summary of optical and microphysical properties of aerosols in different atmospheric conditions during the dust field campaign.

	Floating Dust (3/4–7/4)	Floating Dust (9/4–12/4)	Floating Dust (25/4–28/4)	Dust Storm (23/4–25/4)	LZF (Background)	GDD (Background)
Dust particle density (g cm^{-3})	1.32 ± 0.28	1.04 ± 0.17	1.24 ± 0.21	1.16 ± 0.51	1.33 ± 0.44	1.64 ± 0.50
Refractive index	1.53–0.0117*i*	1.53–0.0862*i*	1.53–0.0020*i*	1.53–0.0010*i*	1.53–0.0442*i*	1.53–0.0010*i*
$\sigma^{2.5}_{sp,\ neph}$ (Mm^{-1})	102 ± 37	86 ± 29	127 ± 31	1087 ± 991	49 ± 24	31 ± 9
$\sigma^{2.5}_{sp,\ Mie}$ (Mm^{-1})	107 ± 40	72 ± 30	132 ± 32	1163 ± 992	41 ± 25	31 ± 9
$\sigma^{20}_{sp,\ Mie}$ (Mm^{-1})	153 ± 51	102 ± 31	334 ± 75	2983 ± 2712	66 ± 32	71 ± 27
$PM_{2.5}$ scattering fraction (%)	49.3	85.1	37.9	63.6	74.8	43.7

References

Anderson, T. L. and Ogren, J. A.: Determining aerosol radiative properties using the TSI 3563 Integrating Nephelometer, Aerosol Sci. Tech., 29, 57–69, doi:10.1080/02786829808965551, 1998.

McConnell, C. L., Formenti, P., Highwood, E. J., and Harrison, M. A. J.: Using aircraft measurements to determine the refractive index of Saharan dust during the DODO Experiments, Atmos. Chem. Phys., 10, 3081–3098, doi:10.5194/acp-10-3081-2010, 2010.

Müller, T., Henzing, J. S., de Leeuw, G., Wiedensohler, A., Alastuey, A., Angelov, H., Bizjak, M., Collaud Coen, M., Engström, J. E., Gruening, C., Hillamo, R., Hoffer, A., Imre, K., Ivanow, P., Jennings, G., Sun, J. Y., Kalivitis, N., Karlsson, H., Komppula, M., Laj, P., Li, S. M., Lunder, C., Marinoni, A., Martins dos Santos, S., Moerman, M., Nowak, A., Ogren, J. A., Petzold, A., Pichon, J. M., Rodriquez, S., Sharma, S., Sheridan, P. J., Teinilä, K., Tuch, T., Viana, M., Virkkula, A., Weingartner, E., Wilhelm, R., and Wang, Y. Q.: Characterization and intercomparison of aerosol absorption photometers: result of two intercomparison workshops, Atmos. Meas. Tech., 4, 245–268, doi:10.5194/amt-4-245-2011, 2011.

Müller, T., Schladitz, A., Massling, A., Kaaden, N., Kandler, K., and Wiedensohler, A.: Spectral absorption coefficients and imaginary parts of refractive indices of Saharan dust during SAMUM-1, Tellus B, 61, 79–95, doi:10.1111/j.1600-0889.2008.00399.x,

2009.

Optical and microphysical properties of natural mineral dust and anthropogenic soil dust near dust source regions over northwestern China

Xin Wang[1], Hui Wen[1], Jinsen Shi[1], Jianrong Bi[1], Zhongwei Huang[1], Beidou Zhang[1], Tian Zhou[1], Kaiqi Fu[1], Quanliang Chen[2], and Jinyuan Xin[3]

[1] Key Laboratory for Semi-Arid Climate Change of the Ministry of Education, College of Atmospheric Sciences, Lanzhou University, Lanzhou 730000, China

[2] Plateau Atmospheric and Environment Laboratory of Sichuan Province, College of Atmospheric Sciences, Chengdu University of Information Technology, Chengdu 610225, China

[3] State Key Laboratory of Atmospheric Boundary Layer Physics and Atmospheric Chemistry (LAPC), Institute of Atmospheric Physics, Chinese Academy of Sciences, Beijing 100029, China

Correspondence to: X. Wang (wxin@lzu.edu.cn)

Abstract.

Mineral dust aerosols (MDs) not only influence the climate by scattering and absorbing solar radiation, but also modify cloud properties and change the ecosystem. From 3 April to 16 May 2014, a ground-based mobile laboratory was deployed to measure the optical and microphysical properties of MDs near dust source regions in Wuwei, Zhangye, and Dunhuang (in chronological order) along the Hexi Corridor over northwestern China. Throughout this dust campaign, the hourly averaged (± standard deviation) aerosol scattering coefficients (σ_{sp}, 550 nm) of the particulates with aerodynamic diameters less than 2.5 μm ($PM_{2.5}$) at these three sites were sequentially 101.5 ± 36.8, 182.2 ± 433.1 and 54.0 ± 32.0 Mm^{-1}. Correspondingly, the absorption coefficients (σ_{ap}, 637 nm) were 9.7 ± 6.1, 6.0 ± 4.6 and 2.3 ± 0.9 Mm^{-1}; single scattering albedos (ω, 637 nm) were 0.902 ± 0.025, 0.931 ± 0.037 and 0.949 ± 0.020; and scattering Ångström exponents ($Å_{sp}$, 450–700 nm) of $PM_{2.5}$ were 1.28 ± 0.27, 0.77 ± 0.51 and 0.52 ± 0.31. ~~and backscattering coefficients (σ_{bsp}), single scattering albedo (ω), backscattering fraction (b), scattering Ångström exponent (), ($Å_{sp}$), mass scattering efficiency (MSE)~~mass concentration of $PM_{2.5}$, ~~and aerosol size distribution in the range of 0.5–20 μm~~ were observed, respectively ~~at 5-min intervals. The results indicate that large differences were found between the optical and microphysical properties of anthropogenic and natural dust because of floating dust episodes and dust storms. The values of σ_{sp}, σ_{ap} and ω of $PM_{2.5}$ measured at 550 nm range from ~37–532 Mm^{-1}, ~2.2–55.3 Mm^{-1} and ~0.64–0.98, respectively, because of the presence of anthropogenic soil dust during floating dust episodes, and the corresponding values~~

~~under background conditions are ~21–163 Mm^{-1}, ~1.3–34.8 Mm^{-1}, and ~0.70–0.98, respectively. We note that~~During a severe~~strong~~ dust storm in Zhangye (i.e., from 23 to 25 April), the highest~~r~~ values of $\sigma_{sp}^{2.5}$ (~5074 Mm^{-1}), backscattering coefficient~~s~~ ($\sigma_{bsp}^{2.5}$, ~522 Mm^{-1}) and ω (~0.993), the lowest~~r~~ values of backscattering fraction ($b_{2.5}$, ~0.101) and Å$_{sp}^{2.5}$ (~~–~~0.046) at 450–700 nm, with peak values of aerosol number size distribution (appearing at the particle diameters range of 1–3 μm) ~~indicate~~ exhibit that the atmosphere aerosol~~s particles observed during a strong dust storm in Zhangye~~ were dominated by coarse mode dust aerosols. It is hypothesized that ~~However,t~~The relative higher values of MSE ~~the highest~~ during floating dust episodes in Wuwei and Zhangye are attributed to the~~reveal that the~~ anthropogenic soil dust produced by agricultural cultivations~~. (e.g., land planning, ploughing, and disking)can scatter more solar radiation than coarse mode particles.~~

1 Introduction

The role of mineral dust aerosols (MDs) in the climate system has received considerable attention over recent years ~~Mineral dust is one of the major types of tropospheric aerosols in the atmosphere~~ (Arimoto et al., 2006; Ramanathan et al., 2001). MDs~~Mineral dust~~ has a profound impact on the radiative balance of the Earth by scattering and absorbing solar radiation (Huang et al., 2010, 2014; Wang et al., 2010~~; Huang et al., 2014~~; Li et al., 2016); ~~this dust~~it can also act as cloud condensation nuclei (CCN) to alter the precipitation rate and hydrological cycle of the Earth (Rosenfeld et al., 2001). East Asia includes the Taklimakan, Tengger, Badain Jaran and Gobi Deserts and is thus considered to be one of the major source regions of natural dust in the world, as it produces large amounts of natural mineral dust (Zhang et al., 1997; Wang et al., 2008; Che et al., 2011, 2013; Ge et al., 2014; Xin, 2005, 2010, 2015). ~~Once dust aerosols are lifted into the atmosphere by strong surface winds, they can be transported up to thousands of kilometres away from their source regions (Chen et al., 2013; Liu et al., 2015; Huang et al., 2008).~~ The long-range transport of MDs~~tropospheric aerosols~~ from ~~their~~ dust source regions ~~in East Asia~~ have a significant influence on ~~plays a key role in~~ aerosol radiative forcing and environment changing (Chen et al., 2013; Ge et al., 2011; Liu et al., 2015; Huang et al., 2008~~Ge et al., 2011~~). In order to fully account~~better estimate~~ the climate effects ~~due to~~of MDs~~mineral dust~~ ~~aerosols~~ over eastern Asian regions, several international intensive field campaigns were conducted to measure their optical, physical, and chemical properties ~~in the eastern Asian regions over~~in recent decades, such as the Asian Aerosol Characterization

Experiment (ACE-Asia) (Arimoto et al., 2006), the NASA Global Tropospheric Experiment Transport and Chemical Evolution over the Pacific (TRACE-P) (Jacob et al.~~Christopher~~, 2003), the Atmospheric Brown Clouds-East Asia Regional Experiment (EAREX) (Nakajima et al., 2007~~3~~), and the 2008 China-U.S. joint dust field experiment (Ge et al., 2010; Li et al., 2010; Wang et al., 2010). For instance, Ge et al. (2010) illustrated the mean single scattering albedo (SSA) measured at Zhangye ~~over northwestern China~~ increases with wavelength from 0.76 ± 0.02 at 415 nm to 0.86 ± 0.01 at 870 nm. Seasonal variations of the scattering coefficients and the absorption coefficients were also collected at Dunhuang and Zhangye of Gansu Province as well as Yulin of Shanxi Province~~,in northwestern China~~ (Li et al., 2010; Xu et al., 2004; Yan et al., 2007). However, the systematic review of the optical and microphysical properties of ~~the fine mode mineral dust~~MDs ~~near the dust source regions~~ in eastern Asia is still a challenge due to limited observations, especially for fine mode mineral dust near the dust source ~~region~~areas in northwestern China.

~~to measure their optical, chemical, and microphysical properties in East Asian regions over recent decades. For exampleinstance, the single scattering albedo, which is the measured of the effectiveness of scattering relative to total light extinction by aerosols, is a key variableparameter in assessing the climatic effects (Haywood and Shine, 1995). Dust aerosols are suggested to have SSA values typically greater than 0.95 in the visible wavelengths based on satellite reflectance and Aerosol Robotic Network (AERONET) data (Kaufman et al., 2001; Dubovik et al., 2002). A change in SSA from 0.9 to 0.8 can often change the sign of radiative forcing from negative to positive, which depends on~~

the reflectance of the underlying surface and the altitude of the aerosols (Hensen et al., 1997; Bergstrom et al., 2007). Therefore, the largest source of uncertainty in determining global radiative forcing is associated with the estimation of radiative forcing caused by dust particles, which is mainly due to their non-sphericity and chemical composition (Washington et al., 2003; McConnell et al., 2008,; IPCC, 2013). The Asian Aerosol Characterization Experiment (ACE-Asia) also showed that most of the coarse-particle nitrate and sulfate in post-frontal air was associated with dust (Arimoto et al., 2006). Dubovik and King (2000) pointed out that the average AERONET-retrieved single scattering albedo (SSA) is about 0.9 in the visible wavelength range at all stations, confirming the presence of aerosols with strong absorbing properties based on An International Regional Experiment (EAST-AIRE). The Asian Aerosol Characterization Experiment (ACE-Asia) showed that most of the coarse-particle nitrate and sulfate in post-frontal air was associated with dust, and more remarkably, that competitive or exclusionary processes evidently are involved in the uptake or production of these substances using an aerosol time-of-flight mass spectrometer (Arimoto et al., 2006). Nie et al. (2014) found observational evidence on new particle formation and growth in heavy dust plumes mixed with anthropogenic pollution and suggests an unexpected source of nucleating and condensable vapors via dust-induced heterogeneous photochemical processes based on field measurements at a mountain site in South China. Furthermore, the light-absorbing aerosols such as black carbon, organic carbon and desert dust in Asian monsoon regions may also induce dynamical feedback processes, leading to a strengthening of the early monsoon and

affecting the subsequent evolution of the monsoon (Li et al., 2016; Jin et al., 2015, 2016). The spatiotemporal distributions of dust physical and chemical properties (e.g., aerosol loading, SSA, asymmetry factor, and size distribution) were also measured at numerous sites havingwith different environmental conditions, especially during the EAST-AIRC (Li et al., 2011), Saharan Dust Expriment SHADE (Tanre et al., 2003), Puerto Rico Dust Experiment PRIDE (Reid et al., 2003), and 2008 China-U.S. joint dust field experiment (Ge et al., 2010; Li et al., 2010; Wang et al., 2010).

For instance, Washington et al. (2003) demonstrated that there isWe noted that the large-scale uncertainty is associated with the estimation of radiative forcing caused by dust particles, which is mainly due to their non-sphericity and chemical composition (Washington et al., 2003; McConnell et al., 2008). The single scattering albedo, which is the measured of the effectiveness of scattering relative to total light extinction by aerosols, is a key variable in assessing the climatic effects (Haywood and Shine, 1995). Dust aerosols are suggested to have SSA values typically greater than 0.95 in the midvisible wavelengths based on satellite reflectance and Aerosol Robotic Network (AERONET) data (Kaufman et al., 2001; Dubovik et al., 2002). Lower SSA values (~0.8–0.9) were expected in the source regions for Asian dust particles since they are often mixed with anthropogenic light-absorbing aerosols during transport over the downwelling industrial and urban areas (Kim, 2001; Sohn et al., 2007). Ge et al. (2010) also found similar values of SSA from 0.76 ± +-0.02 at the wavelength of 0.415 μum to 0.86 ± +-0.01 at the wavelength of 0.870 μum at Zhangye over northwestern China. A change in single scattering albedo (SSA) from 0.9 to 0.8 can often change the sign of

radiative forcing from negative to positive, which depends on the reflectance of the underlying surface and the altitude of the aerosols (Hensen et a., 1997; Bergstrom et al., 2007). Compared to natural mineral dust, black carbon (BC), which is generated from the incomplete combustion of fossil fuels and biomass burning, is also a major anthropogenic pollutant. Numerous modelling studies have demonstrated the importance of BC in regional climate change (Ramanathan et al., 2005; Menon et al., 2002). Therefore, the largest source of uncertainty in determining global radiative forcing is the quantification of the direct and indirect effectsoptical and microphysical properties of mineral dustMDs and other anthropogenic aerosols (IPCC, 2013).

Recently, the potential impacts of anthropogenic soil dust have also received an increasing amount of attention (Prospero et al., 2002; Huang et al., 2015a; Tegen and Fung, 1995; Tegen et al., 2002; Shi et al., 2015; Pu et al., 2015; Wang et al., 2015a). Anthropogenic mineral dust can also influence air quality and human health through the processes of their emission, transport, removal, and deposition (Aleksandropoulou et al., 2011; Chen et al., 2013; Huang et al., 2014, 2015a, 2015b; Kim et al., 2009; Li et al., 2009; Mahowald and Luo, 2003; Zhang et al., 2005, 2015). Ginoux et al. (2010) estimated that anthropogenic dust accounts for 25% of all dust aerosols using observational data from MODIS (Moderate Resolution Imaging Spectroradiometer) Deep Blue satellite products combined with a land-use fraction dataset. Nie et al. (2014) found observational evidence on new particle formation and growth in heavy dust plumes mixed with anthropogenic pollution via dust-induced heterogeneous

photochemical processes. ~~Anthropogenic dust primarily originates from urban and regional sources, especially during the winter; this dust is commonly enriched in heavy metals and other toxic elements (Kamani et al., 2015; Li et al., 2013; Wang et al., 2015; Zhang et al., 2013). Nnortheastern China and its surrounding regions are generally regarded as industrial areas that are most strongly affected by human activities.~~ Because anthropogenic dust emissions from disturbed soils are not well constrained, we define anthropogenic dust as mineral dust from areas that have been disrupted by human activities, such as deforestation, overgrazing, and agricultural and industrial activities (Aleksandropoulou et al., 2011; Tao et al., 2014, 2015, 2017; Tegen and Fung, 1995; Tegen et al., 2002, 2004; Thompson et al., 1988); anthropogenic dust is thus different ~~than~~ from natural mineral dust, which originates from desert regions (Che et al., 2011, 2013; Goudie and Middleton, 2001; Li et al., 2012; Park and Park, 2014; Pu et al., 2015; Wang et al., 2008, 2010). This assumption is consistent with the results of a recent study by Huang et al. (2015a), who found that anthropogenic dust comprises 91.8% of regional emissions in eastern China and 76.1% of regional emissions in India ~~(e.g., Figure 10 in Huang et al., 2015a)~~. ~~This may be due to the larger population densities of eastern China and India, which are characterized by intense human activity (Huang et al., 2015a; Wang et al., 2013).~~

Understanding the ~~microphysical and optical properties of~~ natural dust mixed with the ~~other atmospheric~~anthropogenic aerosols ~~produced by human activities~~ in the troposphere has a critical impact on our ability to get insight into~~predict~~ atmospheric compositions and predict global climate change (Nie et al., 2014; Ramanathan et al.,

2007; Spracklen and Rap, 2013; Wang et al., 2015b). Although sSeveral attempts have been made conducted to investigate the significance of the effects of dust on global climate, meteorology, atmospheric dynamics, ecosystems and human health (Rosenfeld et al., 2011; Qian et al., 2004)., only lLimited field campaigns have focused on the properties of natural dust and anthropogenic aerosols, especially those of the anthropogenic dust aerosols produced by human activities near dust source regions. In this paper, In this study, we not only focus on the surface measurements of theed optical and microphysical properties of natural dust and anthropogenic aerosolsdust. This paper presents detailed emission information obtained from measurements made in Wuwei, Zhangye, and Dunhuang over Northwestern northwestern China from 3 April to 16 May in 2014, but also in order to better understand the sources of regional emissions and the mixing state of air pollution with mineral dust. We also used statistical analysis to identify the possible signatures of natural dust storms transported from dust source regions over northwestern China.

2 Methodology

2.1 Measurement Sites dDespcription

The Hexi Corridor is a ~1000km northwest-southeast-oriented chain of oases in northwestern China (mainly in the Gansu Province), surrounded by the Qilian Mountains (elevation: ~4000 m) to the south and southwest, the Beishan Mountains (elevation: ~2500 m), and Heli Mountains (elevation: ~2000 m) to the north, and the Wushao Mountains (elevation: ~3000 m) to the east.; adjacent to the east margin of the

Kumtag Desert, by the Badain Jaran Desert to the northeast and the Tengger Desert to the southeast. The Hexi Corridor is considered to be a heavily polluted area because of the combination of local topography and the human activities occurring over northwestern China (Li et al., 2010Ref...; Wang et al., 2010; Bi et al., 2017).

The dust field campaign was carried out along the Hexi Corridor from 3 April to 16 May 2014. A ground-based mobile facility of the Semi-Arid Climate and Environment Observatory of Lanzhou University (SACOL) for Energy Atmospheric Radiation Measurements was used in three sites, which are was located in Wuwei (37.72°N, 102.89°E; 1691 m a.s.l.; 3–7 April), Zhangye (39.04°N, 100.12°E; 1578 m a.s.l.; 9–28 April), and Dunhuang (39.96°N, 94.33°E; 1367 m a.s.l.; 3–16 May). The locations of these sites are shown in the top panel of Figure 1a. As presentedshown in the bottom panels of Figure 1, the site Huangyang Farmland in Wuwei (HFW in figures and tTables, similarly hereinafter) is located only ~17 km away fromwest of the Tengger Desert and ~20 km away from the Qilian Mountains; therefore, anthropogenic air pollutants originating from Wuwei City can directly influence the sampling site because of the prevailing wind direction along the local topography. The Linze farmland in Zhangye (LFZ) is located in northwestern Zhangye City (~30 km), to the southwest of Linze County (~12 km), encompassed by the Qilian Mountains and the Badain Jaran Desert. The land surface type in Linze farmland in Zhangye (LFZ) is similar with Wuwei (Figure 2b). However, the sampling site in Dunhuang was located approximately 30 km away from the urban area and in the upwind direction of Dunhuang, and the primary components in Dunhuang were dominated by natural

mineral dust (Figure 2c).As shown in Figure 2a and 2b, the site in Wuwei and Zhangye are mainly agricultural fields with similar land surface type, with corn and cotton being the major crops. In general, agricultural and preparation activities were done in April, such as disking, tillage and seeding operations; thus, the local tropospheric aerosols in Wuwei and Zhangye were dominated by anthropogenic soil dust due to agricultural cultivation activityies (e.g., land planning, ploughing, and disking), especially during the floating dust period.. However, the sampling site in Dunhuang is located in Gobi Desert (GDD), ~35 km distantaway from the eastern edge of Kumtag Desert and in the upwind direction of Dunhuang City; there arewas not any significant anthropogenic pollution source around the mobile facility during the sampling period, and the primary components in Dunhuang were dominated by natural mineral dust (Figure 2c).

2.2 Instrumentation

During the 2014 dust field campaign, Automatic automatic measurements of ambient temperature (*T*), relative humidity (RH), pressure (*P*), wind direction (WD), and wind speed (WS) were automatically collectedmeasured with a Wweather Ttransmitter (model WXT 520, Vaisala Inc., Helsinki, Finland) at 1- min intervals based on the microphysical and optical parameters of aerosols described above. The aerosol optical and microphysical properties measured at these three sites consist of We also measured aerosol absorption coefficients (σ_{ap}), and total scattering coefficients (σ_{sp}) and backscattering coefficients (σ_{bsp}), mass concentrations, and aerosol number size distribution during the 2014 dust field campaign. Finally, all datasets measured during

this field campaign were adjusted to standard temperature and pressure conditions (STP; T=273.15 K, P=101.325 kPa),. in which 5 -min and hourly averaged data were used.

The wind direction datasets are associated with the aerosol absorption and scattering coefficients and can be used to determine the origins of natural and anthropogenic dust.

Figure 3a shows the ground-based mobile laboratory of SACOL used deployed in Dunhuang during the dust field campaign along the Hexi Corridor over Northwest northwestern China. The instruments were conducted in the container, whichwhere temperature was maintained at 20°C. To minimize local contaminations, a metal samplering inlet stack (10 cm in diameter) was installed at the top of the ground-based mobile laboratory (~6.5 m above the ground level). The airflow werewas splitedevided into several flows and supplied to different instruments, and the particle size cut measurements arewere obtained using 1 μm and 2.5 μm impactors for different instruments, which are shown in Figure 3b. All of the collectors were operated at 50 °C to dry the aerosols (i.e., to a relative humidity (RH) of less than 40%). For proper operation under the flow conditions in the present experiments, the internal plumbing of the commercial unit has to be modified once a week. Details of the most relevant instrument's accuracy for aerosol and dust measurements are given in Table 1. Finally, all datasets measured were adjusted to standard temperature and pressure conditions (STP; T=273.15 K, P=101.325 kPa), in which 5 min and hourly averaged data were used.

The mass concentration with the particle diameter (D_p) less than 2.5 μm ($PM_{2.5}$) of $PM_{2.5}$ was measured continuously using an ambient particulate monitor (model RP1400a,

R&P Corp., Albany, NY-, USA) with a flow rate of 16.7 L min^{-1} ~~R&P 1400a analyser~~, which is based on the principle of tapered element oscillating microbalance (TEOM) (Patashnick and Rupprecht, 1991), ~~with a flow rate of 16.7 L min^{-1}~~. We checked the main and auxiliary flow rates of TEOM monitor at least once a week, and the Teflon coated glass fiber filters must be exchanged before the filter loading percentage reaches 60% to ensure the validity of the data generated by the TEOM.

~~To compare the properties of coarse and fine mode particles, t~~Two integrating nephelometers (~~TSI M~~model 3563, TSI Inc., Shoreview, MN-, USA) with 1 μm and 2.5 μm impactors were also employed to measure the ~~back and aerosol~~ total scattering and back-scattering coefficients of aerosol particles ~~(σ_{sp}) and backscattering coefficients~~ at three wavelengths of 450, 550, and 700 nm; the detection limits ~~at these three wavelengthsof these instruments were~~are 0.44 ~~× 10~~ Mm^{-1}, 0.17 ~~× 10~~ Mm^{-1}, and 0.26 ~~× 10~~ Mm^{-1} (1 Mm^{-1} = 10^{-6} m^{-1}), respectively., ~~and t~~The nephelometers~~instruments had~~ has a signal-to-noise ratio (S: N) of 2:1 (Anderson et al., 1996; Shi et al., 2013). The two nephelometers were checked with internally filtered particle free air once a day and standard CO_2 every two days. CO_2 calibrations were performed before experiment or when CO_2 check error was greater than 5% (Anderson et al., 1996; Anderson and Ogren, 1998). Multiple calibrations following the manufacture's protocol were performed, and the instrument noise was periodically measured throughout this dust field campaign using an inline HEPA (High Efficiency Particulate Air) filter. The datasets collected by nephelometers were corrected for angular nonidealities, which will cause particle scattering in the near forward direction to be underestimated. For reducing and

quantifying the uncertainties in aerosol optical properties measured by the nephelometers, the data reduction and uncertainty analysis for the scattering datasets due to nonideal detection are processed followeing Anderson and Ogren (1998). Combining these errors could yielded a total uncertainty of ± 8% for a scattering coefficient of 30 Mm^{-1}.

Then, aA multi-angle absorption photometer (MAAP, model 5012, Thermo Scientific, Waltham, MA, USA) was used to determine themeasure aerosol absorption coefficients of $PM_{2.5}$ (σ_{ap}) at 670 637 nm (Müller et al., 2011). with a temporal resolution of 1 min. AThe detailed description of the MAAP could be found in the literatures (Petzold et al. 2002; Petzold and Schönlinner 2004).

The particle size distribution ranging from 0.5 –to 20 μm (52 channels) was measured using an aero-dynamical particle sizer (APS) spectrometer (APS model 3321, TSI Inc., Shoreview, MN, USA), assuming that all aerosols are homogeneous and spherical particles, despite the fact that the observed coarse mode dust particles exhibit non-spherical geometries (Mishchenko et al., 1995). Because of the high aerosol concentrations (i.e., exceeds 1000 cm^{-3}) when the extreme dust storm outbreak, two diluters (model 3302A, TSI Inc., Shoreview, MN USA) with dilution ratio of 20:1 and 100:1 were used on the top of the APS, and the data has taken account of the dilution ratios and particle loss due to the dilutor.

Although the singnalle particle soot photometer (SP2, DMT Inc., Boulder, CO, USA) iswas also used to measure the mass concentration and size distribution of black carbon (BC) in Zhangye from 9 to 28 April, 20174 during this dust field campaign, the datasets

measured by SP2 are used to analyze the mixing status of BC with the other aerosols during this dust field campaign ~~as~~in another manuscript (In preparation). A comparison of the BC mass concentration between SP2 and MAAP instruments is given in Figure S1 in the Supplement. The result indicates that the tendency of BC mass concentrations ~~are~~is much similar, but the values ~~of BC mass concentration~~ measured by MAAP was relatively larger than that measured by SP2. We note the relative large bias between MAAP and SP2 instruments may result from the size distribution of BC measured by using different sampler inlet impactors ~~for~~of 2.5 μm and 1 μm.

2.43 Data analysis methods

The mass absorption coefficient (MAC~~, hereinafter σ_{abs}~~) is a key parameter that can be used to attribute the light absorption of aerosols to BC and to understand its effects on climate. Some studies have attempted to perform this attribution based on the assumption of the wavelength dependence of absorption (e.g. Favez et al., 2009; Yang et al., 2009). Tthese values are calculated by assuming that the imaginary part of the complex refractive index ~~(RI)~~ of BC is independent of the wavelength (λ) and that the absorption cross-section of BC varies as λ^{-1}~~λ^{-1}~~ (Bond and Bergstrom, 2006). ~~The MAC values of BC span a wide range in the literature. For instance, the MAC of BC has been defined as 7.5 m^2 g^{-1} at 550 nm and 12–13 m^2 g^{-1} at ~350 nm (Adler et al., 2010);~~ A narrow range of BC for MAC~~σ_{abs}~~ (6.4–6.6 m^2 g^{-1}) was found to provide a good fit to urban particles collected by previous studies (Arnott et al., 2003; Bond and Bergstrom, 2006; Schwarz et al., 2008)., and ~~A~~a value of ~~σ_{abs} = 6.6 m^2 g^{-1}~~ is

currently used in the ~~instrument~~MAAP. To calculate the aerosol absorption coefficient (~~σ_{ap}~~) at 637 nm ~~(Müller et al., 2011)~~, the following equation is used:

$$\sigma_{ap} = MAC \times m_{BC} \quad (1)$$

where ~~$\alpha = 6.6\ m^2\ g^{-1}$ and~~ m_{BC} is the equivalent mass concentration of BC reported by the MAAP.

The backscattering fractions (b) is defined as the ratio of aerosol scattering in the backward hemisphere to the total scattering ($b = \sigma_{bsp}/\sigma_{sp}$), and related to particle size distribution. The wavelength-dependent variation of σ_{sp} is characterized by the scattering Ångström exponent (SAE, $Å_{sp}$), which is defined as:

$$Å_{sp}(\lambda_1/\lambda_2) = -\frac{\ln\left(\sigma_{sp,\lambda_1}/\sigma_{sp,\lambda_2}\right)}{\ln\left(\lambda_1/\lambda_2\right)} \quad (2)$$

where σ_{sp,λ_1} and σ_{sp,λ_2} are the aerosol scattering coefficients at wavelengths λ_1 and λ_2, respectively. In this paper, we calculated $Å_{sp}$ from 450 to 700 nm (i.e., from using the scattering coefficients measured by nephelometer at 450 ~~$\sigma_{sp,450}$~~ and 700 nm ~~$\sigma_{sp,700}$~~).

~~To calculate the single scattering albedo (ω) at 550 nm, we first adjust the σ_{ap} values from 670 to 550 nm; this equation is listed as follows:~~

~~$$\sigma_{ap,550} = \sigma_{ap,670} \times \left(\frac{\lambda_{670}}{\lambda_{550}}\right)^{AAE} \quad (3)$$~~

~~where λ is wavelength and the absorption Ångström exponent (AAE) corresponds to the λ^{-1} dependence of the absorption of BC, which is typically assumed to be AAE=1. However, we note that the actual AAE of BC can be greater or less than 1, as this value is highly dependent on the internal/external core size and its ageing process (Gyawali~~

~~et al., 2009).~~

The aerosol ~~single scattering albedo~~SSA is a key parameter that can be used to investigate the optical and microphysical properties of atmospheric aerosols (Haywood and Shine, 1995)~~.~~ ~~,~~ ~~The single scattering albedo is~~ which is defined as the ratio of the scattering coefficient to the total extinction coefficient (i.e., the sum of the scattering ~~+~~ and absorption coefficients). To calculate the ~~single scattering albedo~~SSA ~~(ω)~~ at 637 nm, we first interpolate~~adjust~~ the σ_{sp} values to 637 nm using the Ångström law:

$$\sigma_{sp,\,637} = \sigma_{sp,\,550} \times \left(\frac{637}{550}\right)^{-Å_{550\text{-}700}} \quad (3)$$

The SSA (ω) ~~single scattering albedo~~ at ~~550~~ 637 nm was then calculated using Eq. (4):

$$\omega_{637} = \frac{\sigma_{sp,\,637}}{\sigma_{ap,\,637} + \sigma_{sp,\,637}} \quad (4)$$

~~The parameter of m~~Mass scattering efficiency (MSE) is calculated as the slope of the reduced major axis (RMA) linear regression of $\sigma_{sp}^{2.5}$ and $PM_{2.5}$~~, which is calculated using Eq. (5)~~:

$$MSE = \frac{\sigma_{sp}^{2.5}}{PM_{2.5}} \quad (5)$$

where $\sigma_{sp}^{2.5}$ is the aerosol scattering coefficient at 550 nm and $PM_{2.5}$ is the mass concentration measured by TEOM~~ of atmospheric aerosols with size diameters of less than 2.5 μm.~~

In order to estimate the uncertainties of optical properties on our dust aerosol measurements during this dust field campaign, we performed a closure study to compare the $\sigma_{sp}^{2.5}$ measured by nephelometer associated with that calculated based on the particle number size distribution measurements using a modified Mie model. Computer programs based on the Mie theory (Mie, 1908) to calculate scattering of

particles are freely available (e.g., "BHCOAT ~~Model~~" ~~(~~, Bohren and Huffman, 1983~~)~~), and we used an implementation of these algorithms in MATLAB (Mathworks, MA, USA) functions (Mätzler, 2002). Mie scattering calculations of a single spherical particle require the aerosol number size distribution, the aerosol complex refractive index ($m = n+ki$) and the size parameter ($x = \pi D_p/\lambda$) as key input parameters. The scattering coefficients are calculated from the integration of the scattering efficiency (Q_{sp}) over the whole number- size distribution:

$$\sigma_{sp}(x,m) = \int_{D_p} Q_{sp}(x,m) \cdot \frac{\pi D_p^2}{4} \cdot N(\log D_p) \cdot d\log D_p \quad (6)$$

where D_p is the particle diameter, ~~λ is the wavelength of light,~~ and ~~n~~$N(\log D_p)$ represents number-size distribution measured by the APS. In this study, the real part of the refractive index (n) was assumed to be 1.53, which was widely~~often~~ used for mineral dust in literatures (Müller et al., 2009; McConnell et al., 2010); the imaginary part of the refractive index (k) was determined using Mie calculations. ~~The experimentalmeasured scattering values are compared to those calculated withusing Mie scattering theory forat the wavelength of 550nm in Figure 143 and Table 3.~~

3 Results

3.1 Temporal Variability ~~RegionalGeneral Statistics~~

Floating dust is generally defined as a weather phenomenon in which fine mode dust particles suspended in the lower troposphere under calm or low-wind condition, with horizontal visibility less than 10 km; while dust storm is that large quantities of dust particles lofted by strong winds, and horizontal visibility reduced to below 1 km.

(Wang et al., 2005; Wang et al., 2008). During this dust field campaign, ~~four~~ three floating dust episodes (which are shown as dotted boxes in Figure 4) occurred on 3–7 April in Wuwei and on 9–12~~, 14–15~~ and 25–28 April in Zhangye. We also observed the optical and microphysical properties of natural mineral dust during a heavy dust storm (shown as a solid box in Figure 4) from 23 to 25 April ~~2014~~ in Zhangye. Moreover, we identified five clear-sky days in Zhangye (16, 18, 19, 20 and 22 April) and ~~five~~three clear-sky days in Dunhuang (~~3, 10,~~ 11, 14~~,~~ and 15 May) as background weather conditions based on the manual weather recording and the abovementioned measurements. According to the land surface types shown in Figure 2, one of the major ~~aims~~ novelties of this study is to investigate the characteristics of anthropogenic and natural dust~~, which are present in~~ during floating dust ~~episodes~~ and dust storms~~,~~ episodes, respectively~~,~~ ~~and represent the fine mode soil dust that is produced by agricultural cultivations and the coarse mode mineral dust that originates from desert regions, respectively. Therefore, significant differences in the optical and microphysical properties of these aerosols were observed under different atmospheric conditions (e.g., dust storms, floating dust episodes and background conditions).~~

Figure 4 illustrates the temporal variations ~~in~~ of hourly averaged σ_{sp}, σ_{bsp}~~, ω b and MSE at 550 nm~~, σ_{ap} ~~and~~, b, ω ~~at 637 nm~~, as well as $Å_{sp}$~~,~~ ~~those in~~ MSE, ~~$Å_{sp}$ (calculated from 450 nm to 700 nm)~~ and aerosol size distribution in Wuwei, Zhangye, and Dunhuang in chronological order from 3 April to 16 May 2014. ~~These surveys were conducted in Wuwei, Zhangye, and Dunhuang in chronological order, as is illustrated in Figure 4.~~ Note that the time periods denoted in Figure 4 contain

some gaps due to the transportation of ground-based mobile facility or instrument problems. The statistical analyses of the optical parameters ~~measured during this dust field campaign~~ are also summarized in Table ~~1~~2. (~~h~~Hereinafter, these results are given as the mean ± the standard deviation of the ~~5-min~~hourly ~~–~~ averaged datasets~~)~~. Unless otherwise noted, all aerosol scattering measurements discussed here are for the wavelength of 550 nm.

Aerosol optical and microphysical properties are entirely different in these three sites. One of the most significant features in Figure 4a is that the variation of $\sigma_{sp}^{2.5}$ is highly consistent with that of $\sigma_{sp}^{1.0}$ during the whole period of field campaign; the backscatter coefficients shows the same trends with the total scattering coefficients but in a relatively small magnitude. The values of $\sigma_{sp}^{2.5}$ and $\sigma_{sp}^{1.0}$ are very close in Wuwei and Zhangye; however, the large differences observed in Dunhuang. It indicates that fine mode particles dominate the scattering coefficient in farmland regions, whereas coarse mode particles play a more important role in ~~closer to~~ the desert regions ~~of Dunhuang~~. ~~Meanwhile, the large standard deviations of are found in Wuwei and Zhangye, which are possibly attribute to frequent floating dust events and local anthropogenic emissions (Wang et al., 2008, 2015a). Meanwhile, the large standard deviations are found in Wuwei and Zhangye, which are possibly attribute to frequent floating dust events and local anthropogenic emissions (Wang et al., 2008, 2015).~~ Except for the values obtained during a heavy dust storm ~~in Zhangye~~, the ~~overall~~hourly mean $\sigma_{sp}^{2.5}$ ~~values measured at the wavelength of 550 nm using the nephelometer range from ~ 50~429~~ are 101 ± 37 Mm^{-1} and 84 ± 58 ~~~ 20~532~~ Mm^{-1} ~~at~~ at two anthropogenically influenced sites ~~of~~in

Wuwei and Zhangye, respectively; the corresponding $\sigma_{bsp}^{2.5}$ are 12.2 ± 4.4 Mm^{-1} and 9.5 ± 5.9 Mm^{-1}. By contrast, the much lower $\sigma_{sp}^{2.5}$ (54.0 ± 32.0 Mm^{-1}) and $\sigma_{bsp}^{2.5}$ (6.5 ± 3.7 Mm^{-1}) are measured in Dunhuang. Values for ~~. The *b* increased with the wavelengths due to decreasing size parameters. with the~~ $b_{2.5}$ ~~of~~are 0.121 ± 0.005 ~~and~~, 0.~~00~~115 ± 0.007 and 0.122 ± 0.005 in Wuwei, Zhangye, and Dunhuang, respectively, which are consistent with the result ~~from~~in Backgarden (0.124 ± 0.015; Garland et al., 2008), a rural site near the megacity Guangzhou in southeastern China~~, which can be compared to the σ_{ap} values at 637 nm of 9.7 ± 6.0~3.6–69 Mm^{-1} and 5.5 ± 3.8~1.3–64.5 Mm^{-1} measured at Wuwei and Zhangye, respectively.~~, but higher than those observed in Shouxian in eastern China (0.101 ± 0.017; Fan et al., 2010).

Meanwhile, the large standard deviations of $\sigma_{ap}^{2.5}$ are found in Wuwei and Zhangye, which are possibly attribute to frequent floating dust events and local anthropogenic emissions (Wang et al., 2008, 2015a). The lowest value of $\sigma_{ap}^{2.5}$~~σ_{ap}~~ ~~obtained~~ during the field campaign (~~i.e.,~~ 2.~~7~~ 3 ± ~~1.2~~0.9 Mm^{-1}) ~~was~~ are ~~collect~~ obtained~~measured~~ in Dunhuang, which can be compared with the relative higher σ_{ap} values of 9.7 ± 6.0 Mm^{-1} and 5.5 ± 3.8 Mm^{-1} in Wuwei and Zhangye, respectively. This observation reveals that natural mineral dust is still a weaker absorber than anthropogenic soil dust that has been mixed with air pollutants ~~(e.g., BC and OC)~~.

Compared with Figure ~~4a~~4b, Figure ~~4b~~ 4d indicates that the majority of ~~ω_{550}~~ω_{637} values are much higher in Dunhuang than ~~they are~~that in the other two sites~~:~~, where these values range from ~~0.80~~0.874 to 0.~~99~~986, with overall~~a~~ mean value of 0.~~95~~949 ± 0.020. Similar results were also found in other field campaigns in Zhangye

during the dust storm(ω_{550} of 0.95 ± 0.02; Li et al., 2010) and Yulin (ω_{530} of 0.95 ± 0.05; Xu et al., 2004) because of the presence of coarse mode particles. By contrastHowever, only 0.7 % and 21.9 % of the values of $\omega_{550}\omega_{637}$ reach up to 0.95 in Wuwei and Zhangye (except for the dust storm period, as shown in Figure 7), and their average $\omega_{550}\omega_{637}$ values are much lower (0.910.902 ± 0.0253 and 0.930.925 ± 0.040.034, respectively) and also exhibit larger variation than those in Dunhuang (0.949 ± 0.020). This phenomenon most likely indicates that natural dust aerosols are dominateddominanted in Dunhuang, since mineral dust scatters more and absorbs less than other atmospheric aerosols. Figure 4c 4e reveals that the $Å_{sp}$ values of aerosols with diameters of less than 1 μm ($Å_{sp}^{1.0}$) are much higher than those ofless than 2.5 μm ($Å_{sp}^{2.5}$) and that $Å_{sp}$ values decrease significantly from Wuwei to Dunhuang. The overall average MSE values in Wuwei, Zhangye and Dunhuang are 2.8 79 ± 0.57 $m^2 g^{-1}$, 2.21 ± 0.8 64 $m^2 g^{-1}$ and 1.55 ± 0.7 59 $m^2 g^{-1}$, respectively, whichwith 5-minhourly -averaged maximum values of 6.34.37 $m^2 g^{-1}$, 9.54.49 $m^2 g^{-1}$, and 8.53.57 $m^2 g^{-1}$, respectively. The higher MSE values in Wuwei and Zhangye reflect the fact that anthropogenic dust, which is influenced by local soil dust during floating dust episodes, scatters more solar radiation than natural dust (Figure 4d4f).

Aerosol size distribution (hereinafter defined as $dN/d\log D_p$) in the range of 0.5–5 μm areis also presented in Figure 4g, whichFigure 4e 4g indicates that fine mode particles (typically D_p < ~1 μm) that are less than 1 μm in diameter are dominant in Wuwei and Zhangye, except during a strong dust storm that occurred in Zhangye on 23–25 April 2014. Although tThe number concentration of coarsefine mode particles

(typically D_p > ~1 μm) is ~~also~~ higher than that of ~~coarse~~ fine mode particles in Dunhuang (calculated from the integral of the size distribution curve), this region yields hourly averaged number concentration of 7.2 cm^{-3} and 9.0 cm^{-3} for fine mode and coarse mode particles, respectively, with the average percentage of coarse mode particles relative to total atmospheric particles ~~is~~ of ~~55~~455%, which is higher than the relative percentages observed in Wuwei (~16 %) and Zhangye (~33 %) ~~(~16 % and ~33 %, respectively)~~.

On 23–25 April 2014, a severe dust storm occurred in Zhangye, along with a strong northerly wind. The ~~5-min~~hourly-averaged $\sigma_{sp}^{2.5}$ value ~~at 550 nm~~ increased remarkably from ~186 to ~~5813~~ 5074 Mm^{-1}, which is ~10 times higher than that measured in non-dust plume periods in Zhangye (~~532~~ 509 Mm^{-1}~~),~~); while the maximum value of $\sigma_{ap}^{2.5}$ ~~was~~ is ~~59~~37.6 Mm^{-1} during this dust storm, which is slightly ~~lower~~ higher than that measured during non-dust plume periods (~~64.5~~36.0 Mm^{-1}). Figures 4~~b~~d and ~~4c~~ 4e delineate~~indicate~~ that the peaks of ~~ω_{550}~~ω_{637} (> 0.99) ~~that are~~ associated with the ~~lowest~~ negative values of $Å_{sp}$ (< 0)– are close to those observed in another field campaign ~~that studied dust-dominant particles in~~ over ~~Northwestern~~ northwestern China (Li et al., 2010), which is possibly related to the reduce of anthropogenic emissions and the prevalence of coarse mode particles (Cermak et al., 2010). Figure ~~4e~~ 4g demonstrates that the values of aerosol number size distribution peaked at 1–3 μm. Simultaneously~~Meanwhile~~, the number concentration of coarse mode particles ~~(calculated from the integral of the size distribution curve) with diameters of 1~~0.5 5 μm ~~is~~ generally exceed~~higher than~~ ~~900~~ 300 cm^{-3} and even

approach 1200 cm^{-3}, which reveal~~indicate~~s that pure coarse mode particles from desert regions are dominant during the dust storm~~s in Zhangye~~. These results are consistent with those of a previous study, in which the aerosol diameter ~~(De)~~ of PM_{10} was determined to be larger during dust plume periods than it was during non-dust plume periods (Wang et al., 2010).

3.~~3~~2 Diurnal Variations

Here, we also present the diurnal cycles of $\sigma_{sp}^{2.5}$ ~~and~~, $\sigma_{sp}^{1.0}$ ~~at 550 nm~~, $\sigma_{ap}^{2.5}$ and ω_{637}~~at 637 nm, and ω_{550}~~, as well as those of ~~the~~ Å_{sp} and MSE values in Wuwei (red lines), Zhangye (black lines), and Dunhuang (blue lines) throughout the experiment~~these periods~~ (Figure 5). As shown in Figure 5a and 5b, the values of $\sigma_{sp}^{2.5}$, $\sigma_{sp}^{1.0}$ and $\sigma_{ap}^{2.5}$ ~~at 550 nm~~ present prominent bimodal distributions in Wuwei and Zhangye, which are consistent with the variations in ~~ω_{550}~~ω_{637} (Figure ~~5e~~5c)~~.~~. The maximal $\sigma_{ap}^{2.5}$ value (~16.8 Mm^{-1}) appeared at 08:00 LST (local standard time) in Wuwei, with two secondary peak values occurring at 21:00 (~20.2 Mm^{-1}) and 22:00 LST (~18.7 Mm^{-1}). Similarly, two comparable peaks of $\sigma_{ap}^{2.5}$ appeared at 08:00 (~12.2 Mm^{-1}) and 20:30 (~9.7 Mm^{-1}) LST in Zhangye. ~~Two comparable peaksThe highest higher values of $\sigma_{ap}^{2.5}$ appeared at ~08:00 and 20:30 LST (local standard time) in Wuwei and ~7:30 and 21:00 LSTIt is in Zhangye~~ indicate that not only anthropogenic mineral dust but also local air pollutants (e.g., BC and OC) were found in ~~these regions~~Wuwei and Zhangye; these pollutants likely originated from agricultural activities, biomass burning, and the burning of fossil fuels (e.g., domestic coal

combustion, diesel emissions from vehicles). The pronounced diurnal variations in these sites may also associated with the local meteorological elements (Arya, 1999). Compared with the lower ~~ω_{550}~~ω_{637} values that occurred at ~19:30–20:30~~87:00 30–08:30~~ (~0.880) and ~~20~~1907:30~~–20:30~~ LST (~0.864) ~~(local standard time)~~ in ~~Wuwei and Zhangye~~two ~~farmland sites~~Wuwei and Zhangye, respectively, the higher ω_{637} with ~~the presence of~~ only slight variations ~~in ω_{550} ω_{637}~~ in Dunhuang indicates that ~~coarse mode particles (e.g.,~~ natural dust aerosols~~)~~ are dominant near the dust source areas ~~in Dunhuang~~ (Figure 5e). Additionally, ~~a comparison of the $Å_{sp}$ values due to fine mode and coarse mode particles that are less than 1 μm and 2.5 μm in size, respectively, indicates that~~ there are large diurnal variations ~~in~~ of $Å_{sp}^{2.5}$ and $Å_{sp}^{1.0}$ in Wuwei, ranging from ~~1.00.5~~1.0–1.7 and ~1.~~8~~48–2.3, respectively~~:~~. ~~The~~ these lowest values ~~of $Å_{sp}^{2.5}$ and $Å_{sp}^{1.0}$~~ observed in Dunhuang ~~also suggest~~could partly support the conclusion that its atmospheric aerosols are dominated by pure coarse mode ~~–~~particles (Figure 5c~~–~~5d). ~~Another feature is that the $Å_{sp}^{1.0}$ value of fine mode particles is significantly higher than that of $Å_{sp}^{2.5}$.~~ Large diurnal variations in MSE are also found at all three sites; MSE values is the ~~are highest during the floating dust episodes in Wuwei and~~ lowest in Dunhuang because of the amounts of pure coarse mode particles ~~that are present during background surface condition~~near the source areas~~s in Dunhuang~~ (Figure 5f).

~~Diurnal variations in the aerosol number distribution (hereinafter defined as $dN/d\log D_p$) in the range of 0.5 μm $\leq D_p$ (particle diameter) $\leq$ 5 μm were also observed using the aerodynamic particle sizer (APS) instrument APS (Figure 6).~~ As is shown in

Figure 6a, the accumulated fine mode particles ~~(<1 μm)~~ increased in Wuwei, yielding a maximum number distribution concentration~~(calculated from the integral of the size distribution curve)~~ of more than ~~300~~ 100 cm^{-3} due to the frequent outbreaks of floating dust episodes that occurred ~~in Wuwei~~ on 3–7 April 2014. The similar pattern~~s~~ of fine mode particles is found in Zhangye, but with a slightly lower number distribution of fine mode particles (Figure 6b)~~,~~. We suggest that the fine mode particles represent the dominant contributions in Wuwei and Zhangye, which is due to the formation of local anthropogenic soil dust by agricultural cultivations. ~~However, large differences are found in Dunhuang because of its higher percentage of coarse mode particles relative to total atmospheric particles; this region yields 5-min~~hourly averaged number ~~concentration~~distribution ~~values of 203 ± 125~~407.2 ~~cm^{-3} and 234 ± 248~~889.0 ~~cm^{-3} for fine mode and coarse mode particles, respectively (Figure 6c).~~

Figure 7 shows the histograms of the single scattering albedo values ~~observed at 550 637 nm from 3 April to 16 May 2014~~in these three sites. During the floating dust period in Wuwei, the majority of the ~~ω_{550}~~ω_{637} values of fine mode particles that originated from anthropogenic soil dust range from ~0.900–0.~~93~~925; approximately 10~~%~~–20 % of those values range from ~0.~~88~~875–0.900 and ~0.~~93~~925–0.950. The overall range of ~~ω_{550}~~ω_{637} values observed in Zhangye is similar to that observed in Wuwei. The ~~ω_{550}~~ω_{637} values that range from ~0.900 ~~–~~–0.~~93~~–925 are 30 % higher than those in Zhangye. This result is consistent with that of Li et al. (2010), who noted that the SSA of a dust storm was approximately 0.98 for coarse mode particles, while lower SSA values (i.e., ranging from 0.89 to 0.91) were closely related to local air pollution. T~~his~~

~~observation indicates~~hus, we infer that the atmospheric aerosols in Wuwei and Zhangye not only include anthropogenic soil dust that is smaller than 1 μm but also have undergone mixing with air pollutants ~~(e.g., BC)~~ during their transportation from urban and industrial regions. ~~This result is consistent with that of Li et al. (2010), who noted that the SSA of a dust storm was approximately 0.98 for coarse mode particles, while lower SSA values (i.e., ranging from 0.89 to 0.91) were closely related to local air pollution. Thus, we infer that the occurrence of much lower $\omega_{550}\omega_{637}$ values in Wuwei and Zhangye than in Dunhuang is due to the mixing of anthropogenic pollutants with local mineral dust.~~ However, the ~~$\omega_{550}\omega_{637}$~~ values in Dunhuang range from ~0.~~93~~925–0.~~98~~975, with the majority of these values falling between ~0.950–0.~~98~~975 because of the high percentage of coarse mode particles. These results are consistent with that of a previous study, which indicated that the surface measurement of SSA for coarse mode particles from Saharan desert regions at 550 nm yielded a value of 0.97 $\pm$ 0.02 (Cattrall et al., 2003). ~~Additionally, the wind roses in Figure 8 can be used to provide further insights into the correlation between meteorology and the aerosol scattering (absorption) coefficients. The wind direction accompanying $\sigma_{sp}^{2.5}$ and $\sigma_{ap}^{2.5}$ at 550 nm most likely represents the emissions from both local sources and regional transport from remote regions.~~

3.43 Local Emission ~~Implications for Emission Inventories~~Sources ~~a~~Attribution

Additionally, the wind roses ~~in~~described in Figure 8 can be used to provide further

insights into the correlation between the meteorology and local emission sources~~the aerosol scattering (absorption) coefficients~~. The wind direction accompanying $\sigma_{sp}^{2.5}$ ~~at 550 nm~~ and $\sigma_{ap}^{2.5}$ ~~at 637 nm~~ most likely represents the emissions from both local sources and regional transport from remote regions. The dominant wind directions in these three sites ~~is~~ are generally more abundant to the west. Figure~~s~~ 8a ~~and 8b~~ indicate that the higher values of $\sigma_{sp}^{2.5}$ (> 160 Mm^{-1}) are found along with the south~~northwest~~ wind, which implies that dust particles are primarily generated from nearby farmlands~~,,~~; ~~and while~~ the majority of $\sigma_{ap}^{2.5}$ values are dominated by the southeast~~east~~ wind because of the emissions of anthropogenic pollutants from the ~~city centre of Wuwei~~Huangyang Town. ~~However, t~~The fact that the highest values of $\sigma_{sp}^{2.5}$ (> 140 Mm^{-1}) and $\sigma_{ap}^{2.5}$ (> 12 Mm^{-1}) are associated with the west~~ern~~ wind in Zhangye most likely indicates that ~~these emissions originate from both~~ anthropogenic soil dust ~~and~~ mixed with local air pollutants from their upwelling residences~~regions~~ (Figure 8c and 8d). However, both $\sigma_{sp}^{2.5}$ and $\sigma_{ap}^{2.5}$ ~~were~~ are probably influenced by coarse mode mineral dust origin from desert areas due to the prevalent~~presence of~~ northwest wind in Dunhuang (Figure 8e and 8f).

MSE is a key parameter that can be used to estimate the radiative forcing effects due to atmospheric particles on global climate. Therefore, several studies have been performed to determine the optical properties of aerosols using MSE values (Laing et al., 2016). For instance, Hand and Malm (2007) noted that the MSE is mainly dependent

on particle composition (e.g., the particle refractive index and aerosol size distribution). As shown in Figure 9a, coarse mode particles have significantly higher ω_{637}~~$_{550}$~~ (> 0.~~93~~93) and lower MSE (1 < MSE < 2) values because of the presence of natural mineral dust under background weather condition~~s~~ in Dunhuang. However, there appears to be no clear difference between the ~~ω_{550}~~ω_{637} and MSE values due to floating dust periods in Wuwei and Zhangye. The presence of lower ~~and higher~~ MSE ~~values~~ in Wuwei and ~~and~~ higher values in Zhangye~~, respectively~~, suggests that fine mode particles can not only be attributed to floating dust periods (due to local soil dust) but also include BC, OC and other air pollutants that originated from the burning of biomass and fossil fuels. For instance, the large variations in ~~ω_{550}~~ω_{637} ~~(~0.7182–0.95 and ~0.6875–0.9998, respectively)~~ and MSE ~~(~0.91.9–6.34.4 $m^2 g^{-1}$ and ~0.493–94.5 $m^2 g^{-1}$, respectively)~~ observed in Wuwei and Zhangye are consistent with values that were previously measured during dust storms or biomass burning events (Li et al., 2010; Laing et al., 2016). Another notable feature is the remarkable discrepancy between the optical properties of aerosols for a given type of aerosol with diameters of less than 1 μm and 2.5 μm. Although the values of $\sigma_{sp}^{1.0}$ measured during this dust field campaign are only slightly lower than those of $\sigma_{sp}^{2.5}$ (as is indicated in Figures 9b and 9c), the $Å_{sp}^{1.0}$ values range from ~1.~~1~~4–2.~~4~~3 (mean: 2.1) for fine mode particles because of floating dust episodes in Wuwei, compared to the values of $Å_{sp}^{2.5}$ range from ~0.~~2~~5–1.7 (mean: 1.3) observed during the same period in Wuwei. Similar results are also found at the other two sites in Zhangye and Dunhuang.

~~The microphysical and optical properties of aerosols observed during this dust field~~

campaign are summarized in Figure 10. The boxes and whiskers denote the 10th, 25th, median, 75th, and 90th percentiles of the data, with dots marking their average values. We determined that the values of both σ_{sp} and σ_{ap} at 550 nm and σ_{ap} at 637 nm are higher in Wuwei during floating dust episodes than that in Zhangye and Dunhuang during background conditions. The average values of $\sigma_{sp}^{1.0}$, and, $\sigma_{sp}^{2.5}$, and $\sigma_{ap}^{2.5}$ measured at 550 nm, and $\sigma_{ap}^{2.5}$ at 637 nm during this field campaign in Wuwei are 75 744 ± 29 27 Mm^{-1}, 102 101 ± 40 37 Mm^{-1}, and 11.59.7 7 ± 7.86.4 Mm^{-1}, respectively. The 90th percentage of $\sigma_{sp}^{2.5}$ in Zhangye is due to the dust storm that occurred on 23–25 April 2014. However, the highest $\omega_{550}\omega_{637}$ value is found in Dunhuang and is due to the presence of coarse mode particles during background conditions. We note that there are large differences in $Å_{sp}Å_{sp}$ between fine mode and coarse mode particles. The average values of $Å_{sp}^{2.5}$ and $Å_{sp}^{1.0}$ are 1.3 ± 0.3 and 2.1 ± 0.2 during floating dust episodes in Wuwei, respectively, whereas those in Dunhuang are 0.5 ± 0.3 and 0.9 ± 0.4, respectively. The highest MSE in Wuwei and the lowest MSE in Dunhuang indicate that fine mode mineral dust particles scatter more solar radiation than coarse mode particles.

3.54 Case study

Aerosol optical depth (AOD) is a major optical parameter for aerosol particles and is a key factor affecting global climate (Holben et al., 1991, 2001, 2006; Srivastava and Bhardwaj, 2014). AOD can not only represent local air pollution but can also be used to observe dust storms. For instance, Dubovik et al. (2002) demonstrated that non-

spherical mineral dust can be retrieved using the assumption of spherical aerosols for high aerosol loading (AOD >0.5, Å <0.7) in desert regions due to dust events. Figure ~~11~~ 10 illustrates the spatial distribution of deep blue AOD at 550 nm in East Asia retrieved using ~~Terra~~ Terra-MODIS during a heavy dust storm over northern China on 24 April 2014. During this dust storm, the spatial distribution of high aerosol loadings with AOD values of >1.6 over ~~Northwest~~ northwest China was observed; in this distribution, the transport of natural mineral dust from the Taklimakan Desert to the downwelling regions over China can be clearly seen. The most prominent feature in Figure ~~12~~ 11 is that $\sigma_{sp}^{2.5}$ reaches its peak value ~~from ~209~~ 186 ~~Mm^{-1} to~~of ~~5813~~ 5074 Mm^{-1} and that a strong relationship (R^2 = 0.~~91~~9093) existed between $\sigma_{sp}^{2.5}$ and $\sigma_{ap}^{2.5}$ during the dust storm ~~on 23–25 April 2014~~. However, the values of $\sigma_{ap}^{2.5}$ observed during the dust storm are consistent with those measured during floating dust episodes in Wuwei and Zhangye. Therefore, we note that large differences in $\sigma_{sp}^{2.5}$ ~~are found~~ between natural mineral dust and anthropogenic ~~mineral~~ soil dust because of the presence of fine mode particles during floating dust episodes and coarse mode particles ~~during floating dust episodes and~~ during dust storms~~, but that they record similar ranges of $\sigma_{ap}^{2.5}$~~. We also observed the lowest values of $\sigma_{ap}^{2.5}$ and $\sigma_{sp}^{2.5}$ (which range from ~~0.9~~1.2–~~13.1~~7.9 Mm^{-1} and ~~14~~16–~~264~~224 Mm^{-1}, respectively) in Dunhuang ~~on 3–16 May~~, which indicates that natural mineral dust represents the dominant particles under the background conditions. ~~The observed higher $\sigma_{ap}^{2.5}$ and lower $\sigma_{sp}^{2.5}$ values in Wuwei and Zhangye during floating dust episodes suggest that fine mode anthropogenic dust particles were dominant in Wuwei and Zhuangye during floating dust episodes, in~~

~~contrast to the coarse mode particles observed during the dust storm in Dunhuang~~Zhangye~~.~~

Figure ~~13~~ 12 shows the average aerosol number size distribution observed under different weather conditions ~~using the APS instrument~~ during this field campaign. These data clearly show that the dominant particles during the dust storm in Zhangye are coarse mode particles ranging in size from 1 μm to ~~5~~ 5 μm, which peaked at 1.60 μm ~~reach~~ with a maximum dN/dlogD_p value of ~~~~596~~ 590 cm^{-3} ~~at a size of 1.60 μm~~. Compared with dust storms, the ~~value of~~ dN/dlogD_p reaches a peak with values of ~~~~335~~ 336 cm^{-3} and ~~~~345~~ 332 cm^{-3} at 0.67 μm during typical floating dust episodes on 4–7 in Wuwei and 9–~~15~~ 12 April in Zhangye ~~2014~~, respectively. This observation indicates that fine mode anthropogenic soil dust mixed with local air pollutants was dominant during these two floating dust episodes ~~on 3–7 and 9–15 April 2014 in Wuwei and Zhangye~~. However, another floating dust episode that occurred in Zhangye reveals a bimodal variation, ~~of dN/dlogD_p~~ which peaked at 0.67 μm and 1.49 μm. It also should be noted that the lowest value of dN/dlogD_p for fine mode particles was observed in Dunhuang ~~because of~~under the background weather condition~~s~~. These results are very close to those of previous studies that stated that atmospheric particles were dominated by both anthropogenic soil dust and air pollutants during floating dust episodes; however, the amount of coarse mode particles increased sharply during natural dust storms that originated from dust source regions (Wang et al., 2010; Li et al., 2010).

The gravimetric density of fine mode particles is reported to range from 1.00–2.00 g cm^{-3}, with an average value of 1.5 g cm^{-3} (Sloane et al., 1991; Seinfeld and Pandis,

1998). In this study, the gravimetric density of fine mode mineral dust particles was estimated by using the integrated volume concentrations measuredmeasurcalculated by APS data instrument and the mass concentration of $PM_{2.5}$ measured by TEOM. As shown in Figure S2 and Table 3, we found that the gravimetric density of dust particles is in the range of 1.04 ± 0.17 g cm^{-3} ~ to 1.64 ± 0.50 g cm^{-3}, and there is no evidence of significant differences of the dust gravimetric density during floating dust and dust storm episodes.

Then, the volume-weighted mean diameters (VMD) under the diameter of 2.5 μm and 1.0 μm wasare also calculated by using the integrated number size distribution of APS data (DeCarlo et al., 20045) datainstrument. We found that the $VMD_{2.5}$ and $Å_{sp}^{2.5}$ wasare correlated well during the whole dust field campaign (Figure S3 in Supplement). However, there is no significant linear correlation between $VMD_{1.0}$ and $Å_{sp}^{1.0}$. The highly possible explanation is that the $VMD_{1.0}$ is calculated based on the aerosol size diameter ranging from ~0.5 to 1 μm measured by APS, while the variation of $Å_{sp}^{1.0}$ is affected by the aerosol diameter under 1 μm.

Finally, we use the Mie theory and the aerosol number size distribution measured by APS to estimate the scattering coefficient compared with that derived by the nephelometer. As shown in Figure 143, the Mie-calculated scattering coefficient ($\sigma_{sp,\,Mie}$) and the measured scattering coefficient ($\sigma_{sp,\,neph}^{2.5}$) of 550 nm wereare highly correlated. For instance, the imaginary part of the refractive index (0.001) for natural dust during dust storm in Zhangye and the background weather condition in Dunhuang are similar to the result of SAMUM-1 in Saharan (Müller et al., 2009b). However, the

higher value of imaginary part (~0.01–0.08) during floating dust reflects inherently more anthropogenic dust particles, which can absorb more solar radiation than that during dust storm. Based on the Mie calculation in this study, the $PM_{2.5}$ scattering fraction, which defined as the contribution of ~~natural~~ the light scattering ~~for~~of $PM_{2.5}$ to the total scattering (the calculated scattering coefficient in the size range of 0.5–20 μm), is ~36.4 % during dust storm, while is in the range of ~37.9–85.1 % during floating dust episode. Detailed information of Mie-calculated and measured scattering coefficient is summarized in Table 3. Comparisons between $\sigma_{sp,\ Mie}$ ~~measured~~ and $\sigma_{sp,\ neph}$ ~~calculated $\sigma_{sp}^{2.5}$~~ ~~was~~were carried out taking into account the uncertainties of the measurements and the calculations. The $\sigma_{sp,\ Mie}^{2.5}$ ~~calculated of $\sigma_{sp}^{2.5}$~~ is ~6.6% ~~low~~higher than $\sigma_{sp,\ neph}^{2.5}$ ~~that measured by the TSI 3563 nephelometer~~ during dust storm, while ~16.5% ~~high~~lower than that during floating dust from 9 to 12 April. Generally, most of the $\sigma_{sp,\ Mie}^{2.5}$ ~~measured $\sigma_{sp}^{2.5}$~~ agree well with $\sigma_{sp,\ neph}^{2.5}$ ~~the values calculated with the Mie calculation~~, which can reflect a good quality of the datasets of $\sigma_{sp}^{2.5}$ during this dust field campaign.

4 Conclusions

~~To determine the optical and microphysical properties of atmospheric particles in anthropogenic soil dust and natural mineral dust, a ground-based mobile laboratory was deployed near the dust source regions along the Hexi Corridor over Northwest China from 3 April to 16 May 2014. Two of the sampling sites were located in farmland areas~~

~~in Wuwei and Zhangye, and the other site was located near the edge of the Gobi Desert in Dunhuang. Therefore, the land surface types in Wuwei and Zhangye represent anthropogenic soil dust generated by human activities (e.g., ploughing, coal combustion from domestic use, and biomass burning), while the land surface type in Dunhuang represents mineral dust.~~ This study is novel in that we not only captured natural mineral dust near the desert regions but also characterized the properties of anthropogenic soil dust produced by agricultural cultivations, especially during floating dust episodes. ~~During this dust field experiment, which was performed from April to May 2014, four floating dust episodes and one dust storm episode were observed in Wuwei and Zhangye. There are two major findings observed in this study.~~ The most prominent conclusion is that there are significant differences in the optical and microphysical properties of aerosols between anthropogenic soil dust and natural mineral dust under different atmospheric conditions (e.g., dust storm~~s~~, floating dust episodes and background conditions). During the floating dust period in Wuweis ~~in Zhangye~~ (i.e., 3–~~79–12, 14–15, 25–28~~ April), ~~For instance, t~~The average values of $\sigma_{sp}^{2.5}$ ~~at 550 nm~~, $\sigma_{bsp}^{2.5}$, $\sigma_{ap}^{2.5}$, ~~and~~ ω_{550637} ~~at 550 nm at 637 nm~~, $Å_{sp}^{2.5}$, and MSE ~~and $dN/d\log D_p$~~ are 102 ± 37 Mm^{-1}, 12.2 ± 4.4 Mm^{-1}, 9.7 ± 6.1 Mm^{-1}, 0.902 ± 0.025, 1.28 ± 0.27 and 2.79 ± 0.57 $m^2 g^{-1}$, respectively; during two floating dust periods in Zhangye (i.e., 9–12 and 25–28 April), the corresponding values are ~~183–1185~~ ± ~~6436~~ Mm^{-1}, 12.1 ± 4.2 Mm^{-1}, 6.~~9~~ ~~84~~ ± ~~3.74~~.0 Mm^{-1}, 0.935 ± 0.030~~0.91~~, ~~0.90.81~~73 ± 0.59~~7~~, and 2.~~4~~ ~~3~~24 ± 0.57 $m^2 g^{-1}$ and 2072~~±~~ 795 ~~cm^{-3}~~, respectively~~, during floating dust periods in Zhangye (i.e., 9–12, 14–15, 25–28 April);~~ whereas these values are sequentially ~~1108–~~1088 ± 991 Mm^{-1},

114.6 ± 101.6 Mm^{-1}, 13.510.6 ± 7.6 Mm^{-1}, 0.99989 ± 0.004, –0.02014 ± 0.018 , and 1.73 ± 0.20 $m^2 g^{-1}$, and 9923±2698 cm^{-3}, respectively, during dust storms in Zhangye (i.e., 23–25 April). The number concentrations size distribution ($dN/d\log D_p$) of coarse mode particles with diameters of 1–5 3 μm can reach a peak of ~900 590 cm^{-3}, which reveals that pure coarse mode particles from desert regions were dominant during dust storms in Zhangye. However, the overall variations ofin ω_{637} ω_{550}, which ranges from ~0.7182 to 0.95 and ~0.6483 to 0.98 during floating dust episodes in Wuwei and Zhangye, respectively, indicate that atmospheric aerosols not only include anthropogenic soil dust that is smaller than 1 μm but has also undergone mixing with air pollutants (e.g., BC) because of their transportation from urban and industrial regions. In addition to the large discrepancies between fine mode and coarse mode particles observed under different weather conditions, there are also significant differences between the optical and microphysical properties of the given atmospheric particles that are smaller than 1 μm and 2.5 μm. We note that the values of $\sigma_{sp}^{1.0}$ (75 74 ± 29 27 Mm^{-1}) are only slightly lower than those of $\sigma_{sp}^{2.5}$ (102 101 ± 40 37 Mm^{-1}) that are observed in Wuwei. However, there are significant differences between the values of $Å_{sp}^{1.0}$ and $Å_{sp}^{2.5}$, which range from ~1.1–2.4 (mean: 2.1) and ~0.2–1.7 (mean: 1.3)are 2.1 ± 0.2 and 1.3 ± 0.3, respectively, because of the occurrence of floating dust episodes in Wuwei.

By We usinged a modified Mie theory and the aerosol number size distribution measured by APS to estimate the scattering coefficients. The imaginary parts of the refractive indexes (0.0010) fuor natural dust during dust storm in Zhangye and the

background weather condition in Dunhuang are 0.001, while the higher value of imaginary part (0.01–0.08) during floating dust reflects inherently more anthropogenic dust particles, which reflects ~~During the heavy dust storms studied here, atmospheric aerosols sharply increased because of the addition of coarse mode particles ranging in diameter from 1–5 μm. The maximum dN/dlogD_p value for coarse mode particles reached 596 cm^{-3} at 1.60 μm, which is 5 times higher than that observed at the same site under background weather conditions. However, dN/dlogD_p reached its peak values of 335 cm^{-3} and 345 cm^{-3} for fine mode particles at 0.67 μm during floating dust events in Wuwei and Zhangye, respectively. These results indicate~~ that these atmospheric aerosols during this dust field campaign not only were dominated by anthropogenic soil dust produced by agricultural cultivations in ~~Zhangye~~Wuwei and ~~Linze~~Zhangye, but also underwent ~~mixing with local air pollutants because of the burning of biomass and coal~~natural mineral dust originated from the dust source regions over northwestern China. ~~These results are very similar to those of previous studies, which indicated that atmospheric particles were dominated by both anthropogenic soil dust and air pollutants during floating dust events but that natural mineral dust due to dust storms originated from dust source regions.~~

5 Data availability

All data sets and codes used to produce this study can be obtained by contacting Xin Wang (wxin@lzu.edu.cn). The MODIS data used in this study are available at Aerosol Product, https://modis.gsfc.nasa.gov/data/dataprod/mod04.php.

Competing interests. The authors declare that they have no conflict of interest.

Acknowledgements. This research was supported by the Foundation for Innovative Research Groups of the National Science Foundation of China (41521004), the National Science Foundation of China under Grant (41775144 and 41522505)~~, and the Fundamental Research Funds for the Central Universities (lzujbky-2015-k01 and lzujbky-2016-k06)~~. The MODIS data were obtained from the NASA Earth Observing System Data and Information System.

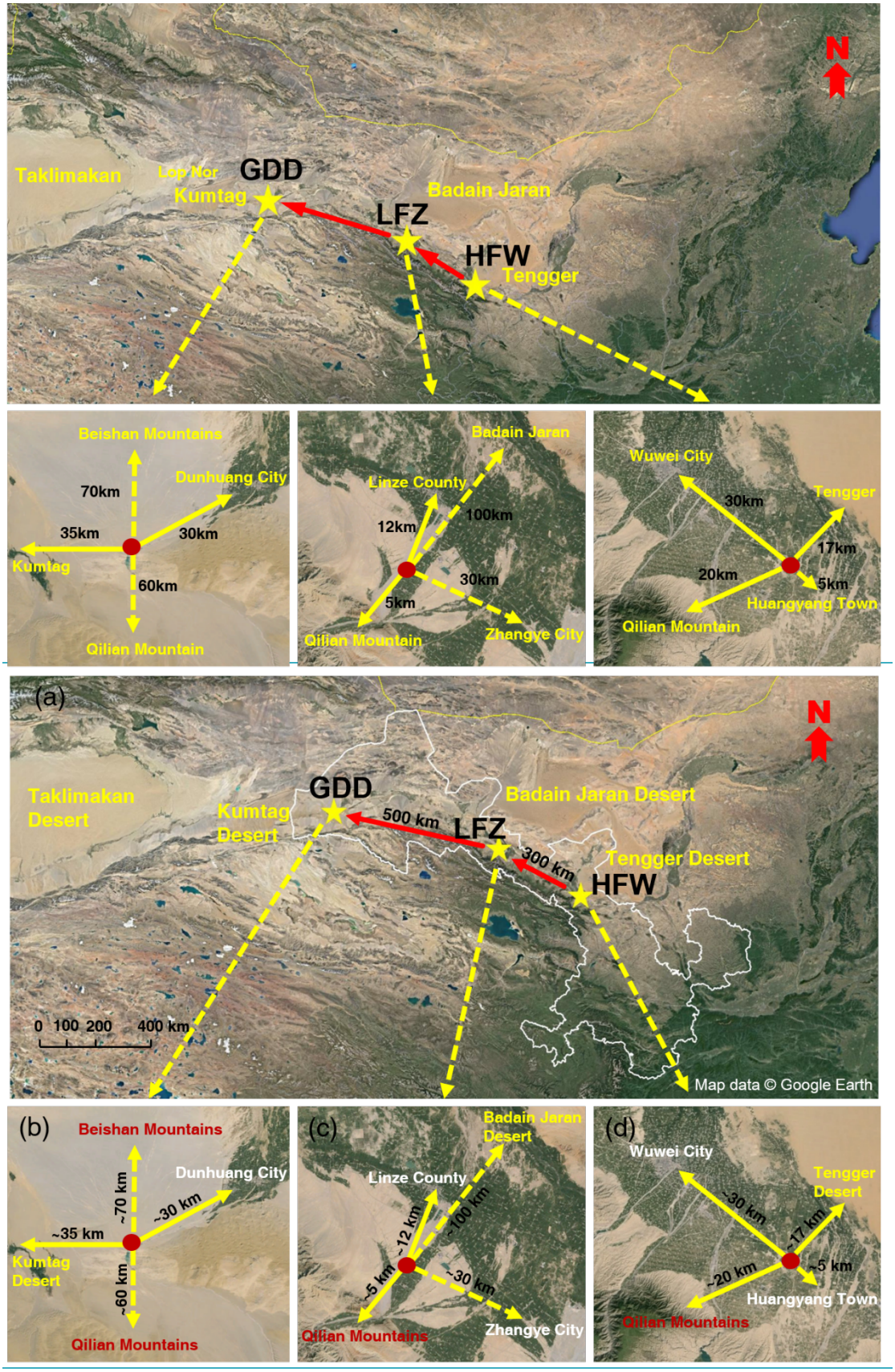

Figure 1. (a) The sampling locations of ground-based mobile laboratory and their

surrounding areas near dust source regions during the 2014 dust field campaigns at **(~~a~~b)** Gobi Desert in Dunhuang (GDD, 39.96°N, 94.33°E; 1367 m a.s.l.)~~Huangyang Farmland in Wuwei (HFW, 37.72°N, 102.89°E; 1691 m a.s.l.)~~, **(~~b~~c)** Linze Farmland in Zhangye (LFZ, 39.04°N, 100.12°E; 1578 m a.s.l.) and **(~~c~~d)** ~~Gobi Desert in Dunhuang (GDD, 39.96°N, 94.33°E; 1367 m a.s.l.)~~ Huangyang Farmland in Wuwei (HFW, 37.72°N, 102.89°E; 1691 m a.s.l.).

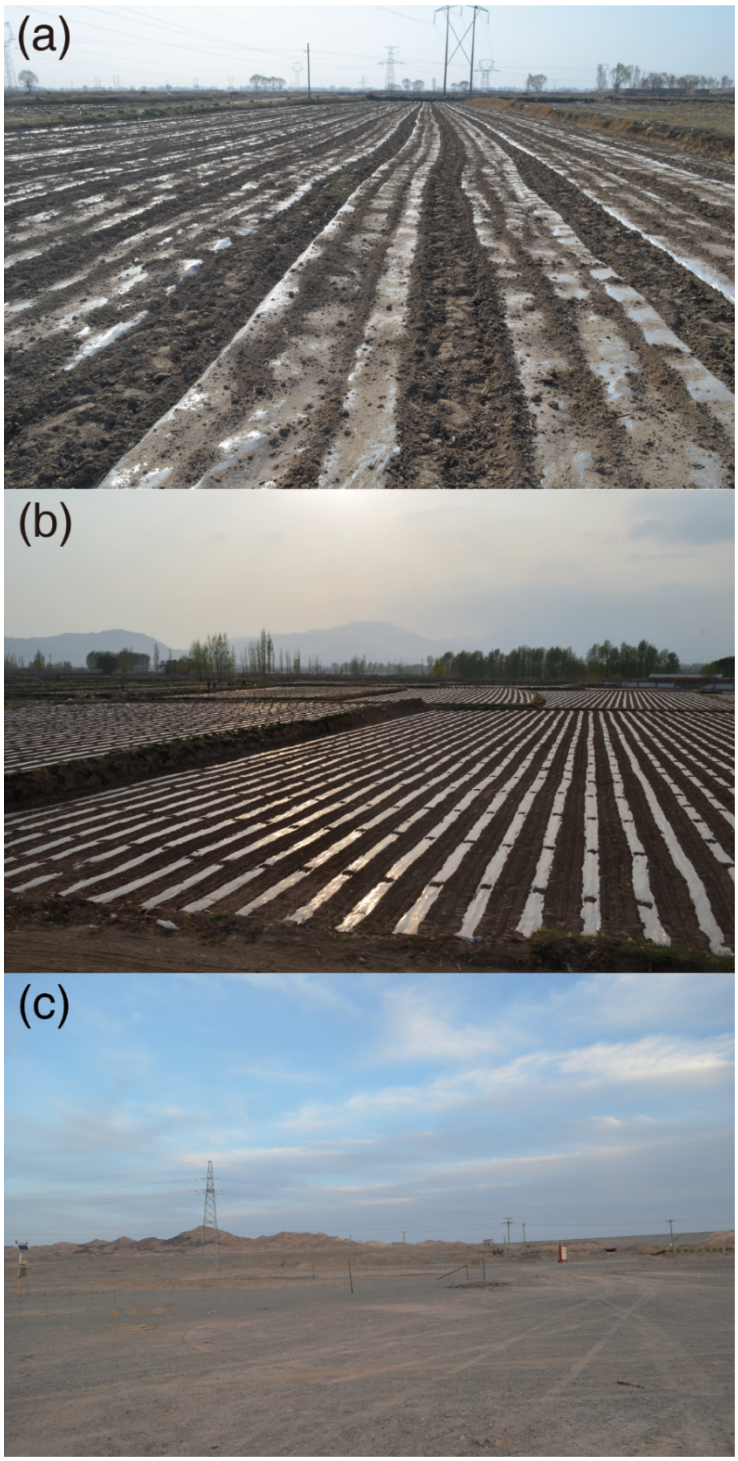

Figure 2. Same as **Figure 1** but for land surface conditions at **(a)** Huangyang Farmland in Wuwei (HFW), **(b)** Linze Farmland in Zhangye (LFZ), and **(c)** Gobi Desert in Dunhuang (GDD).

(a)

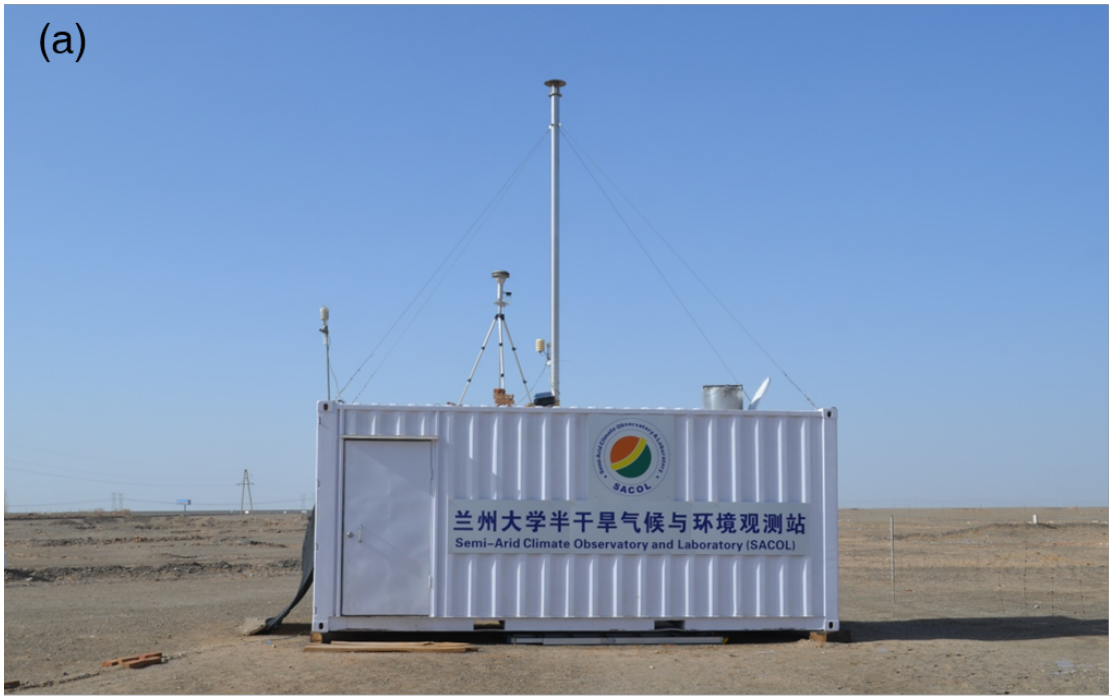
SACOL
兰州大学半干旱气候与环境观测站
Semi-Arid Climate Observatory and Laboratory (SACOL)

(b)

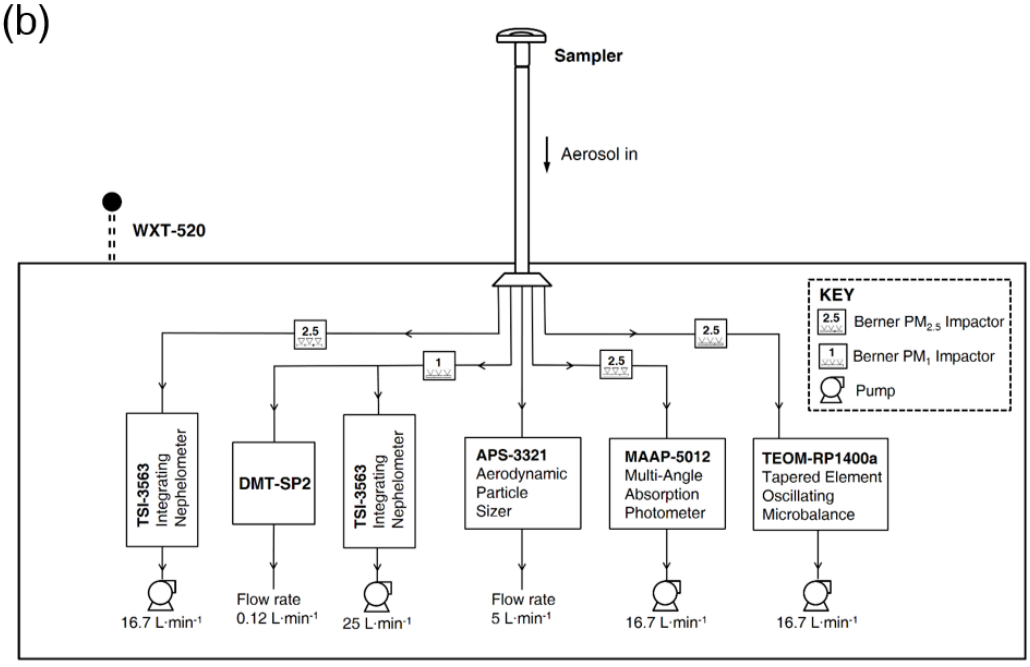
Sampler
Aerosol in
WXT-520
KEY
2.5 Berner PM2.5 Impactor
1 Berner PM1 Impactor
Pump
TSI-3563 Integrating Nephelometer
DMT-SP2
TSI-3563 Integrating Nephelometer
APS-3321 Aerodynamic Particle Sizer
MAAP-5012 Multi-Angle Absorption Photometer
TEOM-RP1400a Tapered Element Oscillating Microbalance
16.7 L·min-1
Flow rate 0.12 L·min-1
25 L·min-1
Flow rate 5 L·min-1
16.7 L·min-1
16.7 L·min-1

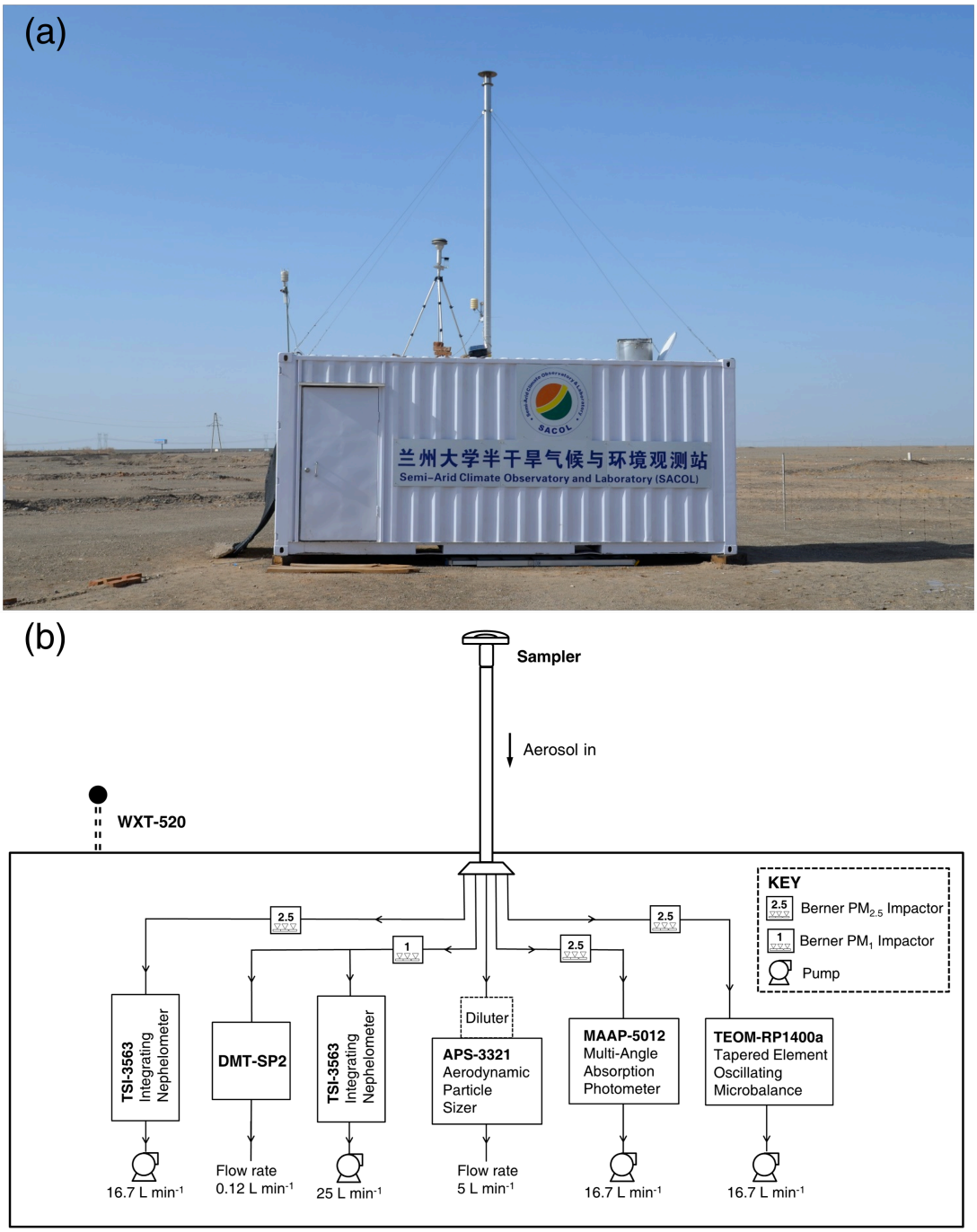

Figure 3. (a) The ground-based mobile laboratory in Dunhuang and **(b)** the schematic diagram of the ensemble instrumentation system.

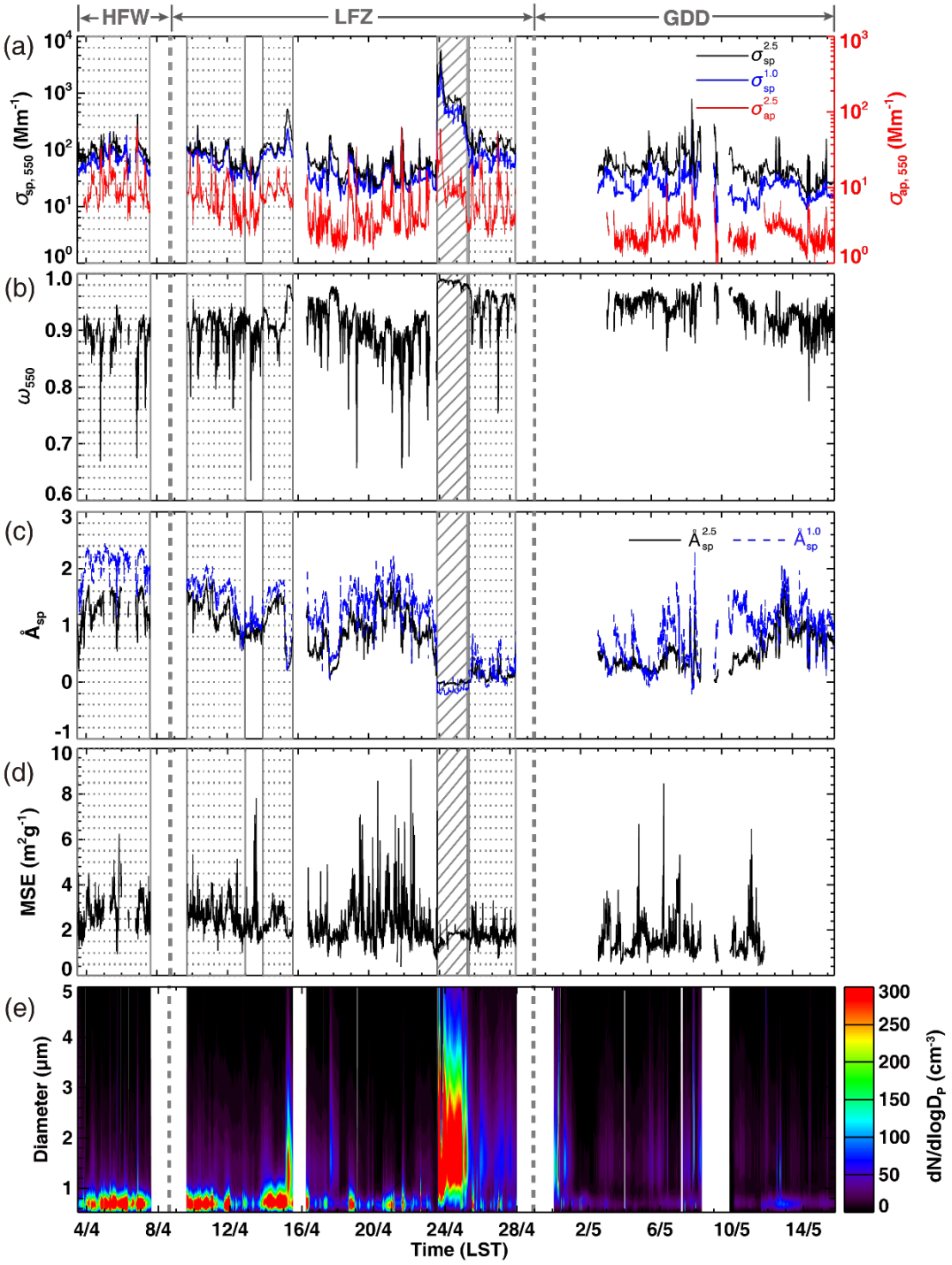
HFW
LFZ
GDD
(a)
$\sigma_{sp,550}$ (Mm^{-1})
$\sigma_{ap,550}$ (Mm^{-1})
$\sigma_{sp}^{2.5}$
$\sigma_{sp}^{1.0}$
$\sigma_{ap}^{2.5}$
(b)
ω_{550}
(c)
Å$_{sp}$
Å$_{sp}^{2.5}$
Å$_{sp}^{1.0}$
(d)
MSE (m^{2}g^{-1})
(e)
Diameter (μm)
dN/dlogD$_P$ (cm^{-3})
4/4
8/4
12/4
16/4
20/4
24/4
28/4
2/5
6/5
10/5
14/5
Time (LST)

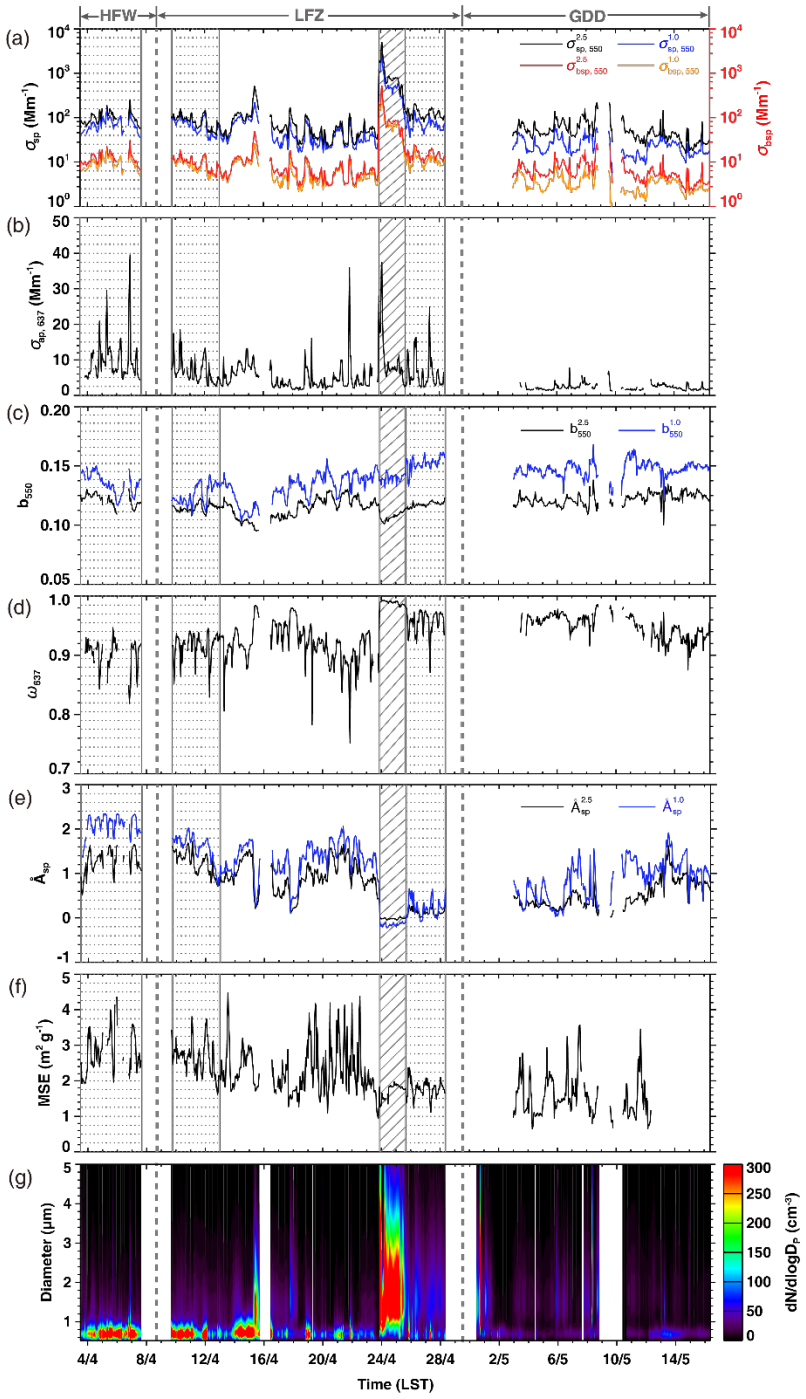

Figure 4. Temporal variations ~~in~~ of hourly ~~-~~averaged **(a)** aerosol scattering ~~(absorption)~~ coefficient at 550 nm and absorption coefficient at 637nm, **(b)** the backscattering fractions at 550 nm **(~~b~~c)** single scattering albedo at ~~550~~ 637 nm, **(~~c~~d)** scattering Ångström exponent (calculated from 450 nm to 700 nm), **(~~d~~e)** mass scattering efficiency (MSE) of $PM_{2.5}$ at 550 nm, and **(~~e~~f)** aerosol size distribution ($dN/d\log D_p$ ~~$dN/d\log D_p$~~, 0.5 μm < D_p ~~D_p~~ < 5 μm) during the entire period from 3 April to 16 May 2014. The shaded box represents a strong dust storm that occurred in Zhangye, and the dotted boxes represent ~~four~~ three floating dust episodes that occurred in Wuwei and

Zhangye.

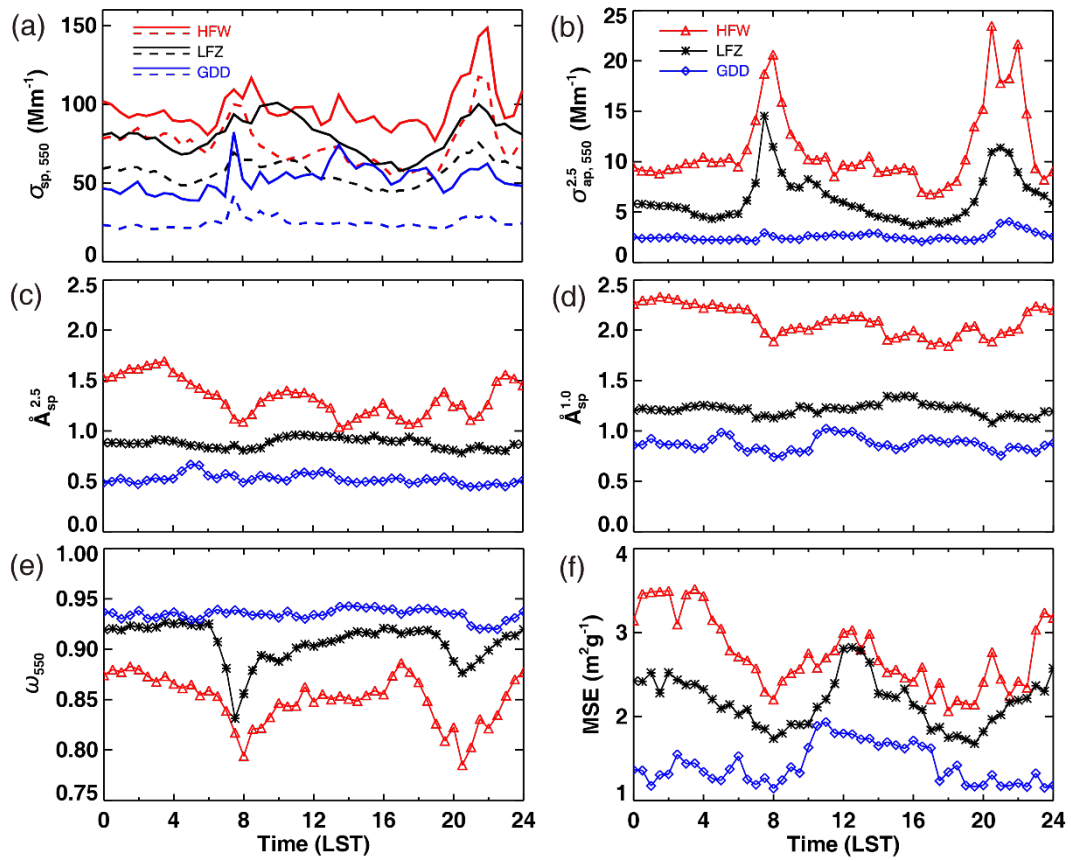
(a)
HFW
LFZ
GDD
$\sigma_{sp,550}$ (Mm^{-1})
(b)
$\sigma^{2.5}_{ap,550}$ (Mm^{-1})
(c)
$Å^{2.5}_{sp}$
(d)
$Å^{1.0}_{sp}$
(e)
ω_{550}
(f)
MSE (m^{2}g^{-1})
Time (LST)
Time (LST)

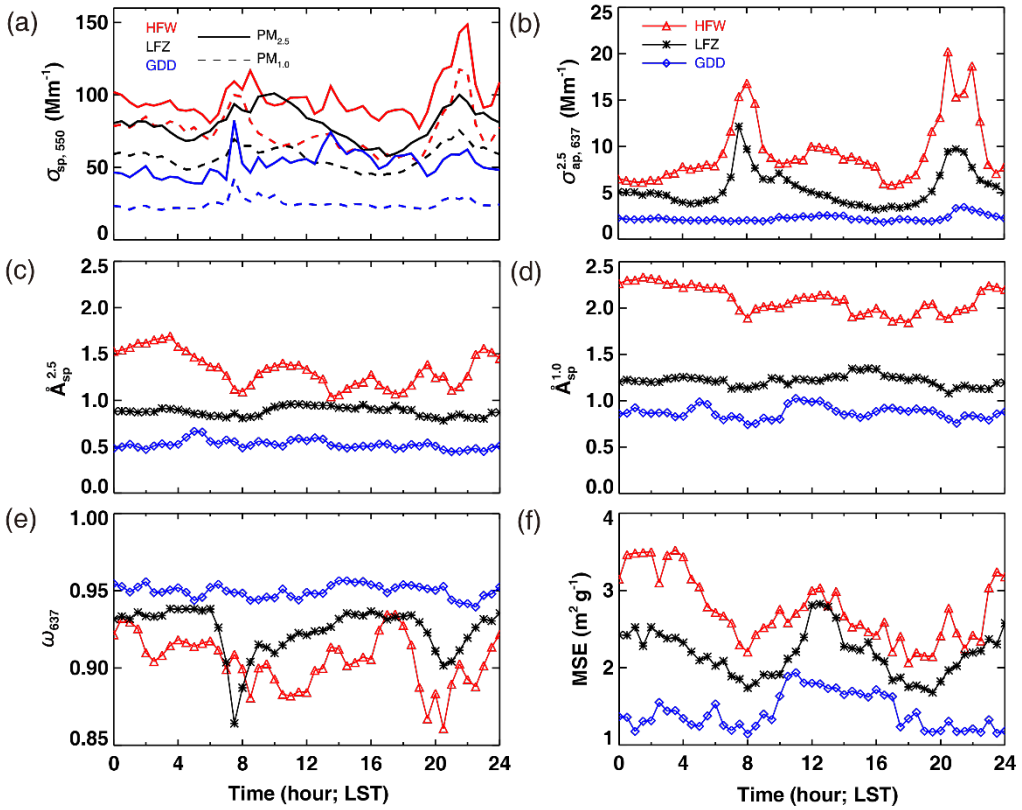

Figure 5. Diurnal variations in **(a)** aerosol scattering coefficient at 550 nm, where solid lines represent the variations ~~in~~ of $PM_{2.5}$ and dotted lines represent the variations ~~in~~ of $PM_{1.0}$; **(b)** the aerosol absorption coefficient at 637 nm and the scattering Ångström exponent for **(c)** $PM_{2.5}$ and **(d)** $PM_{1.0}$ (both calculated from 450 ~~nm~~ to 700 nm); **(e)** single scattering albedo at ~~550~~ 637 nm; and **(f)** mass scattering efficiency (MSE) at 550 nm in Wuwei, Zhangye, and Dunhuang from 3 April to 16 May 2014. Note that data collected during the strong dust storm in Zhangye are excluded.

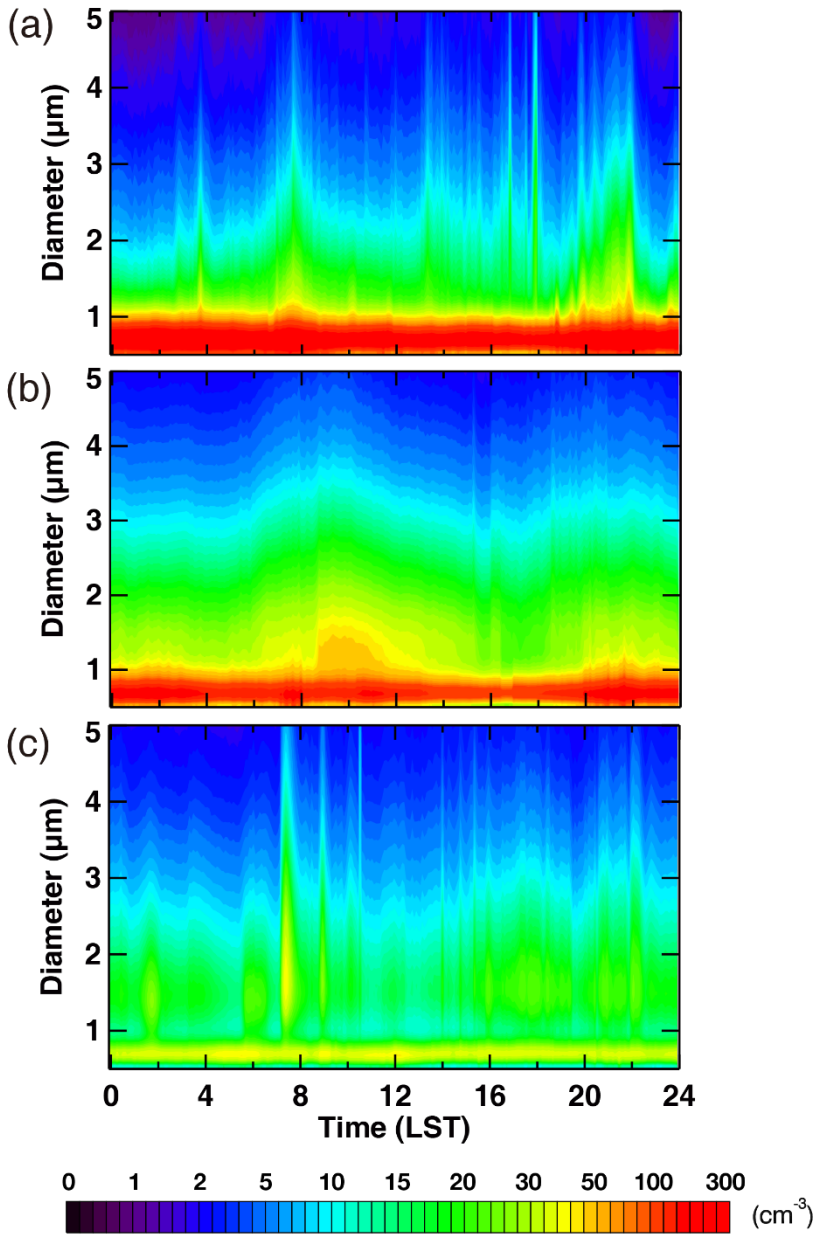
(a)
(b)
(c)
Diameter (μm)
1
2
3
4
5
0
4
8
12
16
20
24
Time (LST)
0
1
2
5
10
15
20
30
50
100
300
(cm-3)

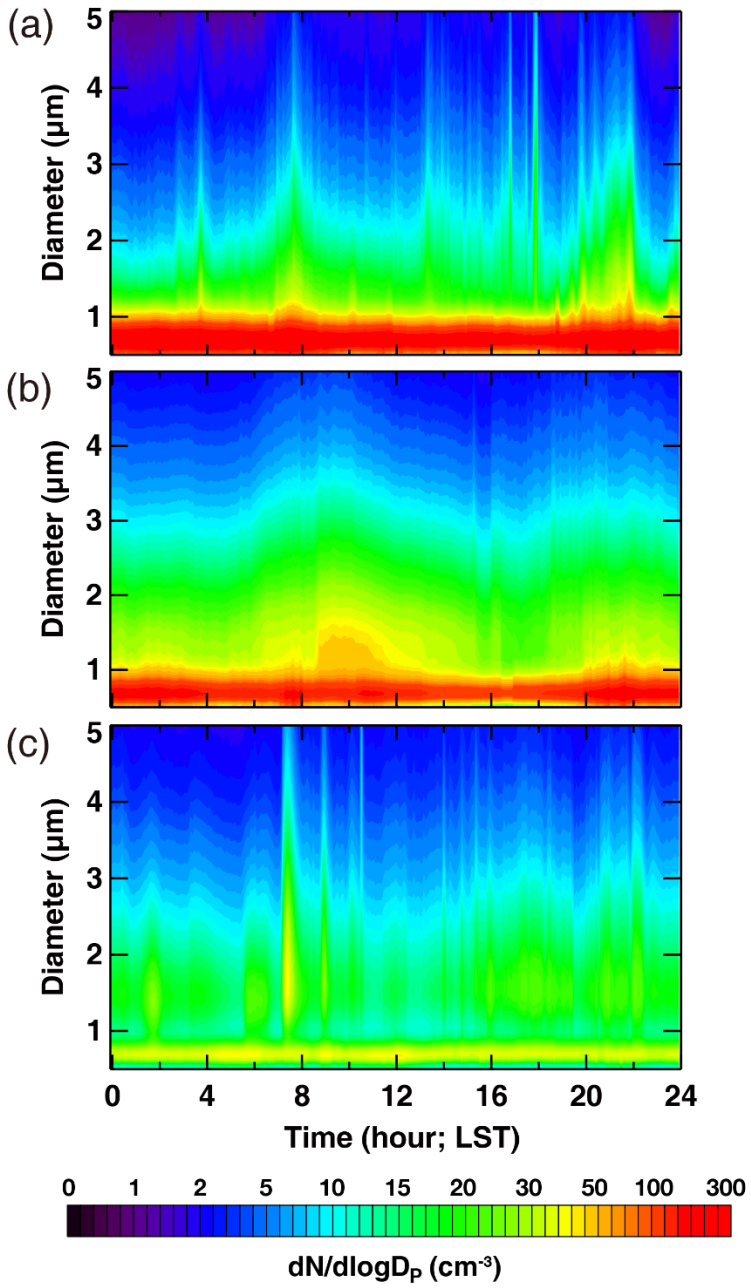

Figure 6. Same as **Figure 5** but for aerosol size distribution (d*N*/dlogD_p ~~dN/dlogD$_p$~~, 0.5 μm < D_p ~~D$_p$~~ < 5 μm) in **(a)** Wuwei, **(b)** Zhangye, and **(c)** Dunhuang from 3 April to 16 May 2014. Note that data collected during the strong dust storm in Zhangye are excluded.

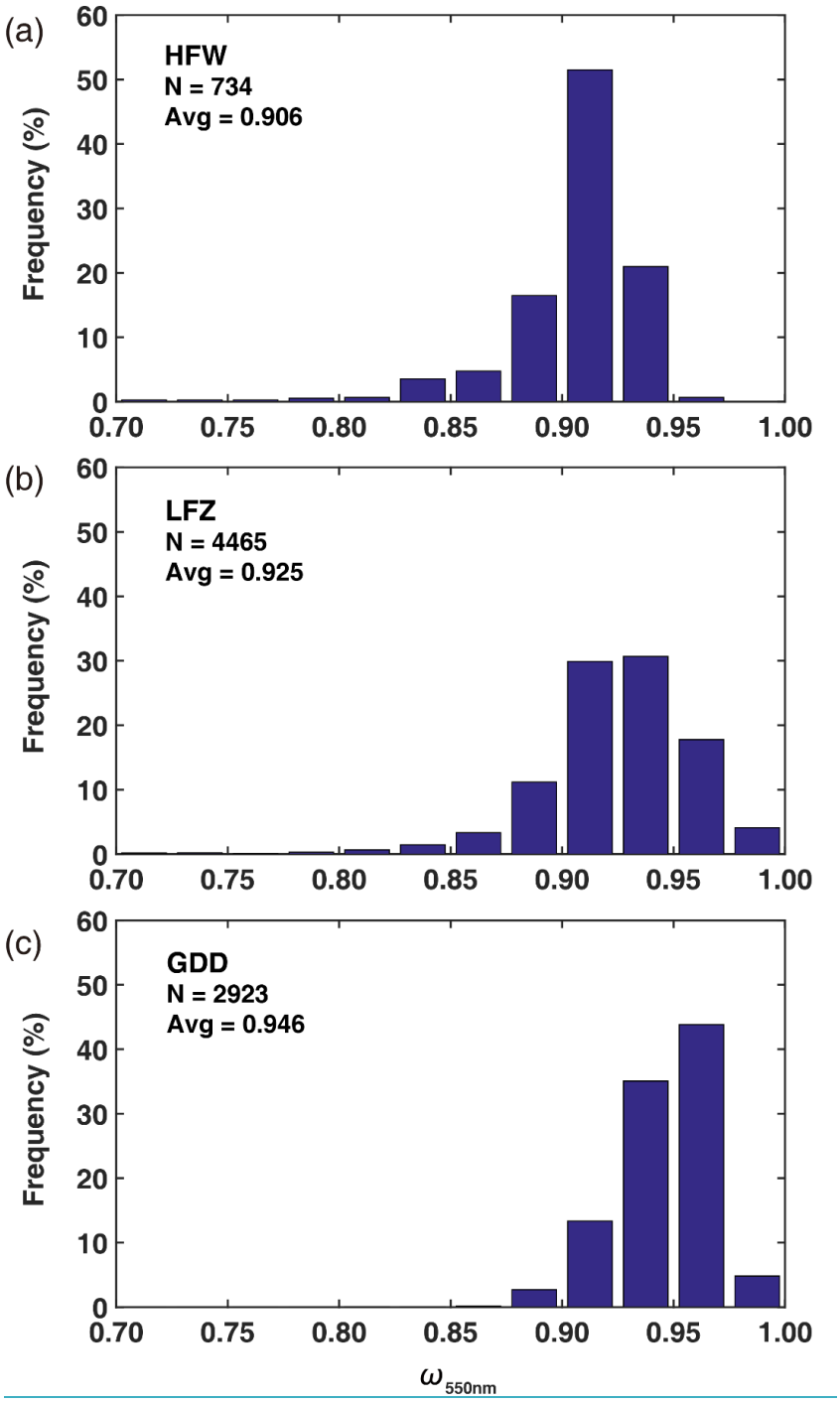
(a)
HFW
N = 734
Avg = 0.906
(b)
LFZ
N = 4465
Avg = 0.925
(c)
GDD
N = 2923
Avg = 0.946
Frequency (%)
0
10
20
30
40
50
60
0.70
0.75
0.80
0.85
0.90
0.95
1.00
ω_{550nm}

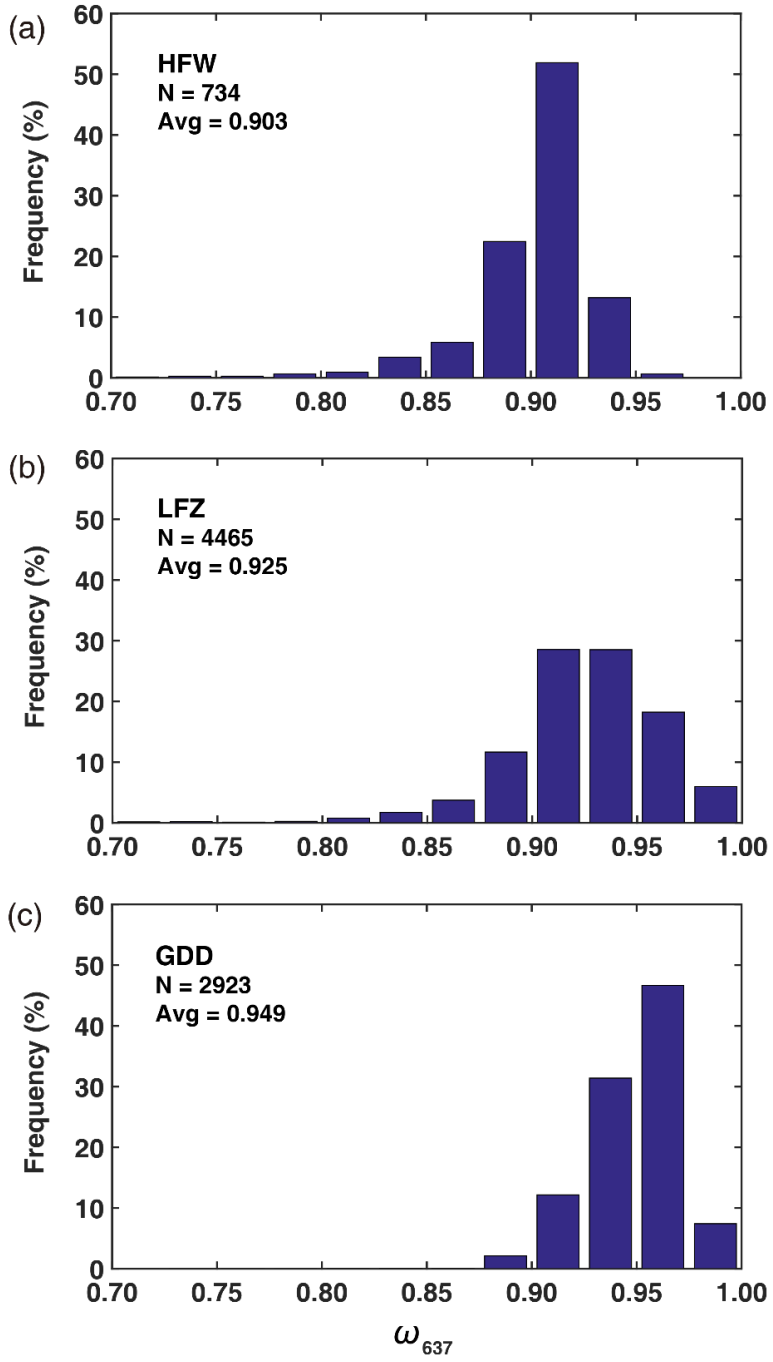

Figure 7. Histograms of 5 min averaged single scattering albedo at 637~~550~~ nm in **(a)** Wuwei, **(b)** Zhangye, and **(c)** Dunhuang. The numbers of samples– and average values are also shown. Note that data collected during the strong dust storm in Zhangye are excluded.

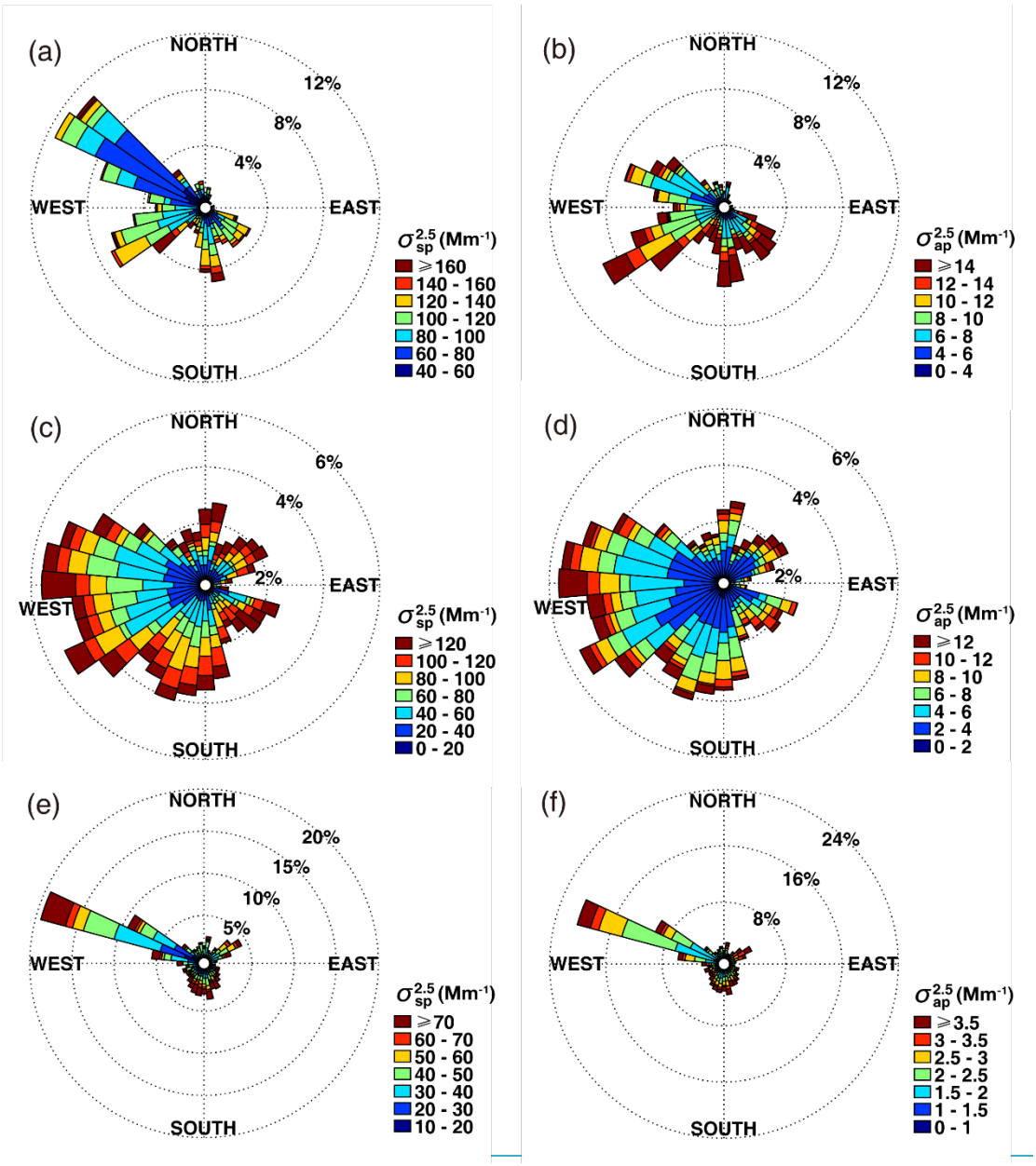
(a)
NORTH
12%
8%
4%
WEST
EAST
SOUTH
$\sigma_{sp}^{2.5}$ (Mm^{-1})
⩾160
140 - 160
120 - 140
100 - 120
80 - 100
60 - 80
40 - 60
(b)
NORTH
12%
8%
4%
WEST
EAST
SOUTH
$\sigma_{ap}^{2.5}$ (Mm^{-1})
⩾14
12 - 14
10 - 12
8 - 10
6 - 8
4 - 6
0 - 4
(c)
NORTH
6%
4%
2%
WEST
EAST
SOUTH
$\sigma_{sp}^{2.5}$ (Mm^{-1})
⩾120
100 - 120
80 - 100
60 - 80
40 - 60
20 - 40
0 - 20
(d)
NORTH
6%
4%
2%
WEST
EAST
SOUTH
$\sigma_{ap}^{2.5}$ (Mm^{-1})
⩾12
10 - 12
8 - 10
6 - 8
4 - 6
2 - 4
0 - 2
(e)
NORTH
20%
15%
10%
5%
WEST
EAST
SOUTH
$\sigma_{sp}^{2.5}$ (Mm^{-1})
⩾70
60 - 70
50 - 60
40 - 50
30 - 40
20 - 30
10 - 20
(f)
NORTH
24%
16%
8%
WEST
EAST
SOUTH
$\sigma_{ap}^{2.5}$ (Mm^{-1})
⩾3.5
3 - 3.5
2.5 - 3
2 - 2.5
1.5 - 2
1 - 1.5
0 - 1

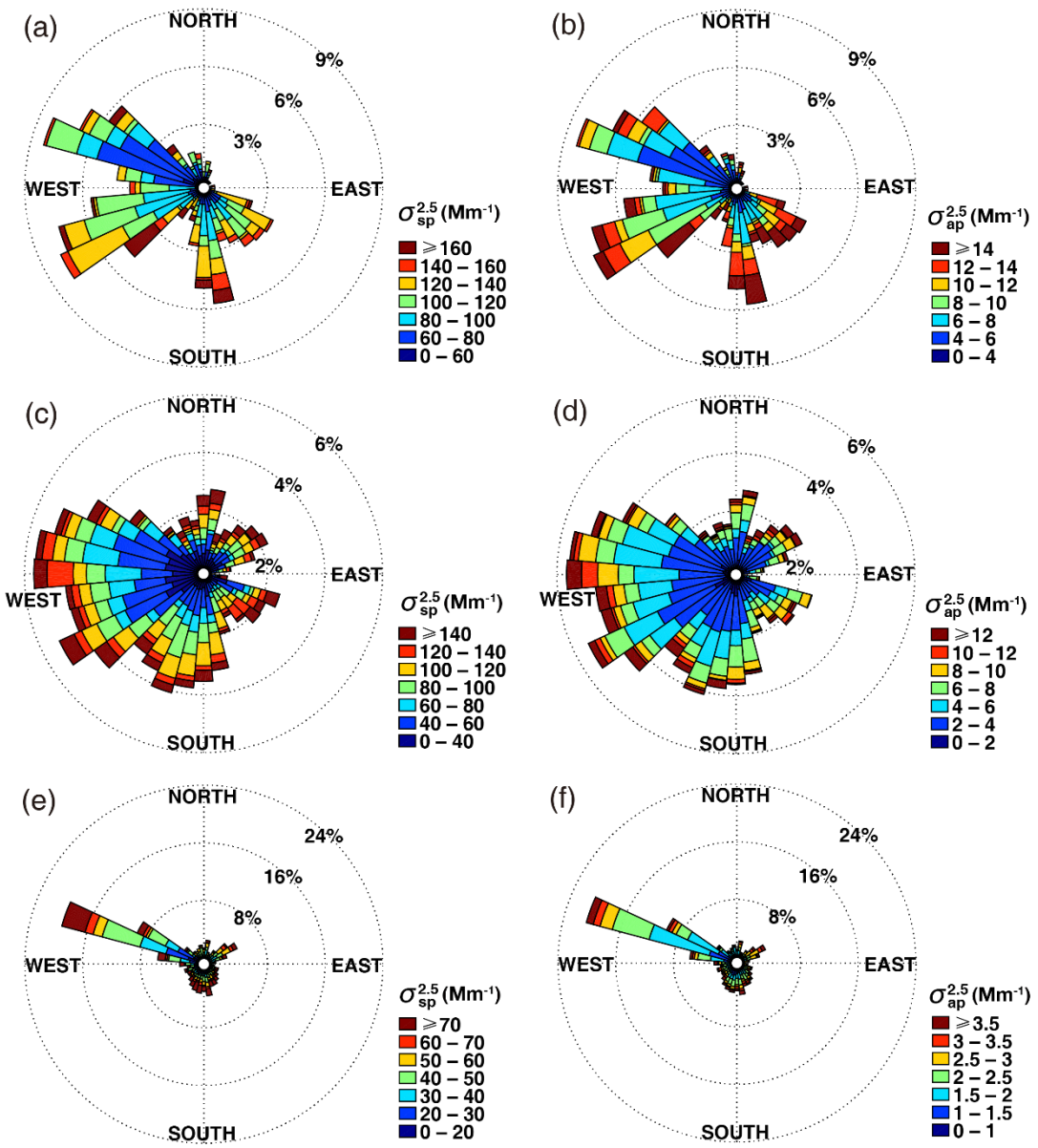

Figure 8. Wind roses for **(a)** aerosol scattering coefficient at 550 nm and **(b)** aerosol absorption coefficient at 637~~550~~ nm in Wuwei; **(c)** and **(d)** are the same as **(a)** and **(b)** but for Zhangye; and **(e)** and **(f)** are the same as **(a)** and **(b)** but for Dunhuang. Note that data collected during the strong dust storm in Zhangye are excluded.

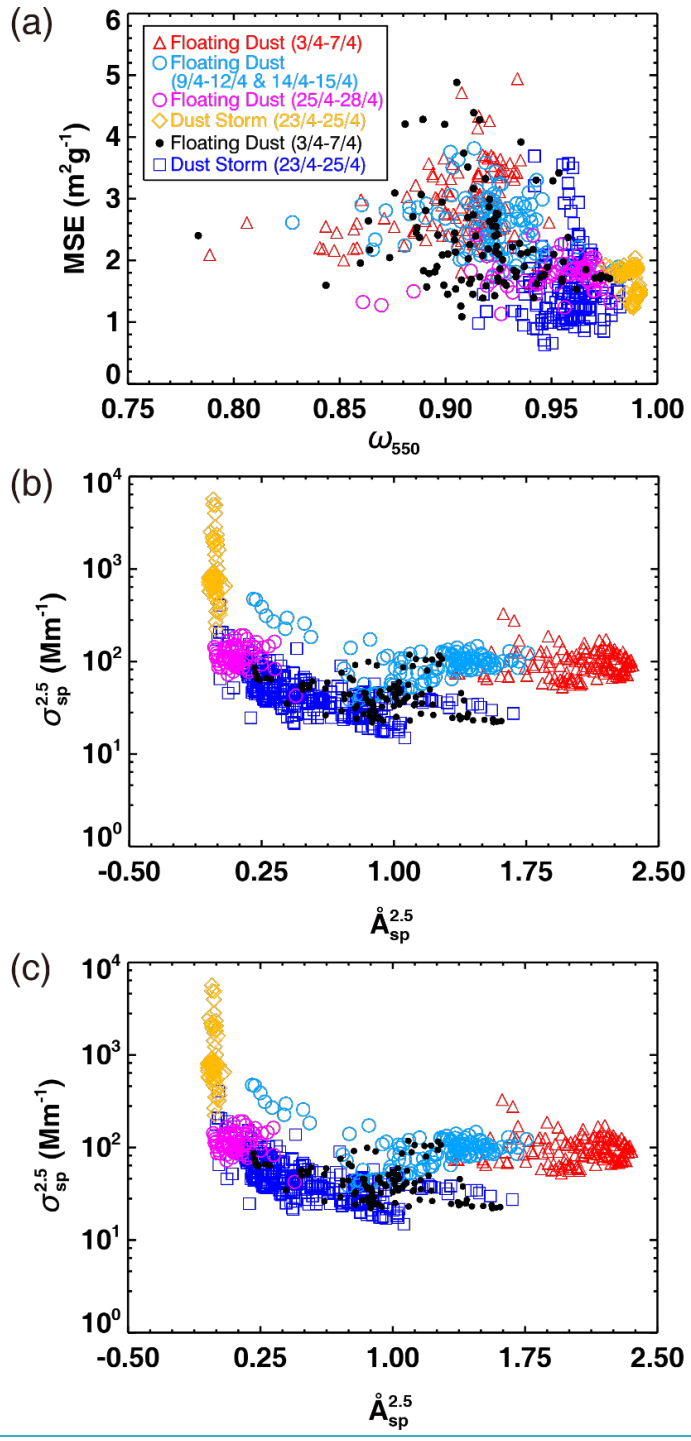
(a)
Floating Dust (3/4-7/4)
Floating Dust (9/4-12/4 & 14/4-15/4)
Floating Dust (25/4-28/4)
Dust Storm (23/4-25/4)
Floating Dust (3/4-7/4)
Dust Storm (23/4-25/4)
MSE (m²g⁻¹)
ω550
(b)
σ2.5sp (Mm⁻¹)
Å2.5sp
(c)
σ2.5sp (Mm⁻¹)
Å2.5sp

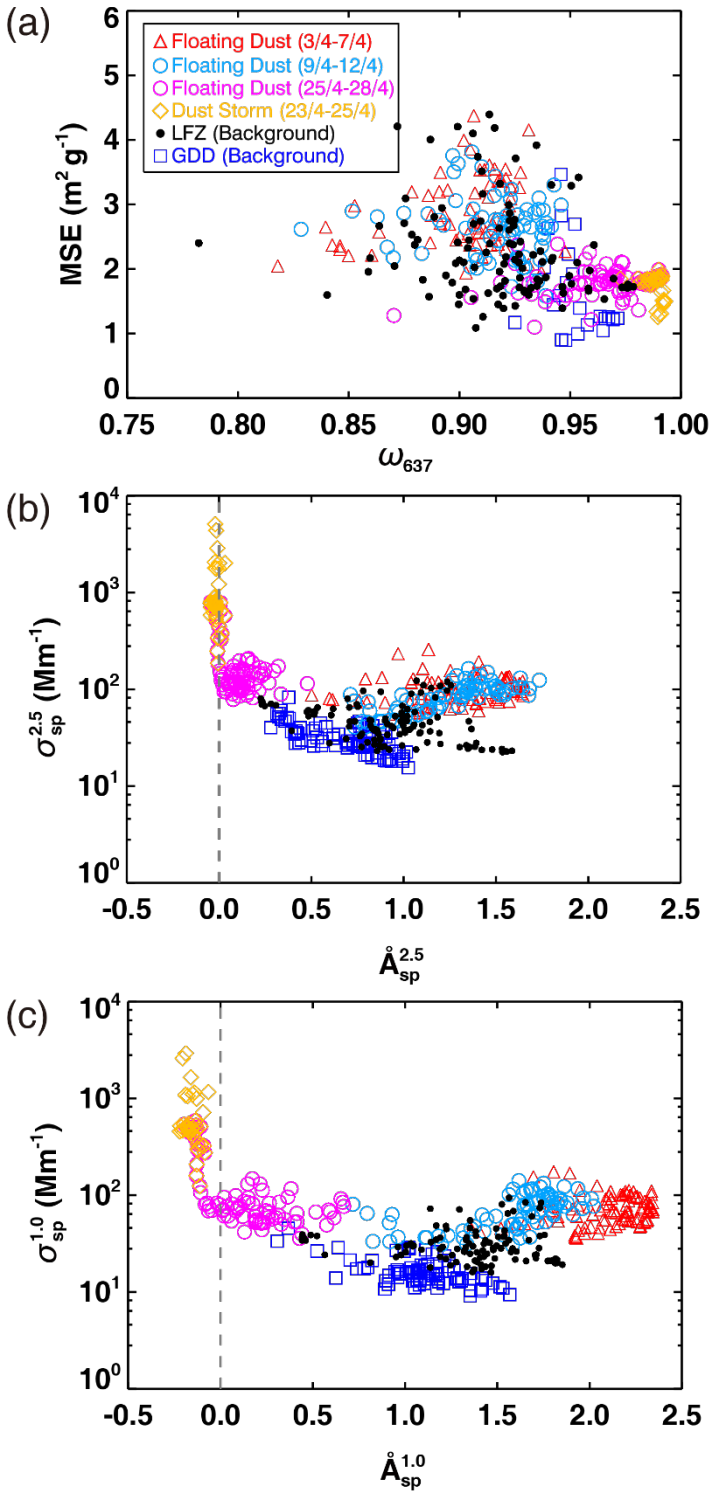

Figure 9. Scatter plots of **(a)** mass scattering efficiency (MSE) versus single scattering albedo (ω) at ~~550~~ 637 nm and **(b)** scattering Ångström exponent at 450–700 nm versus aerosol scattering coefficient ~~for~~ of $PM_{2.5}$ at 550 nm; **(c)** is the same as **(b)** but for $PM_{1.0}$. The color symbols represent different atmospheric conditions during the dust field

campaign.

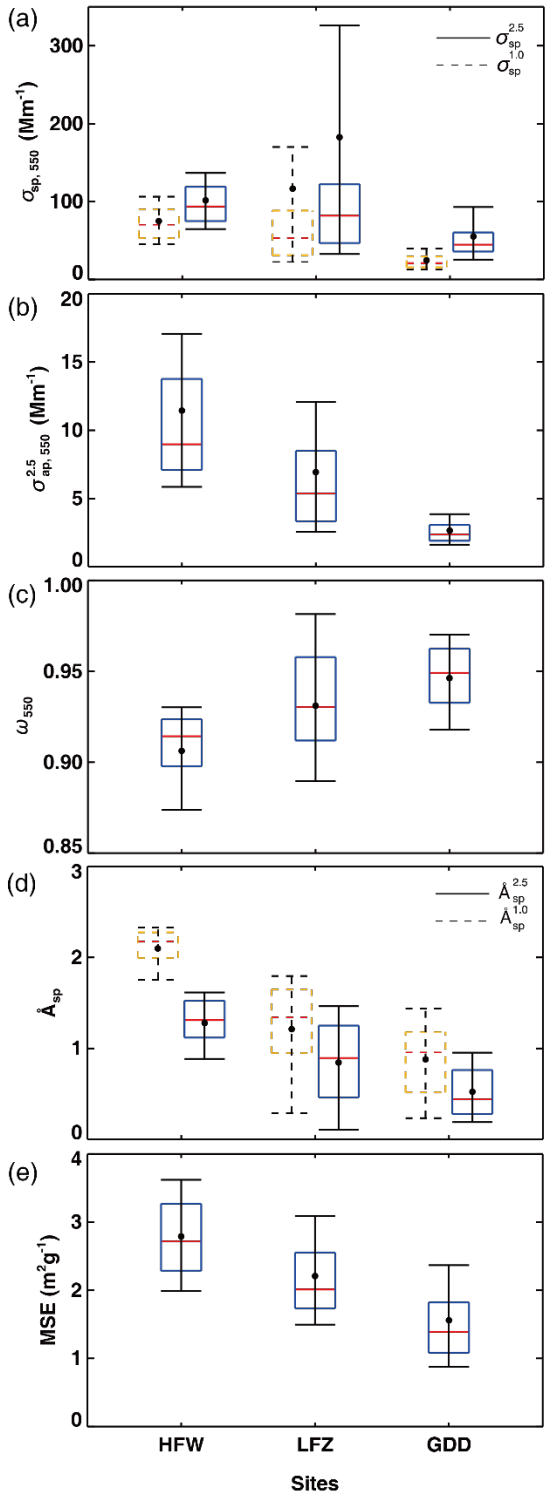

Figure 10. Box plots of (a) scattering coefficient at 550 nm, (b) absorption coefficient at 637 nm, (c) single scattering albedo (ω) at 550 637 nm, (d) scattering Ångström exponent at 450–700 nm, and (e) mass scattering efficiency (MSE) at 550 nm during the dust field campaign. N represents the number of all in-run datasets in Wuwei (HFW), Zhangye (LFZ), and Dunhuang (GDD). The lines, moving from lower to upper,

~~represent the 10th, 25th, 75th, and 90th percentiles. The red lines and black dots represent the median and mean values, respectively.~~

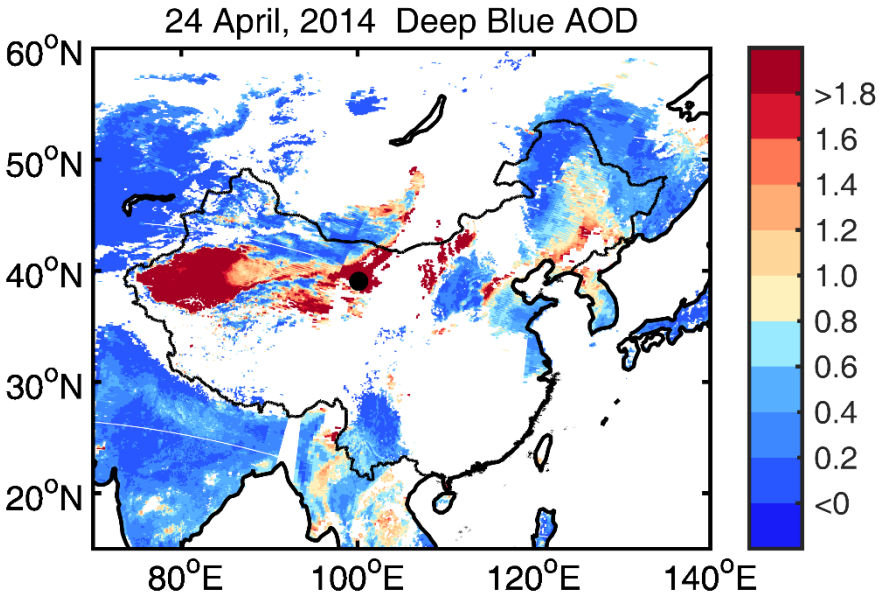

Figure ~~11~~10. Terra MODIS Deep Blue AOD measured at 550 nm by the NASA Giovanni system during a heavy dust storm on 24 April 2014. The black dot represents the location of the ground-based mobile laboratory at Zhangye.

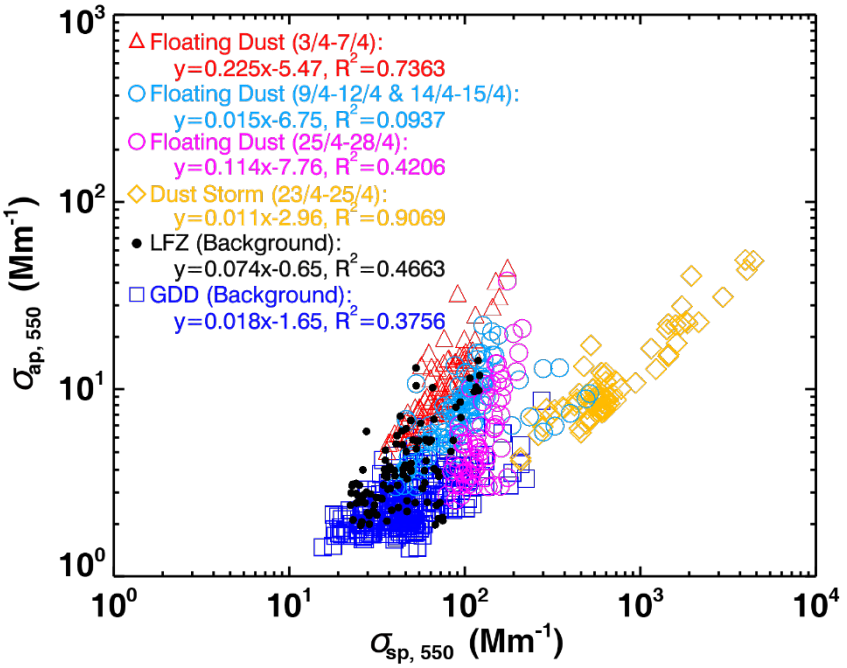

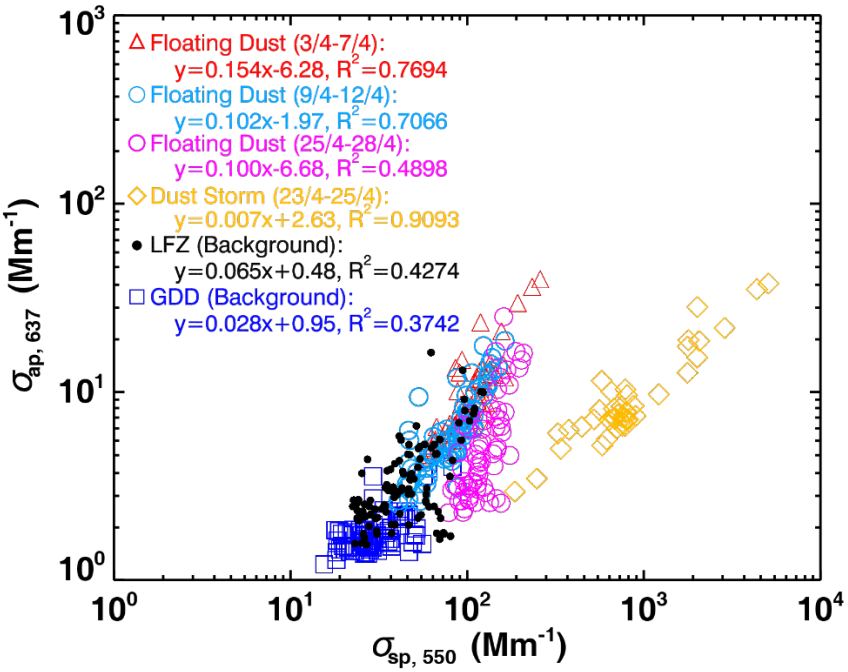

Figure ~~12~~11. Scatter plot of aerosol absorption coefficients versus scattering coefficients from 3 April to 16 May 2014. The colo~~u~~red symbols represent different atmospheric conditions during the dust field campaign.

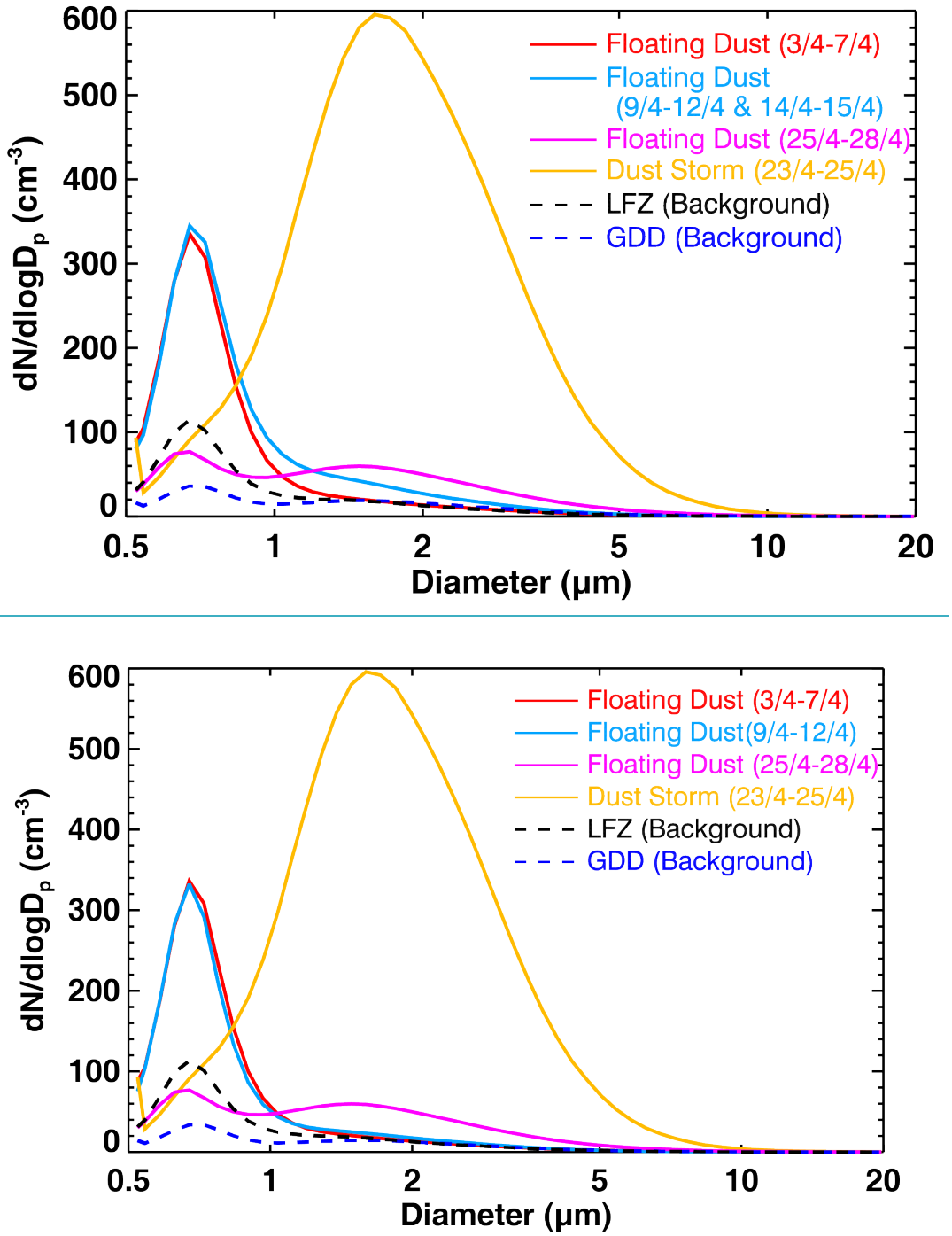

Figure ~~13~~12. Average aerosol size distribution (d*N*/dlogD_p~~dN/dlogD$_p$~~, cm^{-3}) based on all run data collected ~~in~~under different weather conditions during the entire campaign.

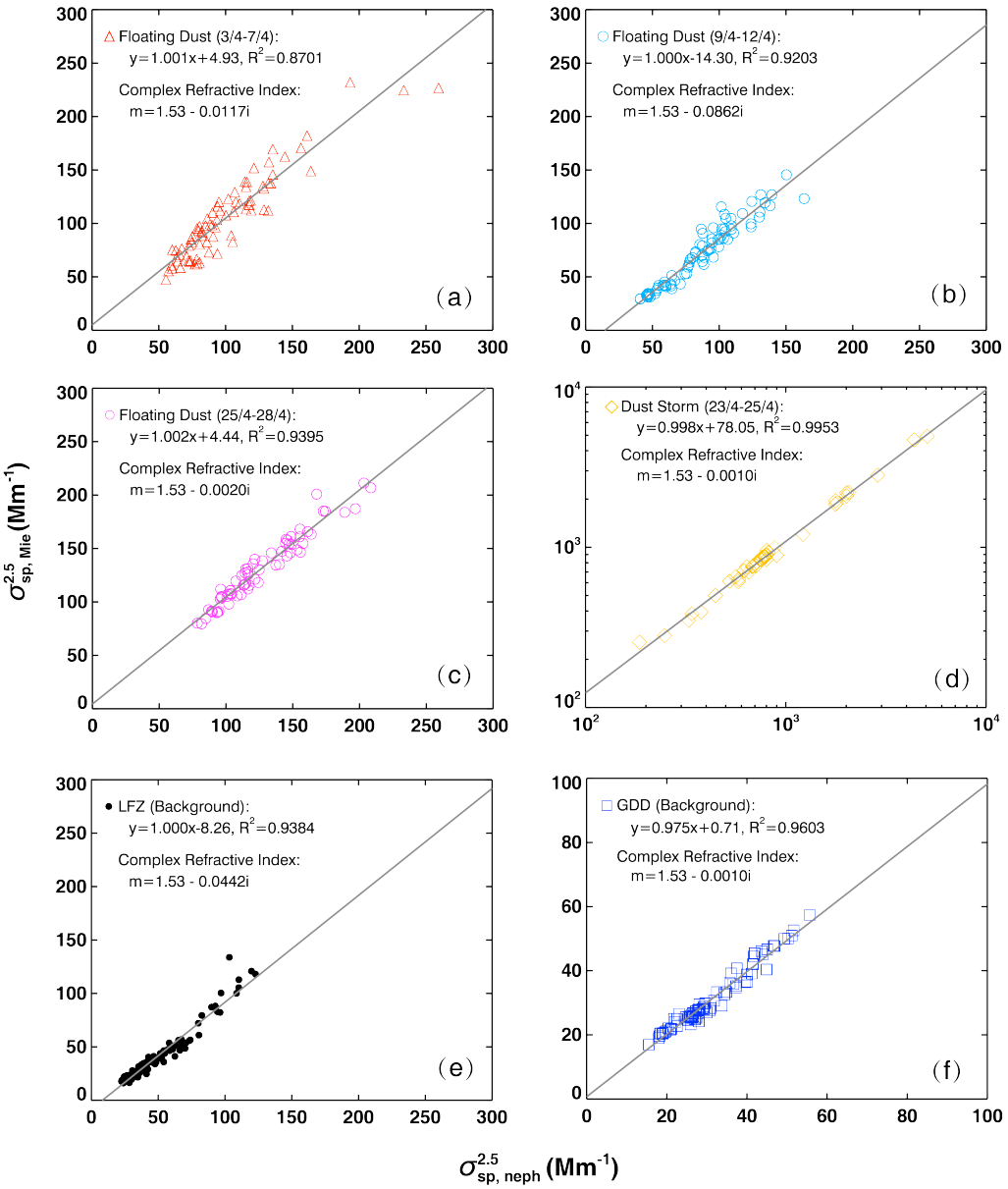

Figure 13. Correlation between $PM_{2.5}$ scattering coefficient calculated from Mie Theory and observed by the nephelometer ~~for $PM_{2.5}$~~ at 550nm ~~in~~under different atmospheric conditions during the dust field campaign.

Table 1. Statistics of optical properties of aerosols measured at three sites.

	λ (nm)	HFW	LFZ			GDD
			All	No dust	Dust storm	
b_{ext} (Mm^{-1})	450	111.2±41.4	124.6±240.8	70.4±40.4	643.0±548.3	28.7±12.4
	550	74.9±29.1	116.6±260.3	57.1±33.6	686.2±589.7	23.8±11.9
	700	44.0±17.9	104.3±265.4	43.0±27.7	691.4±597.5	20.6±12.2
b_{sca} (Mm^{-1})	450	132.8±49.8	193.4±432.1	98.2±63.2	1088.9±1009.9	58.4±33.0
	550	101.6±39.8	182.6±442.7	84.3±59.1	1108.0±1029.8	53.5±33.4
	700	75.7±32.0	169.2±440.4	70.6±55.3	1097.5±1018.7	48.5±33.0
b_{abs} (Mm^{-1})	550	11.45±7.76	6.93±5.91	6.32±5.01	12.48±9.53	2.65±1.20
ω	550	0.906±0.029	0.931±0.038	0.925±0.035	0.987±0.004	0.946±0.021
$Å_{1.0}$	450–700	2.10±0.24	1.05±0.67	1.18±0.57	-0.15±0.05	0.88±0.44
$Å_{2.5}$	450–700	1.28±0.29	0.77±0.52	0.86±0.48	-0.02±0.02	0.53±0.32
MSE ($m^2 g^{-1}$)	550	2.79±0.68	2.21±0.78	2.26±0.79	1.72±0.23	1.55±0.73

Table 1. The main aerosol observations and ground-based instrumentations at three sites.

Observation	Instrumentation	Model & manufacturer	Accuracy
Meteorological elements	Weather transmitter	WXT 520, Vaisala, Helsinki, Finland	*T*: ± 0.3; RH: 0.1 %; *P*: 0.1 hPa; WS: 0.1 m s^{-1}; WD: 1°
$PM_{2.5}$ concentration	Ambient particulate monitor	RP1400a, R&P Corp., Albany, NY-, USA	0.1 μg m^{-3}
Aerosol total scattering/backscattering coefficient	Integrating nephelometer	TSI 3563, TSI Inc., Shoreview, MN, USA	0.44, 0.17, and 0.26 Mm^{-1} at the wavelengths of 450, 550, and 700 nm, respectively
Aerosol absorption coefficient	Multi-angle absorption photometer	MAAP 5012, Thermo Scientific, Waltham, MA, USA	0.66 Mm^{-1}
Aerosol size distribution	Aerodynamic particle sizer	APS 3321, TSI Inc., Shoreview, MN, USA	0.001 cm^{-3}

Table 2. Statistics of optical properties of aerosols measured at the three sites from 3 April to 16 May 2014 .Results are given as the mean ± the standard deviation, which based on hourly averaged data.

	λ (nm)	HFW	LFZ			GDD
			All	Non-dust	Dust storm	
$\sigma_{sp}^{1.0}$ (Mm^{-1})	450	109.7 ± 39.4	125.0 ± 240.8	70.7 ± 39.2	626.1 ± 520.1	28.8 ± 11.6
	550	74.0 ± 27.2	117.0 ± 254.0	57.2 ± 32.5	668.0 ± 559.2	23.9 ± 11.1
	700	43.5 ± 16.4	104.7 ± 259.1	43.1 ± 26.8	673.0 ± 566.5	20.7 ± 11.4
$\sigma_{sp}^{2.5}$ (Mm^{-1})	450	132.7 ± 47.3	193.1 ± 422.7	98.3 ± 62.0	1068.4 ± 971.8	58.9 ± 31.5
	550	101.5 ± 36.8	182.2 ± 433.1	84.3 ± 58.1	1087.1 ± 990.8	54.0 ± 32.0
	700	75.6 ± 28.4	168.8 ± 430.9	70.5 ± 54.5	1076.8 ± 979.7	49.1 ± 31.7
$\sigma_{bsp}^{1.0}$ (Mm^{-1})	450	12.8 ± 4.7	16.7 ± 34.8	8.5 ± 4.3	92.3 ± 76.5	4.0 ± 1.7
	550	9.9 ± 3.6	15.8 ± 35.3	7.5± 3.9	92.9 ± 77.4	3.5 ± 1.6
	700	7.8 ± 2.7	15.6 ± 36.5	6.9 ± 4.0	95.5 ± 79.6	3.3 ± 1.6
$\sigma_{bsp}^{2.5}$ (Mm^{-1})	450	15.3 ± 5.5	22.0 ± 48.5	10.9 ± 6.6	124.0 ± 110.1	7.6 ± 4.0
	550	12.2 ± 4.4	19.7 ± 44.9	9.5 ± 5.9	114.6 ± 101.6	6.5 ± 3.7
	700	11.2 ± 4.0	19.8 ± 46.7	9.1 ± 6.0	118.8 ± 105.5	6.5 ± 3.8
$\sigma_{ap}^{2.5}$ (Mm^{-1})	637	9.7 ± 6.1	6.0 ± 4.6	5.5 ± 3.8	10.6 ± 7.6	2.3 ± 0.9
ω	637	0.902 ± 0.025	0.931 ± 0.037	0.925 ± 0.034	0.989 ± 0.004	0.949 ± 0.020
$b_{1.0}$	450	0.117 ± 0.009	0.126 ± 0.018	0.123 ± 0.017	0.148 ± 0.004	0.137 ± 0.007
	550	0.135 ± 0.009	0.135 ± 0.013	0.134 ± 0.013	0.140 ± 0.003	0.147 ± 0.007
	700	0.181 ± 0.007	0.161 ± 0.012	0.163 ± 0.011	0.143 ± 0.003	0.159 ± 0.012
$b_{2.5}$	450	0.115 ± 0.007	0.113 ± 0.008	0.113 ± 0.008	0.118 ± 0.003	0.131 ± 0.004
	550	0.121 ±0.005	0.114 ± 0.007	0.115 ± 0.007	0.107 ± 0.003	0.122 ± 0.005

	700	0.150 ± 0.007	0.131 ± 0.012	0.133 ± 0.011	0.113 ± 0.003	0.136 ± 0.010
$Å_{sp}^{1.0}$	450–700	2.09 ± 0.22	1.05 ± 0.66	1.18 ± 0.56	–0.15 ± 0.04	0.87 ± 0.42
$Å_{sp}^{2.5}$	450–700	1.28 ± 0.27	0.77 ± 0.51	0.86 ± 0.47	–0.01 ± 0.02	0.52 ± 0.31
MSE (m^2 g^{-1})	550	2.79 ± 0.57	2.21 ± 0.64	2.26 ± 0.65	1.73 ± 0.20	1.55 ± 0.59

Table 3. Statistical summary of optical and microphysical properties of aerosols in different atmospheric conditions during the dust field campaign.

~~Episodes~~	Floating Dust (3/4–7/4)	Floating Dust (9/4–12/4)	Floating Dust (25/4–28/4)	Dust Storm (23/4–25/4)	LZF (Background)	GDD (Background)
Dust particle density (g cm^{-3})	1.32 ± 0.28	1.04 ± 0.17	1.24 ± 0.21	1.16 ± 0.51	1.33 ± 0.44	1.64 ± 0.50
Refractive index	1.53–0.0117-*i*	1.53–0.0862-*i*	1.53–0.0020-*i*	1.53–0.0010-*i*	1.53–0.0442-*i*	1.53–0.0010-*i*
$\sigma^{2.5}_{sp,\ neph}$ (Mm^{-1})	102 ± 37	86 ± 29	127 ± 31	1087 ± 991	49 ± 24	31 ± 9
$\sigma^{2.5}_{sp,\ Mie}$ (Mm^{-1})	107 ± 40	72 ± 30	132 ± 32	1163 ± 992	41 ± 25	31 ± 9
$\sigma^{20}_{sp,\ Mie}$ (Mm^{-1})	153 ± 51	102 ± 31	334 ± 75	2983 ± 2712	66 ± 32	71 ± 27
$PM_{2.5}$ scattering fraction (%)	49.3	85.1	37.9	63.6	74.8	43.7

References

~~Adler, G., Riziq, A. A., Erlick, C., and Rudich, Y.: Effect of intrinsic organic carbon on the optical properties of fresh diesel soot, P. Natl. Acad. Sci. USA, 107, 6699–6704, doi:10.1073/pnas.0903311106, 2010.~~

Aleksandropoulou, V., Torseth, K., and Lazaridis, M.: Atmospheric Emission Inventory for Natural and Anthropogenic Sources and Spatial Emission Mapping for the Greater Athens Area, Water Air Soil Pollut., 219, 507–526, doi:10.1007/s11270-010-0724-2, 2011.

Anderson, T. L., Covert, D. S., Marshall, S. F., Laucks, M. L., Charlson, R. J., Waggoner, A. P., Ogren, J. A., Caldow, R., Holm, R. L., Quant, F. R., Sem, G. J., Wiedensohler, A., Ahlquist, N. A., and Bates, T. S.: Performance characteristics of a high-sensitivity, three-wavelength total scatter-backscatter nephelometer, J. Atmos. Ocean. Tech., 13, 967–986, 1996.

Anderson, T. L. and Ogren, J. A.: Determining aerosol radiative properties using the TSI 3563 Integrating Nephelometer, Aerosol Sci. Tech., 29, 57–69, doi:10.1080/02786829808965551, 1998.

Arimoto, R., Kim, Y. J., Kim, Y. P., Quinn, P. K., Bates, T. S., Anderson, T. L., Gong, S., Uno, I., Chin, M., Huebert, B. J., Clarke, A. D., Shinozuka, Y., Weber, R. J., Anderson, J. R., Guazzotti, S. A., Sullivan, R. C., Sodeman, D. A., Prather, K. A., and Sokolik, I. N.: Characterization of Asian Dust during ACE-Asia, Global Planet. Change, 52, 23–56, doi:10.1016/j.gloplacha.2006.02.013, 2006.

Arnott, W. P., Moosmuller, H., Sheridan, P. J., Ogren, J. A., Raspet, R., Slaton, W. V., Hand, J. L., Kreidenweis, S. M., and Collett, J. L.: Photoacoustic and filter-based ambient aerosol light absorption measurements: Instrument comparisons and the role of relative humidity, J. Geophys. Res-Atmos, 108, 4034, doi:10.1029/2002jd002165, 2003.

Arya, S. P.: Air Pollution Meteorology and Dispersion, 310 pp., Oxford University Press, New York, 1999.

~~Bergstrom, R. W., Pilewskie, P., Russell, P. B., Redemann, J., Bond, T. C., Quinn, P. K., and Sierau, B.: Spectral absorption properties of atmospheric aerosols, Atmos. Chem. Phys., 7, 5937–5943, doi:10.5194/acp-7-5937-2007, 2007.~~

Bi, J., Huang, J., Shi, J., Hu, Z., Zhou, T., Zhang, G., Huang, Z., Wang, X., and Jin, H.: Measurement of scattering and absorption properties of dust aerosol in a Gobi farmland region of northwestern China–a potential anthropogenic influence, Atmos. Chem. Phys., 17, 7775–7792, doi:10.5194/acp-17-7775-2017, 2017.

Bohren, C. F. and Huffman, D. R.: Absorption and Scattering of Light by Small Particles, John Wiley, Hoboken, N. J., 1983.

Bond, T. C. and Bergstrom, R. W.: Light Absorption by Carbonaceous Particles: An Investigative Review, Aerosol Sci. Tech., 40, 27–67, doi:10.1080/02786820500421521, 2006.

Cattrall, C., Carder, K. L., and Gordon, H. R.: Columnar aerosol single-scattering albedo and phase function retrieved from sky radiance over the ocean: measurements of Saharan dust, J. Geophys. Res.-Atmos., 108, 4287, doi:10.1029/2002jd002497, 2003.

Cermak, J., Wild, M., Knutti, R., Mishchenko, M. I., and Heidinger, A. K.: Consistency of global satellite-derived aerosol and cloud data sets with recent brightening observations, Geophys. Res. Lett., 37, 5, doi:10.1029/2010gl044632, 2010.

Che, H. Z., Wang, Y. Q., and Sun, J. Y.: Aerosol optical properties at Mt. Waliguan Observatory, China, Atmos. Environ., 45, 6004–6009, doi:10.1016/j.atmosenv.2011.07.050, 2011.

Che, H. Z., Wang, Y. Q., Sun, J. Y., Zhang, X. C., Zhang, X. Y., and Guo, J. P.: Variation of Aerosol Optical Properties over the Taklimakan Desert in China, Aerosol Air Qual. Res., 13, 777–785, doi:10.4209/aaqr.2012.07.0200, 2013.

Chen, S. Y., Huang, J. P., Zhao, C., Qian, Y., Leung, L. R., and Yang, B.: Modeling the transport and radiative forcing of Taklimakan dust over the Tibetan Plateau: A case study in the summer of 2006, J. Geophys. Res.-Atmos., 118, 797–812, doi:10.1002/jgrd.50122, 2013.

DeCarlo, P. F., Slowik, J. G., Worsnop, D. R., Davidovits, P., and Jimenez, J. L.: Particle morphology and density characterization by combined mobility and aerodynamic diameter measurements. Part 1: Theory, Aerosol Sci. Tech., 38, 1185–1205, doi:10.1080/02786820590928897, 2005.

Dubovik, O., Holben, B. N., Eck, T. F., Smirnov, A., Kaufman, Y. J., King, M. D., Tanré, D., and Slutsker, I.: Variability of absorption and optical properties of key aerosol types observed in worldwide locations, J. Atmos. Sci., 59, 590–608, 2002.

Fan, X. H., Chen, H. B., Xia, X. G., Li, Z. Q., and Cribb, M.: Aerosol optical properties from the Atmospheric Radiation Measurement Mobile Facility at Shouxian, China, J. Geophys. Res.-Atmos, 115, 13, doi:10.1029/2010jd014650, 2010.

Favez, O., Cachier, H., Sciare, J., Sarda-Esteve, R., and Martinon, L.: Evidence for a significant contribution of wood burning aerosols to PM2.5 during the winter season in Paris, France, Atmos. Environ., 43, 3640–3644, doi:10.1016/j.atmosenv.2009.04.035, 2009.

Garland, R. M., Yang, H., Schmid, O., Rose, D., Nowak, A., Achtert, P., Wiedensohler, A., Takegawa, N., Kita, K., Miyazaki, Y., Kondo, Y., Hu, M., Sha, M., Zeng, L. M., Zhang, Y. H., Andreae, M. O., and Poschl, U.: Aerosol optical properties in a rural environment near the mega-city Guangzhou, China: implications for regional

air pollution, radiative forcing and remote sensing, Atmos. Chem. Phys., 8, 5161–5186, doi:10.5194/acp-8-5161-2008, 2008.

Ge, J. M., Huang, J. P., Xu, C. P., Qi, Y. L., and Liu, H. Y.: Characteristics of Taklimakan dust emission and distribution: A satellite and reanalysis field perspective, J. Geophys. Res.-Atmos., 119, 11772–11783, doi:10.1002/2014jd022280, 2014.

Ge, J. M., Su, J., Ackerman, T. P., Fu, Q., Huang, J. P., and Shi, J. S.: Dust aerosol optical properties retrieval and radiative forcing over northwestern China during the 2008 China-U.S. joint field experiment, J. Geophys. Res-atmos, 115, doi:10.1029/2009jd013263, 2010.

Ge, J. M., Su, J., Fu, Q., Ackerman, T. P., and Huang, J. P.: Dust aerosol forward scattering effects on ground-based aerosol optical depth retrievals, J. Quant. Spectrosc. Ra., 112, 310–319, doi:10.1016/j.jqsrt.2010.07.006, 2011.

Ginoux, P., Garbuzov, D., and Hsu, H. C.: Identification of anthropogenic and natural dust sources using Moderate Resolution Imaging Spectroradiometer (MODIS) Deep Blue level 2 data, J. Geophys. Res.-Atmos., 115, D05204, doi:10.1029/2009jd012398, 2010.

Goudie, A. S. and Middleton, N. J.: Saharan dust storms: Nature and consequences, Earth-Sci. Rev., 56, 179–204, doi:10.1016/S0012-8252(01)00067-8, 2001.

~~Gyawali, M., Arnott, W. P., Lewis, K., and Moosmuller, H.: In situ aerosol optics in Reno, NV, USA during and after the summer 2008 California wildfires and the influence of absorbing and non-absorbing organic coatings on spectral light absorption, Atmos. Chem. Phys., 9, 8007–8015, doi: 10.5194/acp-9-8007-2009, 2009.~~

Hand, J. L. and Malm, W. C.: Review of aerosol mass scattering efficiencies from ground-based measurements since 1990, J. Geophys. Res.-Atmos., 112, D16203, doi:10.1029/2007jd008484, 2007.

~~Hansen, J., Sato, M., and Ruedy, R.: Radiative forcing and climate response, J. Geophys. Res.-Atmos, 102, 6831–6864, doi:10.1029/96jd03436, 1997.~~

Haywood, J. M., and Shine, K. P.: The Effect of Anthropogenic Sulfate and Soot Aerosol on the Clear-Sky Planetary Radiation Budget, Geophys. Res. Lett., 22, 603–606, doi:10.1029/95gl00075, 1995.

Holben, B. N., Eck, T. F., and Fraser, R. S.: Temporal and Spatial Variability of Aerosol Optical Depth in the Sahel Region in Relation to Vegetation Remote-Sensing, Int. J. Remote Sens., 12, 1147–1163, doi: 10.1080/01431169108929719, 1991.

Holben, B. N., Eck, T., Slutsker, I., Smirnov, A., Sinyuk, A., Schafer, J., Giles, D., and Dubovik, O.: AERONET Version 2.0 quality assurance criteria, in: Remote Sensing of the Atmosphere and Clouds, Proc. of SPIE, Goa, India, 13–17 November, 6408, doi:10.1117/12.706524, 2006.

Holben, B. N., Tanre, D., Smirnov, A., Eck, T. F., Slutsker, I., Abuhassan, N., Newcomb, W. W., Schafer, J. S., Chatenet, B., Lavenu, F., Kaufman, Y. J., Castle, J. V., Setzer, A., Markham, B., Clark, D., Frouin, R., Halthore, R., Karneli, A., O'Neill, N. T., Pietras, C., Pinker, R. T., Voss, K., and Zibordi, G.: An emerging ground-based aerosol climatology: Aerosol optical depth from AERONET, J.

Geophys. Res.-Atmos., 106, 12067–12097, doi:10.1029/2001jd900014, 2001.
Huang, J. P., Liu, J. J., Chen, B., and Nasiri, S. L.: Detection of anthropogenic dust using CALIPSO lidar measurements, Atmos. Chem. Phys., 15, 11653–11665, doi:10.5194/acp-15-11653-2015, 2015a.
Huang, J. P., Yu, H. P., Guan, X. D., Wang, G. Y., and Guo, R. X.: Accelerated dryland expansion under climate change. Nat. Clim. Change, 6, 166–172, doi:10.1038/nclimate2837, 2015b.
Huang, J. P., Minnis, P., Chen, B., Huang, Z. W., Liu, Z. Y., Zhao, Q. Y., Yi, Y. H., and Ayers, J. K.: Long-range transport and vertical structure of Asian dust from CALIPSO and surface measurements during PACDEX, J. Geophys. Res.-Atmos., 113, D23212, doi:10.1029/2008jd010620, 2008.
Huang, J. P., Minnis, P., Yan, H., Yi, Y., Chen, B., Zhang, L., and Ayers, J. K.: Dust aerosol effect on semi-arid climate over Northwest China detected from A-Train satellite measurements, Atmos. Chem. Phys., 10, 6863–6872, doi:10.5194/acp-10-6863-2010, 2010.
Huang, J. P., Wang, T. H., Wang, W. C., Li, Z. Q., and Yan, H. R.: Climate effects of dust aerosols over East Asian arid and semiarid regions, J. Geophys. Res.-Atmos., 119, 11398–11416, doi:10.1002/2014jd021796, 2014.
~~Intergovernmental Panel on Climate Change (IPCC): Climate Change 2013: The Physical Science Basis, Contribution of Working Group I to the Fifth Assessment Report of the Intergovernmental Panel on Climate Change, edited by Stocker, T. F., D. Qin, G.-K. Plattner, M. Tignor, S. K. Allen, J. Boschung, A. Nauels, Y. Xia, V. Bex and P. M. Midgley. Cambridge University Press, Cambridge, United Kingdom and New York, NY, USA, 2013.~~
Jacob, D. J., Crawford, J. H., Kleb, M. M., Connors, V. S., Bendura, R. J., Raper, J. L., Sachse, G. W., Gille, J. C., Emmons, L., and Heald, C. L.: Transport and Chemical Evolution over the Pacific (TRACE-P) aircraft mission: Design, execution, and first results, J. Geophys. Res.-Atmos, 108, 1–19, doi:10.1029/2002jd003276, 2003.
~~Kaufman, Y. J., Tanre, D., Dubovik, O., Karnieli, A., and Remer, L. A.: Absorption of sunlight by dust as inferred from satellite and ground-based remote sensing, Geophys. Res. Lett., 28, 1479–1482, doi:10.1029/2000gl012647, 2001.~~
~~Kamani, H., Ashrafi, S. D., Isazadeh, S., Jaafari, J., Hoseini, M., Mostafapour, F. K., Bazrafshan, E., Nazmara, S., and Mahvi, A. H.: Heavy Metal Contamination in Street Dusts with Various Land Uses in Zahedan, Iran, B. Environ. Contam. Tox., 94, 382–386, doi:10.1007/s00128-014-1453-9, 2015.~~
Kim, W., Doh, S. J., and Yu, Y.: Anthropogenic contribution of magnetic particulates in urban roadside dust, Atmos. Environ., 43, 3137–3144, doi:10.1016/j.atmosenv.2009.02.056, 2009.
Laing, J. R., Jaffe, D. A., and Hee, J. R.: Physical and optical properties of aged biomass burning aerosol from wildfires in Siberia and the Western USA at the Mt. Bachelor Observatory, Atmos. Chem. Phys., 16, 15185–15197, doi:10.5194/acp-16-15185-2016, 2016.
Li, C., Tsay, S.-C., Fu, J. S., Dickerson, R. R., Ji, Q., Bell, S. W., Gao, Y., Zhang, W., Huang, J., Li, Z., and Chen, H.: Anthropogenic air pollution observed near dust

source regions in northwestern China during springtime 2008, J. Geophys. Res.-Atmos., 115, doi:10.1029/2009jd013659, 2010.

Li, G. J., Chen, J., Ji, J. F., Yang, J. D., and Conway, T. M.: Natural and anthropogenic sources of East Asian dust, Geology, 37, 727–730, doi:0.1130/g30031a.1, 2009.

Li, J., Wang, Z. F., Zhuang, G., Luo, G., Sun, Y., and Wang, Q.: Mixing of Asian mineral dust with anthropogenic pollutants over East Asia: a model case study of a super-duststorm in March 2010, Atmos. Chem. Phys., 12, 7591–7607, doi:10.5194/acp-12-7591-2012, 2012.

Li, Z. Q., Lau, W. K. M., Ramanathan, V., Wu, G., Ding, Y., Manoj, M. G., Liu, J., Qian, Y., Li, J., Zhou, T., Fan, J., Rosenfeld, D., Ming, Y., Wang, Y., Huang, J., Wang, B., Xu, X., Lee, S. S., Cribb, M., Zhang, F., Yang, X., Zhao, C., Takemura, T., Wang, K., Xia, X., Yin, Y., Zhang, H., Guo, J., Zhai, P. M., Sugimoto, N., Babu, S. S., and Brasseur, G. P.: Aerosol and monsoon climate interactions over Asia, Rev. Geophys., 54, 866–929, doi:10.1002/2015rg000500, 2016.

~~Li, Z. Q., Li, C., Chen, H., Tsay, S. C., Holben, B., Huang, J., Li, B., Maring, H., Qian, Y., Shi, G., Xia, X., Yin, Y., Zheng, Y., and Zhuang, G.: East Asian Studies of Tropospheric Aerosols and their Impact on Regional Climate (EAST-AIRC): An overview, J. Geophys. Res.-Atmos, 116, D00k34, doi:10.1029/2010jd015257, 2011.~~

Liu, Y., Sato, Y., Jia, R., Xie, Y., Huang, J., and Nakajima, T.: Modeling study on the transport of summer dust and anthropogenic aerosols over the Tibetan Plateau, Atmos. Chem. Phys., 15, 12581–12594, doi:10.5194/acp-15-12581-2015, 2015.

Mahowald, N. M. and Luo, C.: A less dusty future?, Geophys. Res. Lett., 30, 1903, doi:1910.1029/2003grl017880, 2003.

~~Maring, H., Savoie, D. L., Izaguirre, M. A., Custals, L., and Reid, J. S.: Mineral dust aerosol size distribution change during atmospheric transport, J. Geophys. Res.-Atmos, 108, 797–812, 2003.~~

Mätzler, C.: MATLAB functions for Mie scattering and absorption, Res. Rep. 2002–08, Inst. Fur Angew. Phys., Bern, 2002.

McConnell, C. L., Formenti, P., Highwood, E. J., and Harrison, M. A. J.: Using aircraft measurements to determine the refractive index of Saharan dust during the DODO Experiments, Atmos. Chem. Phys., 10, 3081–3098, doi:10.5194/acp-10-3081-2010, 2010.

~~McConnell, C. L., Highwood, E. J., Coe, H., Formenti, P., Anderson, B., Osborne, S., Nava, S., Desboeufs, K., Chen, G., and Harrison, M. A. J.: Seasonal variations of the physical and optical characteristics of Saharan dust: Results from the Dust Outflow and Deposition to the Ocean (DODO) experiment, J. Geophys. Res.-Atmos, 113, 19, doi:10.1029/2007jd009606, 2008.~~

~~Menon, S., Hansen, J., Nazarenko, L., and Luo, Y. F.: Climate effects of black carbon aerosols in China and India, Science, 297, 2250–2253, doi:10.1126/science.1075159, 2002.~~Mie, G.: Beiträge zur optic trüber Medien speziell kolloidaler Metallösungen, Ann. Phys., 25, 377–445, 1908.

Mishchenko, M. I., Lacis, A. A., Carlson, B. E., and Travis, L. D.: Nonsphericity of Dust-Like Tropospheric Aerosols – Implications for Aerosol Remote-Sensing and

Climate Modeling, Geophys. Res. Lett., 22, 1077–1080, doi:10.1029/95gl00798, 1995.

Müller, T., Henzing, J. S., de Leeuw, G., Wiedensohler, A., Alastuey, A., Angelov, H., Bizjak, M., Collaud Coen, M., Engström, J. E., Gruening, C., Hillamo, R., Hoffer, A., Imre, K., Ivanow, P., Jennings, G., Sun, J. Y., Kalivitis, N., Karlsson, H., Komppula, M., Laj, P., Li, S. M., Lunder, C., Marinoni, A., Martins dos Santos, S., Moerman, M., Nowak, A., Ogren, J. A., Petzold, A., Pichon, J. M., Rodriquez, S., Sharma, S., Sheridan, P. J., Teinilä, K., Tuch, T., Viana, M., Virkkula, A., Weingartner, E., Wilhelm, R., and Wang, Y. Q.: Characterization and intercomparison of aerosol absorption photometers: result of two intercomparison workshops, Atmos. Meas. Tech., 4, 245–268, doi:10.5194/amt-4-245-2011, 2011.

Müller, T., Schladitz, A., Massling, A., Kaaden, N., Kandler, K., and Wiedensohler, A.: Spectral absorption coefficients and imaginary parts of refractive indices of Saharan dust during SAMUM-1, Tellus B, 61, 79–95, doi:10.1111/j.1600-0889.2008.00399.x, 2009.

Nakajima, T., Sekiguchi, M., Takemura, T., Uno, I., Higurashi, A., Kim, D., Sohn, B. J., Oh, S. N., Nakajima, T. Y., Ohta, S., Okada, I., Takamura, T., and Kawamoto, K.: Significance of direct and indirect radiative forcings of aerosols in the East China Sea region, J. Geophys. Res.-Atmos, 108, 16, doi:10.1029/2002jd003261, 2003.

Nie, W., Ding, A. J., Wang, T., Kerminen, V. M., George, C., Xue, L. K., Wang, W. X., Zhang, Q. Z., Petaja, T., Qi, X. M., Gao, X. M., Wang, X. F., Yang, X. Q., Fu, C. B., and Kulmala, M.: Polluted dust promotes new particle formation and growth, Sci. Rep., 4, 6634, doi:10.1038/srep06634, 2014.

Park, S. U., and Park, M. S.: Aerosol size distributions observed at Naiman in the Asian dust source region of Inner Mongolia, Atmos. Environ., 82, 17–23, doi:10.1016/j.atmosenv.2013.09.054, 2014.

Patashnick, H. and Rupprecht, E. G.: Continuous PM-10 Measurements Using the Tapered Element Oscillating Microbalance, J. Air Waste Manage., 41, 1079–1083, doi:10.1080/10473289.1991.10466903, 1991.

Petzold, A., and Schönlinner, M.: Multi-angle absorption photometry—a new method for the measurement of aerosol light absorption and atmospheric black carbon, J. Aerosol Sci., 35, 421–441, doi:10.1016/j.jaerosci.2003.09.005, 2004.

Petzold, A., Kramer, H., and Schonlinner, M.: Continuous measurement of atmospheric black carbon using a multi-angle absorption photometer, Environ. Sci. Pollut. R., 78–82, 2002.

Prospero, J. M., Ginoux, P., Torres, O., Nicholson, S. E., and Gill, T. E.: Environmental characterization of global sources of atmospheric soil dust identified with the Nimbus 7 Total Ozone Mapping Spectrometer (TOMS) absorbing aerosol product, Rev. Geophys., 40, 1002 , doi:10.1029/2000rg000095, 2002.

Pu, W., Wang, X., Zhang, X. Y., Ren, Y., Shi, J. S., Bi, J. R., and Zhang, B. D.: Size Distribution and Optical Properties of Particulate Matter (PM10) and Black Carbon (BC) during Dust Storms and Local Air Pollution Events across a Loess Plateau Site, Aerosol Air Qual. Res., 15, 2212–2224,

doi:10.4209/aaqr.2015.02.0109, 2015.

Qian, W. H., Tang, X., and Quan, L. S.: Regional characteristics of dust storms in China, Atmos. Environ., 38, 4895–4907, doi:10.1016/j.atmosenv.2004.05.038, 2004.

Ramanathan, V., Chung, C., Kim, D., Bettge, T., Buja, L., Kiehl, J. T., Washington, W. M., Fu, Q., Sikka, D. R., and Wild, M.: Atmospheric brown clouds: Impacts on South Asian climate and hydrological cycle, P. Natl. Acad. Sci. USA, 102, 5326–5333, doi:10.1073/pnas.0500656102, 2005.

Ramanathan, V., Crutzen, P. J., Kiehl, J. T., and Rosenfeld, D.: Atmosphere - Aerosols, climate, and the hydrological cycle, Science, 294, 2119–2124, doi:10.1126/science.1064034, 2001.

Ramanathan, V., Ramana, M. V., Roberts, G., Kim, D., Corrigan, C., Chung, C., and Winker, D.: Warming trends in Asia amplified by brown cloud solar absorption, Nature, 448, 575–578, doi:10.1038/nature06019, 2007.

Rosenfeld, D., Clavner, M., and Nirel, R.: Pollution and dust aerosols modulating tropical cyclones intensities, Atmos. Res., 102, 66–76, doi:10.1016/j.atmosres.2011.06.006, 2011.

Schwarz, J.P., Gao, R.S., Spackman, J.R., Watts, L.A. and Thomson, D.S.: Measurement of the Mixing State, Mass, and Optical Size of Individual Black Carbon Particles in Urban and Biomass Burning Emissions, Geophys. Res. Lett., 35, 13810–13814, doi:10.1029/2008gl033968, 2008.

Rosenfeld, D., Rudich, Y., and Lahav, R.: Desert dust suppressing precipitation: A possible desertification feedback loop, Proc. Natl. Acad. Sci., 98, 5975–5980, doi:10.1073/pnas.101122798, 2001.

Seinfeld, J. H. and Pandis, S. N.: Atmospheric Chemistry and Physics, John Wiley and Sons, Inc., 2003.

Shi J. S., Tian P. F., Zhou T., and Huang Z. W.: Aerosol optical properties in spring in Agricultural area in Hexi Corridor, J. Arid Meteo., 33, 38–44, doi:10.11755/j.issn.1006-7639(2015)-01-0038, 2015 (in Chinese).

Shi J. S., Zhao M. G., Ge J. M., Bi J. R., Wang X., and Chen M.: The calibration of three-wavelength integration nephelometer, China Environ. Sci., 33, 1372–1378, 2013 (in Chinese).

Sloane, C. S., Rood, M. J., and Rogers, C. F.: Measurements of Aerosol-Particle Size - Improved Precision by Simultaneous Use of Optical-Particle Counter and Nephelometer, Aerosol Sci. Tech., 14, 289–301, doi:10.1080/02786829108959491, 1991.

Spracklen, D. V., and Rap, A.: Natural aerosol-climate feedbacks suppressed by anthropogenic aerosol, Geophys. Res. Lett., 40, 5316–5319, doi:10.1002/2013gl057966, 2013.

Srivastava, K. and Bhardwaj, R.: Analysis and very short range forecast of cyclone “AILA” with radar data assimilation with rapid intermittent cycle using ARPS 3DVAR and cloud analysis techniques, Meteorol. Atmos. Phys., 124, 97–111, doi:10.1007/s00703-014-0307-7, 2014.

Tanre, D., Haywood, J., Pelon, J., Leon, J. F., Chatenet, B., Formenti, P., Francis, P., Goloub, P., Highwood, E. J., and Myhre, G.: Measurement and modeling of the

Saharan dust radiative impact: Overview of the Saharan Dust Experiment (SHADE), J. Geophys. Res.-Atmos, 108, 8574, doi:10.1029/2002jd003273, 2003.

Tao, J., Zhang, L., Cao, J., and Zhang, R.: A review of current knowledge concerning PM2. 5 chemical composition, aerosol optical properties and their relationships across China, Atmos. Chem. Phys., 17, 9485-9518, https://doi.org/10.5194/acp-17-9485-2017, 2017.

Tao, J., Zhang, L., Gao, J., Wang, H., Chai, F., and Wang, S.: Aerosol chemical composition and light scattering during a winter season in Beijing, Atmos. Environ., 110, 36-44, 2015.

Tao, J., Zhang, L., Ho, K., Zhang, R., Lin, Z., Zhang, Z., Lin, M., Cao, J., Liu, S., and Wang, G.: Impact of PM2.5 chemical compositions on aerosol light scattering in Guangzhou - the largest megacity in South China, Atmos. Res., 135–136, 48–58, 2014.

Tegen, I., and Fung, I.: Contribution to the Atmospheric Mineral Aerosol Load from Land-Surface Modification, J. Geophys. Res.-Atmos., 100, 18707–18726, doi:10.1029/95jd02051, 1995.

Tegen, I., Harrison, S. P., Kohfeld, K. E., Engelstaedter, S., and Werner, M.: Emission of soil dust aerosol: Anthropogenic contribution and future changes, Geochim. Cosmochim. Ac., 66, A766, 2002.

Tegen, I., Werner, M., Harrison, S. P., and Kohfeld, K. E.: Relative importance of climate and land use in determining present and future global soil dust emission. Geophys. Res. Lett., 31, L05105, doi:10.1029/2003gl019216, 2004.

Thompson, L. G., Davis, M. E., Mosleythompson, E., and Liu, K. B.: Pre-Incan Agricultural Activity Recorded in Dust Layers in 2 Tropical Ice Cores, Nature, 336, 763–765, doi:10.1038/336763a0, 1988.

Wang, S. G., Wang, J. Y., Zhou, Z. J., and Shang, K. Z.: Regional characteristics of three kinds of dust storm events in China, Atmos. Environ., 39, 509–520, doi:10.1016/j.atmosenv.2004.09.033, 2005.

Wang, X., Doherty, S. J., and Huang, J.: Black carbon and other light absorbing impurities in snow across Northern China, J. Geophys. Res.-Atmos., 118, 1471–1492, doi:10.1029/2012jd018291, 2013.

Wang, X., Huang, J. P., Zhang, R. D., Chen, B., and Bi, J. R.: Surface measurements of aerosol properties over northwest China during ARM China 2008 deployment, J. Geophys. Res.-Atmos., 115, doi:10.1029/2009jd013467, 2010.

Wang, X., Huang, J., Ji, M., and Higuchi, K.: Variability of East Asia dust events and their long-term trend, Atmos. Environ., 42, 3156–3165, doi:10.1016/j.atmosenv.2007.07.046, 2008.

Wang, X., Huang, J. P., Zhang, R. D., Chen, B., and Bi, J. R.: Surface measurements of aerosol properties over northwest China during ARM China 2008 deployment, J. Geophys. Res.-Atmos., 115, doi:10.1029/2009jd013467, 2010.

Wang, X., Pu, W., Shi, J., Bi, J., Zhou, T., Zhang, X., and Ren, Y.: A comparison of the physical and optical properties of anthropogenic air pollutants and mineral dust over Northwest China, J. Meteorol. Res., 29, 180–200, doi:10.1007/s13351-015-

4092-0, 2015a.

Wang, X., Pu, W., Zhang, X., Ren, Y., and Huang, J.: Water-soluble ions and trace elements in surface snow and their potential source regions across northeastern China, Atmos. Environ., 114, 57–65, doi:10.1016/j.atmosenv.2015.05.012, 2015b.

Washington, R., Todd, M., Middleton, N. J., and Goudie, A. S.: Dust-storm source areas determined by the total ozone monitoring spectrometer and surface observations, Ann. Assoc. Am. Geogr., 93, 297–313, doi:10.1111/1467-8306.9302003, 2003.

Xin, J. Y., Du, W. P., Wang, Y. S., Gao, Q. X., Li, Z. Q., and Wang, M. X.: Aerosol Optical Properties Affected by a Strong Dust Storm over Central and Northern China, Adv. Atmos. Sci., 27, 562–574, doi:10.1007/s00376-009-9023-5, 2010.

Xin, J. Y., Wang, S. G., Wang, Y. S., Yuan, J. Y., Zhang, W. Y., and Sun, Y.: Optical properties and size distribution of dust aerosols over the Tengger Desert in Northern China, Atmos. Environ., 39, 5971–5978, doi:10.1016/j.atmonsenv.2005.06.027, 2005.

Xin, J. Y., Wang, Y. S., Pan, Y. P., Ji, D. S., Liu, Z. R., Wen, T. X., Wang, Y. H., Li, X. R., Sun, Y., Sun, J., Wang, P. C., Wang, G. H., Wang, X. M., Cong, Z. Y., Song, T., Hu, B., Wang, L. L., Tang, G. Q., Gao, W. K., Guo, Y. H., Miao, H. Y., Tian, S. L., and Wang, L.: The Campaign on Atmospheric Aerosol Research Network of China Care-China, B. Am. Meteorol. Soc., 96, 1137–1155, doi:10.1175/BAMS-D-14-00039.1, 2015.

Xu, J., Bergin, M. H., Greenwald, R., Schauer, J. J., Shafer, M. M., Jaffrezo, J. L., and Aymoz, G.: Aerosol chemical, physical, and radiative characteristics near a desert source region of northwest China during ACE–Asia, J. Geophys. Res., 109, D19S03, doi:10.1029/2003jd004239, 2004

Yan, H.: Aerosol scattering properties in northern China, Atmos. Environ., 41, 6916–6922, doi:10.1016/j.atmosenv.2007.04.052, 2007.

Yang, M., Howell, S. G., Zhuang, J., and Huebert, B. J.: Attribution of aerosol light absorption to black carbon, brown carbon, and dust in China – interpretations of atmospheric measurements during EAST-AIRE, Atmos. Chem. Phys., 9, 2035–2050, doi:10.5194/acp-9-2035-2009, 2009.

Zhang, R., Hegg, D. A., Huang, J., and Fu, Q.: Source attribution of insoluble light-absorbing particles in seasonal snow across northern China, Atmos. Chem. Phys., 13, 6091–6099, doi:10.5194/acp-13-6091-2013, 2013.

Zhang, X. Y., Arimoto, R., and An, Z. S.: Dust emission from Chinese desert sources linked to variations in atmospheric circulation, J. Geophys. Res.-Atmos., 102, 28041–28047, doi:10.1029/97jd02300, 1997.

Zhang, X. Y., Wang, L., Wang, W. H., Cao, D. J., Wang, X., and Ye, D. X.: Long-term trend and spatiotemporal variations of haze over China by satellite observations from 1979 to 2013, Atmos. Environ., 119, 362–373, doi:10.1016/j.atmosenv.2015.08.053, 2015.

Zhang, X. Y., Wang, Y. Q., Wang, D., Gong, S. L., Arimoto, R., Mao, L. J., and Li, J.: Characterization and sources of regional-scale transported carbonaceous and dust aerosols from different pathways in coastal and sandy land areas of China, J. Geophys. Res.-Atmos., 110, D15301, doi:10.1029/2004jd005457, 2005.